ABSTRACT

Title of thesis: CHROMIUM OXIDATION-REDUCTION CHEMISTRY CONTROLLED BY IRON AND MANGANESE (HYDR)OXIDE SURFACES AND SOILS: COLUMN LEACHING AND SPECTROSCOPIC STUDIES

Christina Langlois Miller, Master of Science, 2014

Thesis directed by: Professor Bruce R. James
Department of Environmental Science and Technology

Soil interfaces, including those defined by horizons and iron (Fe(III)) and manganese (Mn(III,IV)) (hydr)oxide mineral surfaces, are a largely unstudied area in soils research, especially in terms of their oxidation-reduction properties. This study attempted to address two questions related to this research deficiency. The first: how chromium (Cr) redox changes throughout mineralogically different soil horizons, and the second: how Cr redox structurally alters Fe(III) and Mn(III,IV) (hydr)oxides in synthetic, soil, and microbial systems. Both parts of the study used column leaching experiments along with Cr speciation techniques to study simulated soil horizon interfaces and Fe/Cr and Mn/Cr redox systems. X-ray absorption spectroscopic techniques were also utilized to analyze the mineral structure of Fe(III) and Mn(III,IV) (hydr)oxides. The results of the study indicate that there are significant interfacial properties affecting Cr(VI) reduction and that Cr(III) oxidation does change the mineral structures of synthetic, soil, and fungal Mn(III,IV)(hydr)oxides to varying degrees.

CHROMIUM OXIDATION-REDUCTION CHEMISTRY CONTROLLED BY IRON AND MANGANESE (HYDR)OXIDE SURFACES AND SOILS: COLUMN LEACHING AND SPECTROSCOPIC STUDIES

By

Christina Lynne Langlois Miller

Thesis submitted to the Faculty of the Graduate School of the
University of Maryland, College Park in partial fulfillment
for the requirements for the degree of
Master of Science
2014

Advisory Committee:

Professor Bruce R. James, Chair
Special Member of the Graduate Faculty Cara M. Santelli
Professor Martin C. Rabenhorst
Assistant Professor Stephanie A. Yarwood
Adjunct Professor Edward R. Landa

ACKNOWLEDGEMENTS

I wish to acknowledge and sincerely thank the many people who, without their assistance, completing this study would not be possible.

I would like to thank Bruce James, who has been a phenomenal advisor, mentor, and teacher for the entire duration of my time at the University of Maryland. Only with his support and guidance could this work have been completed.

I would also like to thank Cara Santelli for a wonderful collaboration opportunity. Without her expertise and assistance, I would never be able to coherently analyze manganese mineralogy.

Finally, I would like to thank Elaine Brice and Alan Marquez for their assistance in the lab and my family and friends for their continued encouragement and support.

TABLE OF CONTENTS

LIST OF FIGURES

LIST OF TABLES

CHAPTER 1

LITERATURE REVIEW

I. Current Knowledge

The oxidation-reduction properties of chromium (Cr), governed by both biotic and abiotic processes, have been studied extensively. Microbial reduction of Cr(VI), oxidation of Cr(III) by Mn(III,VI)(hydr)oxides and reactive oxygen species produced by microbes, and reduction of Cr(VI) by organic acids, Fe(II), and S^{2-}, are all proven mechanisms governing the redox status of Cr in soils (Bartlett, 1991; Brose and James, 2013; Fendorf et al., 2000; Tsu and Yang, 1996). Figure 1.1 illustrates these mechanisms of the Cr redox cycle. Aqueous forms of Cr(III) include hexaquo Cr^{3+}, the dominant species at pH < 3.6, $CrOH^{2+}$ and $Cr(OH)_2^+$, at higher pHs, and $Cr(OH)_4^-$, which forms at pH > 11.5. At near neutral pHs, Cr(III) is almost exclusively in the solid form, as $Cr(OH)_3$ or Cr_2O_3, but soluble organic complexes with Cr(III) may also be stable in this pH range. Aqueous forms of Cr(VI) include CrO_4^{2-}, which dominates at pH > 6.5, $HCrO_4^-$, which dominates at pH < 6.5, and $Cr_2O_7^{2-}$, which forms under slightly acidic conditions with high Cr(VI) concentrations (> 1.0 mM) (Cifuentes et al., 1996). While low concentrations of Cr(VI) may be reduced relatively quickly, high concentrations of Cr(VI) in soils may exhaust the oxidizable species present, allowing for toxic Cr(VI) to potentially remain for long periods of time (Bartlett, 1991). Reduction of Cr(VI) is highly dependent on organic matter and pH, while oxidation of Cr(III) relies on the presence of Mn(III,IV)(hydr)oxides (Chen et al., 2013; Kozuh et al., 1999; Negra et al., 2005).

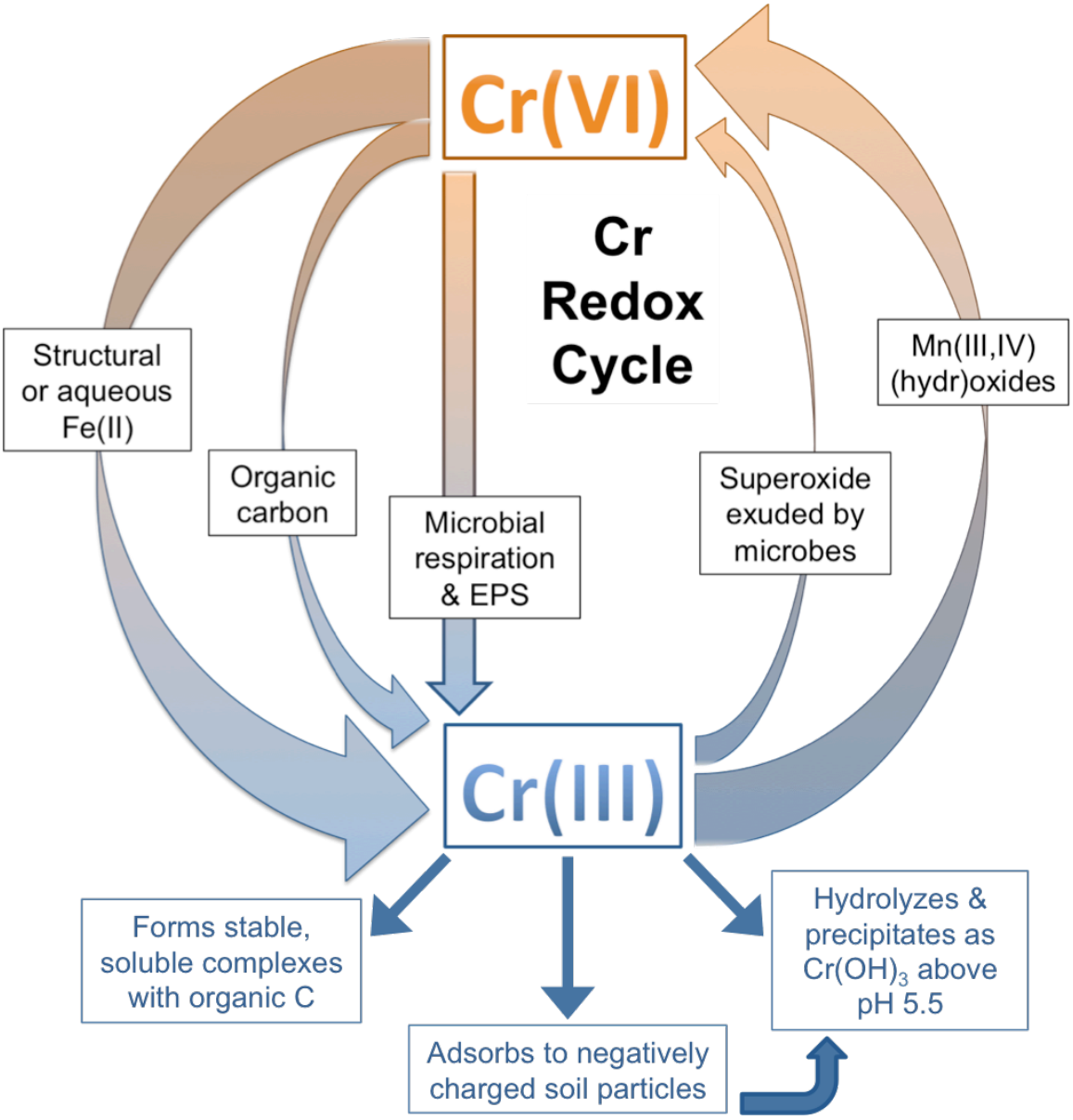

Figure 1.1 Chromium oxidation-reduction cycle in natural soil conditions

a. Sorption of Cr(III) and Cr(VI) in soils

Sequestration of soluble forms of Cr(III) via sorption (including both adsorption and surface precipitation) in soils is greatly enhanced by high clay content, high pH (> 5.5), high cation exchange capacity, and high amounts of organic carbon (C) (Choppala et al., 2013). This sequestration is not affected by Fe(III) or Mn(III,IV) (hydr)oxide content. Adsorption of Cr(III) by soil particles increases with increasing clay content, and decreases in the presence of dissolved organic ligands, which may complex Cr(III) (Cifuentes et al., 1996). Soil pH affects Cr(III) adsorption: at alkaline pHs, $Cr(OH)_3$ precipitation is favored over adsorption, while at acidic pHs, soluble cationic Cr(III) species, which can be more readily adsorbed, will be favored. Higher pH (> 5.5) increases surface precipitation of Cr(III) hydroxides, while low pH favors adsorption of Cr(III) to negatively charged soil particles via inner-sphere monodentate complexes on silica (Stewart et al., 2003). Cation exchange capacity is correlated with Cr(III) sorption because a high CEC indicates a large negative charge on colloidal clay particles (Choppala et al., 2013). In addition to being negatively charged, these colloids have a high surface area, increasing the number of possible sorption sites. The combination of these factors allows for the formation of electrostatic bonds between cationic Cr(III) species and the negatively charged sorption sites on soil colloids (Stewart et al., 2003). Carbonates increase Cr(III) sorption by creating a localized high pH on the surface, which causes the surface precipitation of $Cr(OH)_3$ even when the bulk soil pH is acidic (Stewart et al., 2003).

Sorption of Cr(VI) by soils, which occurs to a significantly lesser extent than Cr(III) sorption, increases with increasing Cr(VI) concentration and is not correlated with

clay content (Choppala et al., 2013; Cifuentes et al., 1996). Adsorption of CrO_4^{2-} is lower in higher pH soils than under more acidic conditions, especially those with large proportions pH-dependent charge, due to the decrease in positive charge with the increase in pH (James and Bartlett, 1983a; Jardine et al., 2013; Zachara et al., 1987). Soils with large amounts of paracrystalline sesquioxides which are coated with organic compounds tend to adsorb Cr(VI) in such a way that it remains oxidized, even in the presence of reducing agents, while soils with large amounts of Fe(III)(hydr)oxides tend to adsorb Cr(VI) in such a way that reduction is enhanced, a process that is not well understood (James and Bartlett, 1983a; Jardine et al., 2013). Goethite, an Fe(III)(hydr)oxide mineral with the chemical formula α-FeO(OH), adsorbs both Cr(III) and Cr(VI) (Fendorf, 1995). Adsorption of Cr(VI) by goethite occurs through a surface complexation reaction, while other Fe(III)(hydr)oxides such as magnetite (Fe_3O_4) reductively precipitate Cr(VI) at Fe(II) sites. This reductive precipitation process occurs via sorption of CrO_4^{2-} onto the Fe_3O_4 surface and then reduction of Cr(VI) to Cr(III) by structural Fe(II), as opposed to reduction of CrO_4^{2-} by Fe(II) in solution (Deng et al., 1996; Dossing et al., 2011). Paracrystalline Fe(III)(hydr)oxides are also able to sorb CrO_4^{2-} through an anion exchange reaction (Aoki and Munemori, 1982; Music et al., 1986). Iron (III) (hydr)oxides in soils have been found to inhibit the oxidation of Cr(III) by Mn(III,IV)(hydr)oxides by adsorbing Cr(III), thus immobilizing it (Fendorf and Zasoski, 1992).

b. Reduction of Cr(VI) by Fe(II)

Soil minerals bearing Fe(II), including biotite ($K(Mg,Fe)_3AlSi_3O_{10}(F,OH)_2$), magnetite ($Fe_3O_4$), ilmenite ($FeTiO_3$), iron sulfides (FeS and FeS_2), and siderite ($FeCO_3$), as well as zero-valent iron (Fe^0), are capable of reducing Cr(VI) (Buerge and Hug, 1998).

Structural Fe(II) is a stronger reducing agent than aqueous Fe^{2+} and is able to reduce chromate, principally as $HCrO_4^-$ below pH 7; the optimum molar ratio of structural Fe(II) to Cr(VI) for chromate reduction is 2.4:1, which is lower than the 3:1 molar ratio of aqueous Fe(II) to Cr(VI) needed for complete chromate reduction (Jung et al., 2007; Loyaux-Lawniczak et al., 2001). Naturally occurring, thick, green clay layers made up of Fe-rich phyllosilicates such as glauconite and Fe-smectite can act as barriers preventing Cr(VI) from entering the groundwater by ensuring reduction by Fe(II) (Loyaux-Lawniczak et al., 2001; White and Peterson, 1996). According to Buerge and Hug (1997), in low pH environments (< 4), the following redox reaction occurs:

$$3\,Fe^{2+} + HCrO_4^- + 7\,H^+ \rightarrow 3\,Fe^{3+} + Cr^{3+} + 4\,H_2O$$

In environments with pH values between 4 and 6, the following redox reaction occurs:

$$3\,Fe^{2+} + HCrO_4^- + 3\,H_2O \rightarrow 3\,Fe(OH)_2^+ + CrOH^{2+}$$

And in environments with a pH > 6, the following redox reaction occurs:

$$3\,Fe^{2+} + HCrO_4^- + 8\,H_2O \rightarrow 3\,Fe_3Cr(OH)_{12}(s) + 5\,H^+$$

The products of each redox reaction change depending on the pH, but all of the reactions require 3 equivalents of Fe(II) for every equivalent of Cr(VI). Regardless of pH, the reduction of Cr(VI) to Cr(III) by Fe(II) can be described as three one-electron transfers, of which the first electron transfer (Cr(VI) to Cr(V)) is the rate determining step (Buerge and Hug, 1997). The second electron transfer from Cr(V) to Cr(IV) accompanies the change from tetrahedral ligand coordination (Cr(VI) and Cr(V)) to octahedral ligand coordination (Cr(IV) and Cr(III)), and is followed by a third electron transfer from Cr(IV) to Cr(III) (Buerge and Hug, 1997). In reality, Cr(V) is the dangerously toxic form of Cr, but it is so short lived in the environment that Cr toxicity concern is expressed as Cr(VI),

as the reduction of Cr(VI) within living tissue can cause cancer and cell mutations (Vasant et al., 2001).

Hexavalent chromium reduction by Fe(II) in the presence of Fe(III)(hydr)oxides such as goethite and lepidocrocite (γ-FeOOH) is fast, and the relationship can be used effectively to reduce Cr(VI), as the Fe(II) reduces the Cr(VI) and the Fe(III)(hydr)oxide catalyzes the reduction and facilitates surface precipitation of $Cr(OH)_3$ at neutral-to-alkaline pHs (Buerge and Hug, 1998). This reductive precipitation can result in the surface precipitation of paracrystalline Cr(III)-Fe(III) mixed (hydr)oxides or crystalline Cr(III)-substituted goethite with Ksp values up to 10^3 times lower than in the pure Cr(III) and Fe(III) (hydr)oxides. Paracrystalline phases may dominate at high pH, and crystallinity is also dependent on the Cr(III)-to-Fe(III) ratio (Buerge and Hug, 1998; Chang et al., 2012). Adsorption of Fe(II) on goethite, lepidocrocite, montmorillonite, and kaolinite occurs via a fast step (< 1 minute) followed by a slow step (> 1 day) (Jeon et al., 2003). This adsorption appears to follow second order kinetics. The kinetics of Cr(VI) reduction by Fe(II) are also second order, which indicates that the electron transfer is the rate-determining step (Buerge and Hug, 1998). If adsorption of Fe(II) was the rate-determining step, the kinetics would appear to be first order and would not be dependent on the Cr(VI) concentration. Chromate reduction kinetics are dependent on pH, as the reduction rate decreases as the pH increases up to pH 4 and above pH 4, the reduction rate begins to increase (Buerge and Hug, 1997; Xiao et al., 2012).

c. Fe(III)(hydr)oxides in soils

Iron oxides, oxyhydroxides, and hydrated oxides are ubiquitous in soils. They are generally red, yellow, or orange and are responsible for the brown or reddish colors of

many soils (Schwertmann and Taylor, 1989). Goethite (α-FeOOH) is one of the most common soil Fe(III)(hydr)oxides. It is yellowish-brown and is commonly associated with other Fe(III)(hydr)oxides in soils. Structurally it is orthorhombic, where double chains of Fe-O-OH octahedra bind to each other via Fe-O-Fe and hydrogen (H) bonds (Liu et al., 2013; Schwertmann and Taylor, 1989). Hematite (α-Fe_2O_3) is bright red in color and is often found in older soils. Its crystal structure is trigonal, consisting of layers of oxygen with Fe(III) occupying vacancies in two thirds of the octahedra (Blanchard et al., 2010; Schwertmann and Taylor, 1989). Magnetite (Fe_3O_4) is unique in its structural Fe(II) content. It has a cubic crystal structure and contains both tetrahedral and octahedral Fe (Schwertmann and Taylor, 1989). It is black in color and generally forms in reducing soils, although it transforms to maghemite (γ-Fe_3O_4), which also contains structural Fe(II), when exposed to oxygen (Peterson et al., 1996; Schwertmann and Taylor, 1989). Another common soil Fe(III) mineral is ferrihydrite. Ferrihydrite forms as a result of the hydrolysis of Fe(III) in water, and therefore is common in reduced soils as they become newly oxidized (Saleh and Jones, 1984). Ferrihydrite is paracrystalline, unlike the other Fe(III)(hydr)oxide minerals, and transforms over time to goethite and hematite (Cornell and Giovanoli, 1985).

In general, Fe(III)(hydr)oxides have points of zero charge (PZCs) between pH 7 and 9, indicating that below pH 7 they are generally fully protonated and positively charged, while above pH 9 they are generally fully deprotonated and negatively charged, although the PZCs can change depending on the soil environment (Arias et al., 1995; Schwertmann and Taylor, 1989). This surface charge attracts ions and organic compounds, which can adsorb to the oxide surface. Soil Fe(III)(hydr)oxides are also

easily reduced to soluble Fe^{2+} by microorganisms. When O_2 becomes deficient in the soil environment, anaerobic bacteria and other microbes use Fe(III) as an electron acceptor as they oxidize organic C, reducing the Fe in the process (Bongoua-Devisme et al., 2013). Other microorganisms are capable of creating Fe(III)(hydr)oxides by oxidizing organic C compounds which have complexed with Fe(III). When the organic C is oxidized, Fe^{3+} is released and, upon contact with O_2 it precipitates out of solution. There has also been evidence for the direct oxidation of Fe(II) by microorganisms (Emerson et al., 2013). Due to the high crystallinity of most Fe(II,III)(hydr)oxides, they are relatively easily quantified and identified in soils. X-ray diffraction is a commonly used method of identification, as most Fe minerals have unique patterns of detectable X-ray diffraction lines, with the exception of paracrystalline ferrihydrite (Wang et al., 1993).

d. Reduction of Cr(VI) and Complexation of Cr(III) by Phenolic and Carboxylic Acids

Both organic matter and living organisms in soils have the capacity to reduce Cr(VI). Humus, which can be represented by fulvic acid (fulvic acids reduce Cr(VI) approximately 100 times faster than do humic acids), and organic phenolic compounds can also reduce Cr(VI) (Fendorf et al., 2000; Wittbrodt and Palmer, 1996). In acidic soil environments, organic matter facilitates the reduction of Cr(VI) to Cr(III) according to the following reaction (Jardine et al., 2011):

$$4\,CrO_4^{2-} + 3\,CH_2O + 20\,H^+ \rightarrow 4\,Cr^{3+} + 3\,CO_2 + 13\,H_2O.$$

Trivalent Cr complexes with organic acids can be soluble in soil solution, or can sorb to soil particles depending on the organic acid and soil sorbent surface properties. These complexes can be very resistant to microbial degradation (Puzon et al., 2008).

Organic-Cr(III) complexes formed after the reduction of Cr(VI) in the presence of organic ligands can be either soluble or insoluble. Soluble organic-Cr(III) complexes account for a large portion of mobile Cr(III) in soils (Puzon et al., 2005). Complexation of Cr(III) by organic acids increases the rate of reduction of Cr(VI), a phenomenon which is not well understood. Organic Cr(III) complexes also decrease the total amount of Cr(III) oxidized by Mn (hydr)oxides and have significantly slower oxidation rates than inorganic Cr(III) complexes (James and Bartlett, 1983b). Recent studies have deduced that the presence of Mn(II) enhances Cr(VI) reduction by the organic acids citrate and tartrate (Brose and James, 2013; Sarkar et al., 2013). Organic-Cr(III) complexes that have been detected in soils include, Cr(III)-malate, Cr(III)-cysteine, Cr(III)-oxaloacetate, Cr(III)-serine, Cr(III)-citrate, Cr(III)-oxalate, and Cr(III)-salicylate. While the toxicity of these compounds has not been determined, their mobility in soils could result in contact with Mn(III,IV)(hydr)oxides, which could induce Cr(III) oxidation (Puzon et al., 2005; Yang et al., 2014).

e. Reduction of Cr(VI) by soil microorganisms

The general reaction sequence of microbial chromate reduction is as follows (where CRB represents chromate-reducing bacteria):

$$CrO_4^{2-} + 8H^+ + 3e^- \xrightarrow{CRB} Cr^{3+} + 4H_2O \xrightarrow{pH\sim 7} Cr(OH)_3(s) + 3H^+ + 3H_2O.$$

This microbial reduction of chromate is enzyme mediated and attributed to either soluble proteins or cell membranes. It is known that in some cases, bacterial reduction can lead to soluble Cr(III) complexes with organic carboxylic acid groups, as opposed to the typical inorganic $Cr(OH)_3$ product, which has the potential to precipitate out of solution. These soluble Cr(III) complexes are formed in the presence of cellular organic metabolites and

their formation is related to microbial exopolymeric substances (EPS). Toxic conditions, such as high Cr(VI) levels, are known to facilitate microbial production of EPS, and thus could increase the occurrence of soluble Cr(III)-organic complexes (Dogan et al., 2011). Recently, Kantar et al. (2014) found that the presence of EPS may decrease the amount of Cr(III) that sorbs to soil surfaces.

Research has shown that a higher cell density is proportional to increased Cr(VI) reduction within certain restrictions. A study by Pal and Paul (2004) concluded that the rate of Cr(VI) reduction increased with cell density up to 10^{10} cells/mL; in general, the increase in cell density in aerobic soil environments is much greater than in anaerobic soil environments, however chromate reduction is significantly lower in aerobic environments than in anaerobic ones. Research published by Contreras et al. (2011) demonstrated aerobic Cr(VI) reduction coupled with both growth and biomass decay, indicating that aerobic Cr(VI) reduction may also be significant. Rates of Cr(VI) reduction have been found to increase with increasing initial Cr(VI); however, higher concentrations of Cr(VI) require longer incubation times (Pal and Paul, 2004). At a certain point, which varies for individual bacterial species, the initial Cr(VI) concentration becomes inhibitory to microbial growth. Camargo et al. (2003) found that isolates were inhibited by Cr(VI) concentrations between 250 and 1500 mg/L, which is a large range, but the values are higher than those tested in many other studies.

There is often debate whether Cr(VI) reduction is biotically or abiotically mediated. Both mechanisms are possible; however, while abiotic chemical processes do have the ability to reduce chromium, reduction is nearly 70% more efficient when mediated biotically, as found by Dotro et al. (2011) in simulated gravel wetlands. This

biological reduction is much less consistent than the physicochemical reduction, however, leading to greater variability in the efficiency and less predictable results. While most soils have an inherent tendency towards chromate reduction, biotic reduction enhanced by the addition of an appropriate carbon source, such as glucose, can increase the Cr(VI) reduction rate by increasing the microbial biomass (Leita et al., 2011). A study by Dogan et al. (2011) showed that simulated biological EPS, including galacturonic acid, glucuronic acid, alginic acid, and extracted microbial EPS, reduced Cr(VI). Controls with no microbial cells added exhibited little to no Cr(VI) reduction, indicating that the process is heavily dependent on microorganisms.

Microbiological reduction of Cr(VI) to Cr(III) can occur either directly as a result of microbial respiration or indirectly as a result of the appearance of an extracellular byproduct of microbial metabolism. Wielinga et al. (2001) proposed a pathway for indirect Cr(VI) reduction, which included two reactions. In the first reaction, Fe^{3+} is used as the terminal electron acceptor for microbial respiration, reducing it to Fe^{2+}. The second reaction involves the Fe(II) re-oxidizing to Fe(III), reducing Cr(VI) to Cr(III) in the process. The electron shuttle nature of the proposed pathway was tested and it was determined that iron was cycled nearly twice over the course of the experiment, proving that ferric iron acts as a catalyst (Brose and James, 2010; Wielinga et al., 2001).

Chromate reduction enzymes can be either membrane-bound or soluble within the cytoplasm, depending on the Cr(VI)-reducing microbial species. The membrane-bound Cr(VI) reductase mechanism ensures that the cell is protected from Cr(VI) toxicity through the precipitation of $Cr(OH)_3$ on the cell surface, while the soluble Cr(VI) reductase mechanism can lead to the uptake of Cr(VI) concentrations which are toxic to

the cell. The presence of membrane-bound Cr(VI) reduction enzymes can be determined by comparing Cr(VI) reductase activity in the cellular supernatant fractions S_{32} (centrifuged at 32,000 x g, contains suspended cell material with associated proteins as well as soluble proteins) and S_{150} (centrifuged at 150,000 x g, contains only soluble proteins) and demonstrating that Cr(VI) reductase activity is higher in the S_{32} fraction than the S_{150} fraction (Pal and Paul, 2004). The presence of soluble Cr(VI) reduction enzymes can be determined by comparing Cr(VI) reductase activity in cellular extract supernatant liquid to the activity in the intact cells, and demonstrating that Cr(VI) reduction does not appreciably change between the two fractions (Chen and Hao, 1998).

In terms of the product of Cr(VI) reduction, Cr(III), Dogan et al. (2011) found that microbial chromium reduction resulted almost entirely in soluble organic Cr(III) complexes, and that the presence of organic ligands increased Cr(III) solubility. These soluble Cr(III)-organic ligand complexes have the potential to protect cells and enzymes critical to Cr(VI) reduction. Soluble Cr(III)-organic complexes allow cells to continue growing in high-Cr(VI) environments that would otherwise be toxic because the complexed Cr(III), unlike cationic mineral Cr(III), is unable to sorb to negatively charged microbial cells and inhibit Cr(VI) reduction. The “removal” of Cr(III) by organic complexation also protects Cr(VI) reductase enzymes from being inactivated, as the presence of inorganic Cr(III) was found to be inhibitory to Cr(VI) reduction enzymes (Dogan et al., 2011).

While Cr(VI) is toxic to most microorganisms, the occurrence of Cr(VI) contamination has produced Cr(VI)-resistant bacterial strains. Some examples of common Cr(VI)-resistant bacteria include various species within the following groups

and genera: *Agrobacterium*, *Alcaligenes*, *Arthrobacter*, *Bacillus*, *Corynebacteria*, *Enterobacter*, *Escherichia* (*E. coli*), *Pseudomonas*, *Streptococcus*, *Streptomyces*, sulfate-reducing bacteria, and some yeast species (Chen and Hao, 1998). Resistance to Cr(VI) has also been observed in fungi and algae. It is likely that there are many pathways of Cr(VI) resistance in the diverse populations of Cr(VI)-resistant microorganisms, however some common pathways which have been previously studied are discussed further in the text below.

A common mechanism of Cr(VI) resistance used by many bacteria is Cr(VI) reduction by a Cr(VI)-reducing enzyme, which can be either soluble in the cytoplasm or associated with the cell membrane, as discussed previously. Another mechanism of Cr(VI) resistance in bacteria has been found to be associated with the presence of a plasmid, as a dramatic decrease in Cr(VI) resistance was observed when the plasmid was removed (Cervantes et al., 2001). The mechanism through which Cr(VI) enters bacterial cells is through the sulfate transport pathways. This is because the chromate oxyanion is structurally and reactively similar to the sulfate oxyanion (Cervantes et al., 2001).

A mechanism of Cr(VI) resistance utilized by yeast species is decreasing the accumulation of Cr(VI) from the soil solution within the cell. The decreased accumulation is facilitated by the presence of a thick cellular envelope with low membrane permeability to chromium (Cervantes et al., 2001). However, Cr(VI) can enter yeast cells through the permease system, which is a non-specific anion carrier used to transport anions such as sulfate and phosphate. In this case, Cr(VI) uptake can decrease sulfate uptake enough to be toxic to the cell (Cervantes et al., 2001). In terms of non-bacterial microbial resistance, filamentous fungi appear to develop Cr(VI) resistance as a

result of a defect in the sulfate transport pathway, while the Cr(VI) tolerance mechanisms for algae are still largely unstudied (Cervantes et al., 2001).

While Cr(VI) resistance and Cr(VI) reduction can exist together in some microorganisms, not all Cr(VI)-resistant microbes are also able to reduce Cr(VI). Some examples of Cr(VI)-reducing bacterial genera include *Achromobacter, Acinetobacter*, *Aeromonas*, *Desulfovibrio, Escherichia*, *Enterobacter*, *Pseudomonas*, and *Shewanella*. Within these genera both aerobic and anaerobic Cr(VI) reduction occur (Chen and Hao, 1998). Chromium (VI) reduction and removal has been observed in a variety of systems, including activated sludge, anaerobic sludge digestion, anaerobic wastewater treatment, and biological fixed-film systems. The addition of antibiotics such as penicillin to chromate-reducing microorganisms results in the decrease of Cr(VI) reduction, further evidence that Cr(VI) reduction is enzymatically mediated. Other indications that Cr(VI) reduction is biologically mediated include the increase in reduction rate with higher cell density, the absence of reduction in samples without cells or cell extracts and when cell extracts were heated to 100°C, and higher reduction rates during the exponential growth phase of different microorganisms (Chen and Hao, 1998).

Additional microbially-mediated Cr reactions include bio-sorption and extracellular precipitation. Adsorption of Cr(III), the product of Cr(VI) reduction, by biofilms has been found to occur mostly in mycelial fungi and filamentous algae. This adsorption is dependent on pH as well as Cr oxidation state. At extremely low pHs (≤ 2), Cr(VI) adsorption will be favored, but at higher pHs (3.5-5.5) Cr(III) hydrolysis and adsorption will be favored (Cervantes et al., 2001). The reason for this pH dependence is that, at very low pH values, biological cells can be positively charged, and therefore

attract anionic chromate, but at most pH values common in soils, biological cells are negatively charged, and therefore attract Cr(III) which has soluble, cationic forms. Extracellular precipitation of Cr(III) can be facilitated by bacteria, removing potentially toxic soluble ionic forms of chromium from solution, reducing the potential for toxicity. This phenomenon has been reported in sulfate-reducing bacteria (Cervantes et al., 2001).

f. Oxidation of Cr(III) by Mn(III,IV)(hydr)oxides

Manganese (III,IV) (hydr)oxides can exist in soils as independent nodules or as coatings on other mineral particles (often referred to as manganese stains in soils or desert varnish on exposed bedrock). There are many forms of Mn(III,IV)(hydr)oxide soil minerals, including lithiophorite ($(Al,Li)Mn^{4+}O_2(OH)_2$), hollandite ($Ba(Mn^{4+},Mn^{2+})_8O_{16}$, and birnessite ($(Na,Ca,K)(Mn^{4+},Mn^{3+})_2O_4 \cdot 1.5\ H_2O$), and, as most are fine-grained and paracrystalline, they are often grouped together under the general term “Mn oxides” (Post, 1999). Due to their paracrystalline nature, their nonstoichiometric composition, and the variability in mineralogy of minerals formed under slightly different conditions, Mn(III,IV)(hydr)oxides are difficult to synthesize reproducibly, and especially to analyze (Feng et al., 2007). Manganese (III,IV) (hydr)oxides appear as brown-black stains as well as in redoximorphic features in soils, and they generally have large surface areas and are considered very chemically active, especially in terms of oxidation-reduction reactions and cation exchange reactions. More specifically, Mn(III,IV)(hydr)oxides, such as birnessite, can oxidize Cr(III) to Cr(VI), and pyrolusite (MnO_2) can have a higher cation exchange capacity (CEC) than montmorillonite at alkaline pHs, a clay mineral with high shrink-swell capacity (Negra et al., 2005; Post, 1999). They also generally have PZC

values lower than Fe(III)(hydr)oxides, making them almost exclusively negatively charged in soils and capable of adsorbing large amounts of cations (Tan et al., 2008).

The amount of Cr(III) that soil Mn(III,IV)(hydr)oxides are capable of oxidizing is dependent on the mineralogy of the oxide. This oxidation capacity can be as high as 700 mmol Cr(III) oxidized/kg pure oxide for pyrolusite (18% of the Cr(III) added was oxidized) (Tan et al., 2005), and 1300 mmol Cr(III) oxidized/kg pure oxide for birnessite (unknown volume of 4 mmol Cr(III)/L added) (Feng et al., 2007). This oxidation occurs via the following steps: 1) the formation of a Cr(III) complex on the Mn(III,IV)(hydr)oxide surface, 2) the transfer of electrons from Cr(III) to Mn(III or IV), 3) the formation of a Cr(VI) – Mn(II) complex, and 4) the release of Mn(II) and Cr(VI) into solution (Trebien et al., 2011). Oxidation of Cr(III) by Mn(III,IV)(hydr)oxides has been found to be inhibited by high pH and high Cr(III) concentration, but has not been found to be limited by the presence of the soluble oxidation products, Mn(II) and Cr(VI) (Fendorf and Zasoski, 1992).

Birnessite, specifically, is the most common soil Mn(III,IV)(hydr)oxide and undergoes both oxidation-reduction and cation exchange reactions, making it instrumental in controlling groundwater and soil solution chemistry. It has an octahedral layer structure in which the layers, constructed of edge sharing MnO_6 octahedra, are separated by water molecules (Post and Veblen, 1990). Birnessite is also poorly crystalline, and has a low point of zero charge (PZC, at pH 1.75) and a high average oxidation state (3.96) compared to other Mn(III,IV)(hydr)oxide minerals (Feng et al., 2007). Due to the high surface area of Mn(III,IV)(hydr)oxides, particularly birnessite, these oxide minerals are able to sorb large amounts of heavy metals. Studies on the

mechanism of this sorption indicate that heavy metals may be adsorbed by Mn(III,IV)(hydr)oxides as hydrolyzed cations, which are formed by surface-induced hydrolysis (Weaver et al., 2002).

g. Crystal structure of Mn(III,IV)(hydr)oxides

Manganese(III,IV)(hydr)oxides fall into two main structural groups: layer, or phyllomanganate, structures and tunnel structures, of which the layer structures are the more stable of the two (McKenzie, 1989). Some common layer-structured Mn(III,IV)(hydr)oxides are birnessite ($(Na,Ca)(Mn^{4+},Mn^{3+})_7O_{14}\bullet 2.8\ H_2O$), vernadite ($\delta$-$MnO_2$), rancieite ($(Ca,Mn)Mn_4O_9\bullet n\ H_2O$), and buserite ($Na_4Mn_{14}O_{27}\bullet 21\ H_2O$). Common tunnel-structured Mn(III,IV)(hydr)oxides include pyrolusite (β-MnO_2) and todorokite ($(Na,Ca,K)_{0.3\text{-}0.5}(Mn^{4+}Mn^{3+})_6O_{12}\bullet 3.5\ H_2O$) (Dixon and White, 2002; McKenzie, 1989). As evidenced in the above minerals, several different valence states of Mn can be present in one mineral.

The phyllomanganate birnessite is a common oxide found in desert varnishes and Mn nodules found in the ocean (Post, 1999). Structurally, it consists of layers of edge-linked octahedra 7 Å apart. The interlayers can contain H_2O molecules as well as exchangeable cations (Dixon and White, 2002). Birnessite structures can vary slightly as a result of different interlayer cations, including magnesium, calcium, nickel, copper, and zinc (Kwon et al., 2013; Post and Veblen, 1990). Buserite is structurally the same as birnessite, except with a 10 Å interlayer spacing (Lanson et al., 2000). Upon dehydration, this spacing collapses to 7 Å, becoming birnessite (Cui et al., 2008; McKenzie, 1989). Vernadite is similar to birnessite, but is composed of both edge-sharing octahedra and corner-sharing octahedra (Dixon and White, 2002; Grangeon et al., 2010). It is commonly

found in Mn-rich ore deposits (Filimonova et al., 2010). Rancieite is considered to be similar to birnessite, but with different interlayer cations, namely calcium (Ca) (Cygan et al., 2012; McKenzie, 1989).

Pyrolusite is considered to be the most crystalline, and therefore stable, Mn(III,IV)(hydr)oxide mineral. Single chains of edge-sharing MnO_6 octahedra share corners with each other to form a framework of tunnels (McKenzie, 1989; Post, 1999). Pyrolusite is found in hydrothermal vent deposits, but is not commonly found in soils (Camprubi et al., 2008; Post, 1999). The true structure of todorokite is 3×3 tunnel structure formed by triple chains of octahedra, which share corners (Cui et al., 2008; McKenzie, 1989). It is one of the most common Mn(III,IV)(hydr)oxides in geologic Mn deposits as well as ocean Mn nodules, although in nature, the 3×3 structure deviates to include 3×4 up to 3×9 structures (Post, 1999).

h. Mn(III,IV)(hydr)oxides in soils: Ferromanganese concretions

The formation of ferromanganese concretions, also known as Mn nodules, occurs under conditions of alternating aerobic and anaerobic periods (Zaidel'man and Nikiforova, 2010). A proposed process by which such concretions form is: the reduction of Fe(III) and Mn(III,IV) under reducing (e.g., anaerobic) soil conditions to Fe(II) and Mn(II) results in the solubilization of these elements, which allows them to move with the flow of water. Then, when the water is no longer present, they concentrate and re-oxidize, in the pores around silicate grains, cementing the grains together and forming hard concretions (Schwertmann and Fanning, 1976). A similar but slightly different proposal for the formation of ferromanganese concretions is: reduced, soluble Mn(II) moves to the inside of the soil ped, where the conditions are more oxidizing. There it

oxidizes, becoming an insoluble, amorphous Mn(III,IV)(hydr)oxide. As the environment becomes more reducing, the process repeats with Fe. Over time, as soil conditions change, layers of Fe(III)(hydr)oxides, Mn(III,IV)(hydr)oxides, and clays build up, increasing the size of the concretion (Jien et al., 2010). Studies have shown that concretions have banded structures with different amounts of Fe and Mn in the concentric layers, which can be used to infer the oxidation-reduction processes occurring at the time of formation of each layer (Gasparatos et al., 2005).

While Fe(III)(hydr)oxides in concretions can be present in high amounts without the presence of Mn(III,IV)(hydr)oxides, Mn(III,IV)(hydr)oxides in concretions only exist in the presence of Fe(III)(hydr)oxides (Schwertmann and Fanning, 1976). Even though a very darkly colored concretion is high in both Mn and Fe, it takes on the appearance of Mn(III,IV)(hydr)oxides, as these oxides are more effective pigmenting agents than are Fe(III)(hydr)oxides. Minerals commonly found in ferromanganese concretions include goethite (FeO(OH)), maghemite (γ-Fe_2O_3), hematite (Fe_2O_3) birnessite ($(Na_{0.3}Ca_{0.1}K_{0.1})(Mn^{4+},Mn^{3+})_2O_4 \bullet 1.5\ H_2O$), lithiophorite ($(Al,Li)MnO_2(OH)_2$), todorokite ($(Na,Ca,K,Ba,Sr)_{1-x}(Mn,Mg,Al)_6O_{12} \bullet 3\text{-}4H_2O$), pyrolusite ($MnO_2$), psilomelane ($Ba(Mn^{2+})(Mn^{4+})_8O_{16}(OH)_4$), and cryptomelane ($K(Mn^{4+},Mn^{2+})_8O_{16}$) (D'Amore et al., 2004; Schwertmann and Fanning, 1976).

Ferromanganese concretions, due to their high concentrations of Fe(III) and Mn(III,IV) (hydr)oxides, are known to accumulate heavy metal cations such as cobalt, lead, and cadmium (Zaidel'man and Nikiforova, 2010). Generally, Mn(III,IV)(hydr)oxides are negatively charged at normal soil pH values, so they are

capable of adsorbing large amounts of cations, accounting for this accumulation of heavy metals (Feng et al., 2007; Komarek et al., 2013).

i. Mn(III,IV)(hydr)oxides in soils: Manganiferous soils

Manganiferous soils are uniquely high in Fe(III) and Mn(III,IV) (hydr)oxides. They are not very common throughout the world, but have distinguishing properties, which validates the need to study them. Typical soils throughout the world have less than 1 g/kg Mn, however some select areas including Maryland, Arkansas, and Hawaii, USA, Orissa, India, and Mpumalanga province, South Africa, have manganiferous bedrock and soils with up to 120 g/kg Mn (Bourgault and Rabenhorst, 2011; Dowding and Fey, 2007; Fujimoto and Sherman, 1948). In these locations manganiferous soils form over dolomite bedrock in what is known as manganese wad (i.e., a term used by geologists to indicate black, porous Mn(III,IV)(hydr)oxides)) (Bourgault and Rabenhorst, 2011).

Analysis of the marble bedrock below manganiferous soils in Maryland, USA showed that it was largely dolomite ($CaMg(CO_3)_2$), which is similar to the parent material of the manganiferous soils found in South Africa (Bourgault and Rabenhorst, 2011). However, soils with slightly lower concentrations of Mn were formed from marble bedrock that was dominantly calcite ($CaCO_3$). Divalent Fe and Mn can substitute for calcium and magnesium in the crystal lattices of calcite and dolomite, although the Mn concentrations tend to be higher in dolomite (Bourgault and Rabenhorst, 2011). The process by which Mn(III,IV) and Fe(III) (hydr)oxides form in soils from marble bedrock is thought to take place as follows: over time, the dolomite and calcite marble weathers, and as the marble dissolves, the calcium, magnesium, and carbonate ions become soluble and are leached away. As this happens, Fe(II) and Mn(II) ions are released from the

marble crystal structure, which allows them to oxidize and become insoluble. The Mn(III,IV) and Fe(III) (hydr)oxides accumulate around the edges of marble grains along with silicate residues. As more and more of the carbonate crystals dissolve, the manganiferous material is left behind, creating manganiferous soils (Bourgault and Rabenhorst, 2011).

Although the A and B horizons of manganiferous soils in Maryland, USA are lighter brown in color, indicating the presence of lower amounts of Mn(III,IV)(hydr)oxides, they can still have Mn concentrations of up to 45 g/kg, which is much higher than the average of 1 g/kg Mn in non-manganiferous soils (Bourgault and Rabenhorst, 2011). The lower BC and C horizons are formed in marble residuum and exhibit much darker colors (e.g., 5YR 2/1) and Mn concentrations up to 140 g/kg (Bourgault, 2008).

Manganiferous soils are characterized by their dark, blackish color (e.g., 10YR 2/1). Organic C in the soil can have a similar effect on color; therefore, dark color alone is not enough to indicate the presence of high concentrations of Mn(III,IV)(hydr)oxides. However, the soil horizons with the highest concentrations of Mn(III,IV)(hydr)oxides in manganiferous soils are found below 100 cm depth, where C concentrations are typically very low (e.g., less than 2 g/kg) (Bourgault and Rabenhorst, 2011). These C concentrations are too low to be able to color the soil so intensely black, and therefore at such depths the black color can be attributed to Mn(III,IV)(hydr)oxides.

Although manganiferous soils are darkly colored due to high concentrations of Mn(III,IV)(hydr)oxides, the Mn(III,IV)(hydr)oxides are always accompanied by high concentrations of Fe(III)(hydr)oxides, a similar phenomenon as seen in ferromanganese

concretions, likely due to the chemical association between Fe and Mn and the presence of both Fe and Mn in the parent material (e.g., dolomite or calcite marble bedrock) (Bourgault and Rabenhorst, 2011). An analysis of the mineralogy of the manganiferous soils in Maryland, USA indicated the presence of hematite (Fe_2O_3), goethite (FeO(OH)), lithiophorite ($(Al,Li)MnO_2(OH)_2$), and gibbsite (Al_2O_3, a weathering product of lithiophorite) (Bourgault and Rabenhorst, 2011; Dowding and Fey, 2007).

Manganiferous soils are very rare worldwide. They are only known in three locations, Maryland and Hawaii, USA and Mpumalanga province, South Africa. There are other locations in the United States as well as in India that have the potential to become manganiferous soils, but currently the manganiferous materials are so deep below the soil surface that they are not considered part of the soil zone (Bourgault and Rabenhorst, 2011). Since these manganiferous soils are so limited in the United States and worldwide, there is currently no accounting for them in Soil Taxonomy, nor is it likely that such accounting will occur unless more of these soils are discovered.

Mn(III,IV)(hydr)oxides have distinctive properties that are important to consider in terms of soils with high amounts of such oxides. One of these properties is their chemical reactivity, which allows for small concentrations of Mn(III,IV)(hydr)oxides to have a large impact on soil properties. Another is their high specific surface area, which allows them to adsorb large amounts of heavy metal cations such as lead (Pb^{2+}), cobalt (Co^{2+}), nickel (Ni^{2+}), copper (Cu^{2+}), and zinc (Zn^{2+}) (Dowding and Fey, 2007). Yet another of these properties is their ability to function as an oxidant, which causes them to oxidize contaminants such as Cr(III) to its more toxic form, chromium (Cr) (VI), arsenic (As) (III) to As(V), and selenium (Se) (IV) to Se(VI) (Vodyanitskii et al., 2004).

j. Mn(III,IV)(hydr)oxides in soils: Biogenic Mn(III,IV)(hydr)oxides

In both soil and marine environments microorganisms govern nutrient cycling. Bacteria and fungi have been identified in various environments which oxidize Mn(II) and create Mn(III,IV)(hydr)oxides. These biogenic oxides generally have smaller crystal sizes than their abiotic counterparts, although crystal sizes are variable depending on growth conditions, and due to the associated increase in surface area are considered more reactive (Santelli et al., 2011). A study of Mn(III,IV)(hydr)oxides produced by the marine *Bacillus sp.* strain SG-1 found that the bio-oxides were layer-structured and had average Mn oxidation states between 3.7 and 4.0 (Webb et al., 2005b). It was proposed that the bacterium oxidized Mn(II) to create an initial Mn(III,IV)(hydr)oxide similar to amorphous δ-MnO_2 which was rapidly transformed to hexagonal Ca-birnessite then to triclinic Ca-birnessite (Webb et al., 2005b). Villalobos et al. (2006) determined that the bacterium *Pseudomonas putida* strain MnB1 produced a Mn(III,IV)(hydr)oxide structurally related to H-bearing birnessite but with Mn(IV) in the octahedral layer, which is a characteristic of δ-MnO_2. A later study of *Pseudomonas putida* strain GB-1 proposed that the bacterium first produced a hexagonal Mn(III,IV)(hydr)oxide, which was recrystallized to a triclinic phyllomanganate, which was ultimately transformed to todorokite during refluxing (Feng et al., 2010). This could potentially be a significant source of todorokite in soils.

The fungus *Acremonium* KR21-2 was determined to oxidize Mn(II) to a tunnel-structured oxide similar to todorokite (Saratovsky et al., 2009). Mn(II) oxidation by fungi was also proven to occur much slower (7-10 days) than Mn(II) oxidation by bacteria (6-12 hours) (Saratovsky et al., 2009). Initial growth products of Mn(II)-oxidizing fungi,

specifically *Plectosphaerella cucumerina* strain DS2psM2a2, *Pyrenochaeta* sp. DS3sAY3a, *Stagonospora* sp. SRC11sM3a, and *Acremonium strictum* strain DS1bioAY4a, have been identified as δ-MnO_2, but, depending on growth conditions, the Mn(III,IV)(hydr)oxides evolve over time to secondary birnessite, or todorokite (Santelli et al., 2011). As with biogenic reduction of Cr(VI), discussed above, different species of Mn(II) oxidizers likely utilize different pathways of Mn(II) oxidation, including different enzymes, extracellular polymers, and production of reactive oxygen species during cell differentiation, resulting in a variety of different Mn(III,IV)(hydr)oxide structures (Santelli et al., 2011).

k. Analytical methods for identifying the crystal structure of Mn(III,IV)(hydr)oxides

The majority of soil Mn(III,IV)(hydr)oxides are fine-grained and poorly crystalline, and they usually occur in much lower concentrations than Fe(III)(hydr)oxides. These factors make crystal structure analysis by X-ray diffraction unrealistic in most cases, as the diagnostic peaks are generally weak and tend to overlap with layer silicates (Dixon and White, 2002). Infrared (IR) spectroscopy techniques can be used along with X-ray diffraction to identify Mn(III,IV)(hydr)oxides due to the sensitivity of IR spectroscopy to amorphous materials (McKenzie, 1989). Transmission electron microscopy (TEM) can also be used to identify Mn(III,IV)(hydr)oxides (Post, 1999).

X-ray absorption near-edge structure (XANES) spectroscopy can be used to determine the oxidation state of Mn(III,IV)(hydr)oxides in soils. Regardless of the oxidation state, Mn has an absorption edge at 6539 eV. However, Mn^{2+} has a distinctive

peak at 6552.6 eV and Mn^{4+} has a distinctive peak at 6560.9 eV, allowing for quantitative analysis of Mn oxidation state (Schulze et al., 1995). Extended x-ray absorption fine structure (EXAFS) spectroscopy is commonly used to identify specific Mn(III,IV)(hydr)oxides. Features at 6.8, 8.0, and 9.3 $Å^{-1}$ allow for differentiation between tunnel-structures and layer-structures and analysis of the first shell Mn-O and second shell Mn-Mn distances allows for more specific differentiation between Mn(III,IV)(hydr)oxides (Webb et al., 2005b). Both of these x-ray absorption spectroscopy (XAS) techniques are conducted using a synchrotron as the x-ray source. The synchrotron itself is an electron accelerator that is usually connected to a high-vacuum magnetic storage ring, through which electrons circle. The radiation produced by the electrons is diverted to multiple beamlines with crystal monochromators and mirrors, where samples are placed in the radiation's path. Detectors measure diffraction and scattering from the sample. The raw absorption data collected must be averaged, energy calibrated, dead-time corrected, background subtracted, deglitched and Fourier transformed before analysis (Webb, 2005).

II. Gaps in the Knowledge: Soil Interfaces

Soil interfaces, including those defined by horizons, the rhizosphere, waste disposal sites and at the vadose-saturated zone boundary are a relatively new focus in soils research, especially in terms of oxidation-reduction properties. While the rhizosphere and the soil-water interface have been studied to some extent in the past several decades, studies of soil interfaces including those between horizons, those created by mixed oxides, and those created by waste disposal have been almost nonexistent.

From the few published studies on oxide surface properties and interfacial interactions, we know that metal (Pb and Co) interactions at chromium oxide (Cr_2O_3) – metal oxide interfaces involve oxidation and reduction transformations, creating heterogeneous interfaces (Cheng et al., 2002). Sorption of Fe(II) to Fe(III) oxides and Fe(III)-bearing clay minerals facilitates an interfacial electron transfer, reducing structural Fe(III) and oxidizing sorbed Fe(II) (Schaefer et al., 2011). Reactions at the solid-water interface determine the bioavailabilty and toxicity of chromium through sorption and redox reactions (Fendorf, 1995), so despite this lack of research, understanding these interfaces and their redox properties is essential to the complete understanding of chromium, or other heavy metal, remediation practices.

III. Rationale

To begin to address the significant lack of understanding of soil interfaces, Chapter 2, titled "Chromium Oxidation-Reduction Chemistry at Soil Horizon Interfaces Defined by Iron and Manganese Oxides", will examine the interfaces between soil horizons with regard to Cr(III) oxidation and Cr(VI) reduction. The key question to be addressed was: how does oxidation-reduction of Cr change in mineralogically different soil horizons as affected by various types of interfacial conditions (e.g. defined by pH, Eh, organic matter content, and Fe(III) and Mn(III,IV) (hydr)oxide mineral content)? The working hypothesis for this question was that soil horizon interfaces would have a significant effect on Cr(III) oxidation and Cr(VI) reduction which would not be directly attributable to quantifiable physical characteristics such as pH, Eh, organic matter content, or Fe(III) and Mn(III,IV) (hydr)oxide content.

A second study, detailed in Chapter 3, titled "Surface Spectroscopic Analysis of Fe(III) and Manganese(III,IV) (Hydr)oxide-Chromium Interactions in Synthetic, Fungal, and Soil Systems", will focus on comparing structural differences between various types of Fe(III) and Mn(III,IV) (hydr)oxides before and after Cr oxidation and reduction. There has been a recent surge in Mn(III,IV)(hydr)oxide structural studies coinciding with the development of spectroscopic techniques capable of analyzing the paracrystalline oxides, however very little research has been published regarding structural effects of oxidation and reduction. The key questions for this study were: 1) how are Fe(III) and Mn(III,IV) (hydr)oxides from different origins (e.g. synthetic, soil, and fungal oxides) structurally different from each other? and 2) how does the structure of Fe(III) and Mn(III,IV) (hydr)oxides with different origins change as a result of oxidation or reduction of Cr? The working hypotheses were that the oxides would have different mineralogy depending on their origin and that Mn(III,IV)(hydr)oxide structures would change dramatically as a result of oxidation of Cr and reduction of Mn, but that Fe(III)(hydr)oxides would not change drastically due to their decreased direct involvement in Cr oxidation or reduction. Chapters 2 and 3 will be presented as individual manuscripts, which will be submitted for publication. The final chapter details overall thoughts and conclusions in a summary chapter, with relevant appendices following.

CHAPTER 2

CHROMIUM OXIDATION-REDUCTION CHEMISTRY AT SOIL HORIZON INTERFACES DEFINED BY IRON AND MANGANESE OXIDES

Introduction

Chromium exists in the environment in multiple oxidation states, the most common and stable of which are the trivalent and hexavalent states. Hexavalent chromium (Cr(VI)) is carcinogenic, is highly toxic when ingested or inhaled, and can cause skin burns upon dermal contact (Fendorf et al., 2000). In soils, most forms of Cr(VI) are highly soluble, increasing the possibility of Cr(VI) leaching into the groundwater, where it could become a problem for drinking water (Bartlett, 1991). Trivalent chromium (Cr(III)), on the other hand, is an essential micronutrient for human health, and does not pose any of the health risks listed above unless ingested in extremely high quantities (Anderson, 1997). Unlike Cr(VI), Cr(III) is insoluble in under most soil conditions, and therefore is not a water quality concern (Kozuh et al., 1999).

The difference between Cr(III) and Cr(VI) is the number of electrons each oxidation state possesses, making the transformation between the two forms redox-based. Trivalent Cr can lose electrons and oxidize to form Cr(VI), while Cr(VI) can gain electrons and reduce to form Cr(III). The forms of Cr present in soils are governed by soil conditions, including factors such as pH, Eh (redox potential), organic matter, sesquioxide minerals, and clay content. While Cr has been demonstrated to be an element of concern, as described above, it is also an instructive element for studying oxidation-reduction properties in soils. While most forms of Cr(VI) are soluble, Cr(III) solubility depends largely on pH. In near-neutral pHs, Cr(III) commonly precipitates out of solution

as $Cr(OH)_3$ or Cr_2O_3, while soluble forms such as $Cr(OH)_2^+$, $CrOH^{2+}$, and Cr^{3+} are possible in increasingly more acidic pH environments (Cifuentes et al., 1996). Chromium (III) can also form complexes with organic carbon (C) compounds in soils and remain soluble even at circumneutral pHs (Yang et al., 2014). Both Cr(III) and Cr(VI) have the potential to sorb to the soil surface, although Cr(III) adsorption is more common due to its cationic nature and the fact that soil particles are generally negatively charged (Choppala et al., 2013). Chromium (VI) adsorption can occur in low pH soils with high amounts of Fe(III)(hydr)oxides which, due to their pH-dependent charge, can be positively charged at low pHs (Jardine et al., 2013). Many of the proposed mechanisms for Cr oxidation, reduction, and precipitated suggest mediation by soil or oxide surfaces, demonstrating the importance of sorption to ion cycling in soils (Loyaux-Lawniczak et al., 2001; Stewart et al., 2003; Trebien et al., 2011). Since Cr can exist as soluble ions or compounds in the soil solution, as sorbed ions on the soil surface, as soluble organic-Cr(III) complexes, or as precipitated compounds; quantitatively determining each of these fractions or species of Cr can isolate and identify key interfacial properties by illustrating sorption processes and sensitivity to redox differences temporally and spatially.

Many types of interfaces exist in soils, and none of these interfaces have been extensively researched. Interfaces can be created by water saturation, which can be affected by the percolation of water down the soil profile as a result of precipitation as well as the seepage of water up the soil profile as a result of capillary action (Hansen et al., 2011). Soil interfaces can also be created by the presence of plant roots, which can create oxidized or reduced zones around them depending on the soil conditions and the

plants' nutritional needs (Fageria and Stone, 2006). These interfaces are called the rhizosphere, and of the many types of soil interfaces, the rhizosphere is one of the most extensively studied. The disposal of waste can also create interfaces in soils by adding a layer of contaminated material on top of an existing soil profile, as well as by the infiltration into the soil profile of potentially hazardous contaminants such as heavy metals (Bahaa-eldin et al., 2011). Natural soil interfaces also exist as a result of the change between one horizon and the next. These interfaces can have variable pH, Eh, redox properties, and oxide mineralogy. Due to the heterogeneous nature of soils, many other types of interfaces may also exist on many different scales, highlighting the importance of studying them.

Iron (III) and Mn(III,IV) (hydr)oxides are prevalent in soils and, in large part, control Cr speciation in soils (Feng et al., 2007). For example, Fe(III)(hydr)oxides are capable of sorbing both Cr(III) and Cr(VI), Fe(II) is capable of reducing Cr(VI), and Mn(III,IV)(hydr)oxides are capable of oxidizing Cr(III) (Fendorf, 1995; Feng et al., 2007; Jung et al., 2007). As with all (hydr)oxides, they have pH-dependent charge, or the ability to be protonated and deprotonated. At pH values below the point of zero charge (PZC) the (hydr)oxide will be positively charged, while at pH values above the PZC the (hydr)oxide will be negatively charged, allowing for sorption of a wide variety of ions. These (hydr)oxides generally have high surface areas, so even when they are found in relatively low concentrations in soils they can have significant effects on ion sorption and cycling (Shaheen et al., 2013). Iron (III) and Mn(III,IV) (hydr)oxides are often found together in soils and can create interfaces within the soil matrix. In ferromanganese concretions, they generally layer in rings indicative of the redox state of the soil at the

time of each ring's formation (Gasparatos et al., 2005). In other soils, they are observed as coatings on soil particles within certain soil horizons. While these oxides exist with many different mineralogical properties depending on the surrounding environment, Fe(II,III)(hydr)oxides, as well as Mn(III,IV)(hydr)oxides can be studied with regard to Cr speciation to enhance the understanding of soil-mediated Cr oxidation, reduction, and sorption (Bartlett, 1991).

This study addresses the key question: how does oxidation-reduction of Cr change in mineralogically different soil horizons as affected by various types of interfacial conditions (e.g. defined by pH, Eh, organic matter content, and Fe(III) and Mn(III,IV) oxide mineral content)? To do this, soil horizon interfaces were simulated from a wide variety of sampled soil horizon materials, encompassing a range of Fe(III)(hydr)oxide, Mn(III,IV)(hydr)oxide, and organic C contents. These interfaces were leached with Cr(III) and Cr(VI) and the soil horizon materials were also individually leached with Cr(III) and Cr(VI) for comparison. Spectrophotometric analyses provided Cr speciation in terms of soluble, adsorbed, and insoluble Cr. The hypothesis for the study was that soil horizon interfaces would have a significant effect on Cr(III) oxidation and Cr(VI) reduction and that this effect would not be directly attributable to quantifiable physical characteristics such as pH, Eh, organic matter content, or Fe and Mn oxide content.

Methods

I. Soil characterization

Seven soils from the Coastal Plain and Piedmont regions of Maryland, U.S. were selected to sample for their varying properties which were capable of oxidizing Cr(III) or

reducing Cr(VI). Soil characterization data are summarized in Tables 2.1 and 2.2. Soils with high Fe content were selected because of the ability of Fe(II) to reduce Cr(VI) and the ability of Fe(III) (hydr)oxides to sorb Cr(III) and Cr(VI). Samples from the Russett-Christiana complex mapping unit (coordinates: 39.012820, -76.854011) were similar to the Russett series (fine-loamy, mixed, semiactive, mesic Aquic Hapludults), and were obtained for their high Fe(III) character. The Ap, AB, and Bt horizons were sampled on June 7, 2011. Samples from the Annapolis mapping unit (coordinates: 38.856533, -76.781593) were similar to the Collington series (fine-loamy, mixed, active, mesic Typic Hapludults), and were chosen for their glauconite (a phyllosilicate mineral which can contain small amounts of Fe(II) under certain conditions) content. The A, AB, and Bt horizons were sampled on June 9, 2011.

Soils with high Mn content were selected because of the ability of Mn(III,IV) (hydr)oxides to oxidize and sorb Cr(III). Samples from the Jackland mapping unit (coordinates: 39.165825, -77.319568) were similar to the Jackland series (fine, smectic, mesic Aquic Hapludalfs), and were chosen for their Mn(III,IV) nodules and their high montmorillonite clay content. The A/AB, Bt, and BC horizons were sampled on June 17, 2011. Samples from the Conestoga mapping unit (coordinates: 39.54805, -77.17803) were not similar to any known soil series, so they were designated ‘Flickinger’ after their location, as suggested by Bourgault (2008). These samples were desirable for our study of redox interfaces due to their unusually high Mn(III,IV)(hydr)oxide content. The Ap, AB, Bt1, and Bt2 horizons were sampled on November 14, 2011.

Soils with varying organic C content were also relevant to this study because of the ability of low molecular weight organic acids to reduce Cr(VI) and form soluble

complexes with Cr(III). Samples from the Askecksy mapping unit (coordinates: 38.214195, -75.522453) were consistent with the Atsion series (sandy, siliceous, mesic, Aeric Alaquods). The O/A, E, Bh, Bs, and C horizons were sampled on June 8, 2011. Samples from the Ingleside mapping unit (coordinates: 38.90295, -76.13712) were consistent with the Unicorn series (coarse-loamy, mixed, semiactive, mesic Typic Hapludults), and were selected for their low organic C content and similarity to typical Mid-Atlantic soils. The Ap, BA, and Bt horizons were sampled on June 7, 2011. Finally, samples from the Glenelg mapping unit (coordinates: 39.2618294, -76.9260483) were similar to the Glenelg series (fine-loamy, mixed, semiactive, mesic Typic Hapludults). They were also chosen for their relatively low organic C content and similarity to typical mid-Atlantic soils, and the A, Ap, Bt1, Bt2, Bt3, and BC horizons were sampled on November 14, 2011.

The soil horizon samples were collected when the matric water potentials were approximately -33 kPa, the standard potentials for "field capacity" moisture. Approximately 8-12 L of soil material were brought back to the lab to be stored field-moist (while remaining aerobic) following sieving through a 4-mm polyethylene screen. The field moist, aerobic soil conditions were maintained by double bagging each sieved soil horizon in 4-mil polyethylene bags, placing wet paper towels between bags, and storing them in closed 16 L polyethylene buckets with lids. The soils were not air-dried due to the severe and undesirable effects air-drying has on soil pH and Mn solubility (Bartlett and James, 1980; Perez et al., 2004).

For characterization purposes, each soil horizon's field-moist color and oven-dry color were determined using the Munsell color book, and water content was determined

by drying at 105°C for 24 h. Soil particle size distribution and textural class were determined by the pipette method (Gee and Bauder, 1986). Percent organic C and nitrogen (N) for each horizon were determined in triplicate on a LECO CHN analyzer. The "free" Fe(III) and Mn(III,IV) (hydr)oxide contents for each soil horizon were determined using citrate-bicarbonate-dithionite (CBD) extractions and flame atomic absorption spectroscopy (FAAS) analysis (Loeppert and Inskeep, 1996).

A Cr redox state assessment method was developed to quantify a soil's potential to reduce Cr(VI) or oxidize Cr(III) following field sampling. According to this procedure, the field moist equivalent of 2.00 g oven dry soil was added to six Oak Ridge-type 50-mL centrifuge tubes for each soil horizon. Ten milliliters of 0.01 M $CaCl_2$ were added to each replicate, and the centrifuge tubes were then capped and shaken for 1 h on a reciprocating shaker at 200 cycles per min. After centrifuging at 10,000 x *g* for 15 min, the salt pH (pH_s) and redox potential (Eh) values were measured in the supernatant liquids using pH and platinum (Pt) combination electrodes with Ag/AgCl reference electrodes. These measurements were taken at an ionic strength of 0.03 in 0.01 M $CaCl_2$ and at a soil:solution ratio of 1:5. The Pt electrode values were corrected to the standard hydrogen electrode (SHE) by adding 199 mV to the meter reading.

Next, 10 mL of 0.2 mM K_2CrO_4 (10.4 mg Cr(VI)/L) were added to three replicates per soil horizon and 10 mL of 0.2 mM $Cr(NO_3)_3$ (10.4 mg Cr(III)/L) were added to the other three, giving an initial concentration of 0.1 mM (5.2 mg Cr/L) and a soil:solution ratio of 1:10 in each replicate. Each centrifuge tube was capped and shaken for 30 min every hour for 12 h. After shaking, 0.2 mL of 1 M phosphate buffer (KH_2PO_4:K_2HPO_4 molar ratio = 1:1, pH 7.2) was added to each replicate to desorb

Cr(VI) (James and Bartlett, 1983b). The centrifuge tubes were capped and shaken for 1 h on a reciprocating shaker, then centrifuged as above.

After centrifugation, 1:5 dilutions of each supernatant liquid were made in glass test tubes with nanopure (18 MΩ) water. Five Cr(VI) standards were made up using concentrated stock K_2CrO_4 solution to span the range of 0.01 – 2.0 mg Cr(VI)/L. Each test tube was vortexed for 15 sec to thoroughly mix the dilution before adding 1.0 mL of 1,5-diphenylcarbazide reagent (DPC) (Bartlett and James, 1979), and continuing to vortex for another 15 seconds. After mixing, the test tubes were left for 15 min to allow completion of the diphenylcarbazide-Cr(VI) redox reaction and the development of the magenta color of the diphenylcarbazone-Cr(III) complex. Color formation occurred as the DPC reagent quantitatively reduced Cr(VI), and the oxidized form of DPC (diphenylcarbazone) immediately complexed the newly-reduced, unhydrated Cr^{3+} cations. DPC does not react with hydrated $Cr(H_2O)_6^{3+}$, and the kinetics of hydration of Cr^{3+} are extremely slow; therefore the colorimetric test quantifies Cr(VI) without interference from Cr(III) species.

The standards and samples were then analyzed colorimetrically on a flow-cell spectrophotometer at 540 nm, and Cr(VI) was quantified by comparison to the standards. Once the dilution was accounted for, Cr(VI) reduced by the soil was calculated by subtracting the Cr(VI) measured in the equilibrium supernatant liquids from the initial Cr(VI) added. Chromium (III) oxidized was calculated as the amount of Cr(VI) measured in the replicates to which Cr(III) was added.

II. Column leaching experiments

For the leaching experiments of simulated interfaces, two horizons, an A and a B horizon, were chosen for each of the 7 soils sampled. The O/A and Bh horizons were chosen for the Atsion soil, the A and Bt horizons were chosen for the Collington soil, the Ap and Bt horizons were selected for the Unicorn soil, the Ap and Bt2 horizons were chosen for the Flickinger soil, the Ap and Bt2 horizons were selected for the Glenelg soil, the A/AB and Bt horizons were chosen for the Jackland soil, and the Ap and Bt horizons were selected for the Russett soil.

The following column leaching experiments were completed in triplicate with 2.0 g of A horizon material to simulate the A horizon by itself, 2.0 g of B horizon material to simulate the B horizon by itself, and 2.0 g of A horizon material stacked on top of 2.0 g of B horizon material to simulate an interface between horizons (represented as A/B in graphs). A fourth experimental protocol consisted of collecting 20 mL of leachate from the A horizon material experiment and leaching that solution through 1.0 g of B horizon material to create a modified "pseudo"-interface where the two horizons were not in physical contact with one another (represented as A→B in graphs). The A/B and A→ treatment data was normalized to be directly comparable to the A and B treatments, even though different total amounts of soil were used.

For each column replicate, a soil:solution ratio of 1:10 was used and all treatments were run in triplicate. For each replicate, the field moist equivalent of 2.0 g of soil material from designated horizons were added in layers separated by plastic spacers in 50 mL syringe barrels. The barrels were placed in a Centurion® mechanical vacuum extractor (MVE). Chromium in the form of 40 mL of 0.05 mM $Cr(NO_3)_3$ (2.6 mg

Cr(III)/L) or 40 mL of 0.05 mM K_2CrO_4 (2.6 mg Cr(VI)/L) solutions were added to syringe tubes corresponding to the appropriate samples. These concentrations were chosen to be directly comparable to the Cr redox assessment batch experiments previously performed on the soil horizon materials. The Cr solutions were made up in 0.01 M KNO_3, a background electrolyte which established an ionic strength in the samples without adding reactive compounds, using concentrated 0.05 M $Cr(NO_3)_3$ and K_2CrO_4 stock solutions, which were created by diluting $Cr(NO_3)_3$ and K_2CrO_4 salts in 0.01 M KNO_3. The flow rate on the MVE was set to 3.03 mL/hr (~13 hours for 40 mL). The replicate leachates were collected in syringe tubes below the soil material and were centrifuged at 25,000 x *g* for 20 min.

Following centrifugation, pH and Eh measurements were taken and 8 mL of centrifuged leachate were added to glass test tubes for total soluble Cr analysis in the centrifuged leachates by FAAS using an air-C_2H_2 flame. These samples were not diluted so the Cr concentrations would be high enough for accurate detection, but were transferred to test tubes to reduce the chance of colloidal re-suspension in the process of transporting the samples. Five Cr(VI) standards spanning from 0.1 to 3 mg Cr/L were created from concentrated stock K_2CrO_4 solutions made up with a background electrolyte of 0.01 M KNO_3. An extensive test of different background solutions, including KNO_3 and nanopure water for FAAS demonstrated the necessity of using the same background electrolyte for the standards as the samples in order for accurate measurements. It was determined that there was no difference between using soluble Cr(III) or soluble Cr(VI) for the standards (data not shown). A blank containing 0.01 M KNO_3 was also created. Additionally, approximately 8 mL of the remaining 0.05 mM $Cr(NO_3)_3$ and K_2CrO_4

solutions that were used for the column leaching experiments were added to test tubes to be analyzed for the concentration of total chromium added and to ensure that Cr remained soluble over time in each solution. Each sample and standard were analyzed for Cr using FAAS. The sample readings were compared to a standard curve to quantify total soluble Cr.

Next, 1:5 dilutions of the centrifuged leachates were made by diluting 2 mL of sample to 10 mL using nanopure H_2O (testing of both nanopure H_2O and 0.01 M KNO_3 backgrounds showed that there was no matrix effect for this method) in test tubes. Additionally, 2 mL of the 0.05 mM $Cr(NO_3)_3$ and K_2CrO_4 solutions were diluted to 10 mL with nanopure H_2O in order to calculate the concentration of added Cr(VI). These samples were analyzed for soluble Cr(VI) by the DPC method, as described above. Once total soluble Cr and soluble Cr(VI) (described below) were measured, soluble Cr(III) was calculated by subtracting soluble Cr(VI) (DPC method) from total soluble Cr (FAAS).

To quantify sorbed Cr(VI), the phosphate buffer solution described above was used to desorb Cr(VI) from the soil materials. To account for residual soluble Cr(VI) in the wet soil materials, the syringe tubes containing soil material were weighed following the original leaching. The difference between the post-leaching mass and the pre-leaching mass can be attributed to Cr solution, the soluble Cr(VI) concentration of which was calculated using the DPC method described above. This amount of soluble Cr(VI) remaining was subtracted from the measured Cr(VI) concentration to give an accurate adsorbed Cr(VI) concentration.

Once the residual solution was accounted for, 40 mL of 0.01 M phosphate buffer (made up using a 1:1 molar ratio of K_2HPO_4 to KH_2PO_4 in nanopure H_2O) was added to

each MVE tube. The MVE was set to the same flow rate as the original leaching and the leachates were collected and centrifuged at 25,000 x *g* for 20 minutes. To quantify adsorbed Cr(VI), 1:5 dilutions of the centrifuged leachates were made in test tubes with nanopure H_2O, and the same seven Cr(VI) standards and blank discussed above were created. The same DPC procedure and spectrophotometric analysis as described above was performed. The adsorbed Cr(VI) was quantified by comparing the sample absorbances to a standard curve. Once the adsorbed Cr(VI) was calculated, insoluble (sorbed/precipitated) Cr(III) was calculated by subtracting the measured soluble Cr(VI), soluble Cr(III), and sorbed Cr(VI) from the concentration of Cr added in the original solution (James and Bartlett, 1983a).

The net Cr(III) oxidized was calculated by dividing the total measured Cr(VI), including both soluble and adsorbed forms, by the total amount of Cr(III) added. The net Cr(III) oxidized represents the amount of oxidation measurable at the end of the experiment. Although newly oxidized Cr(VI) could potentially be reduced back to Cr(III) over the course of the experiment, there is no way to feasibly quantify it. Similarly, net Cr(VI) reduced was calculated by subtracting the total measured Cr(VI) from the total amount of Cr(VI) added to get the total amount of Cr(III), including both soluble and insoluble forms, then dividing by the total amount of Cr(VI) added. While re-oxidation of newly-reduced Cr(III) is possible, quantification of this was impractical, so net Cr(VI) reduction was presented. Ordinary one-way ANOVA multiple comparison tests were performed on the net Cr(III) oxidized and net Cr(VI) reduced data, with statistical significance given to p values less than 0.05.

Results and Discussion

I. Coastal Plain and Piedmont Soils from Maryland, USA

When Cr(III) was added to the the Unicorn soil Ap and Bt horizon soil materials, almost no Cr oxidation occurred (Fig. 2.1(i)). The scale of Fig. 2.1(iii) illustrates this fact, as the Bt horizon, which oxidized the most Cr(III) ($p \leq 0.0005$), only oxidized approximately 2% of the added Cr. This lack of oxidation was expected due to the low concentrations of Mn in the soil (0.03-0.06 g/kg, Table 2.1). When Cr(VI) was added, shown in Fig. 2.1(ii), the Ap treatment reduced the least amount of Cr ($p \leq 0.03$): less than 4% (Fig. 2.1(iv)). The Ap horizon soil material contained more organic C (3.1 g/kg) and less CBD extractable Fe (3.3 g/kg) than the Bt horizon soil material (1.0 g/kg organic C and 13.7 g/kg CBD Fe) (Table 2.1). The Cr redox assessment indicated that this soil horizon material had the potential to reduce 0.14 mmol of Cr(VI) per kg, or 14% of the Cr(VI) added, in the same amount of time (Table 2.1). This indicates that the shorter contact time facilitated by leaching instead of shaking is not sufficient for the maximum amount of Cr(VI) reduction possible, which suggests that the reduction reaction may be occurring slightly slower than the leaching rate allows for. The Ap soil horizon treatment was also the only treatment that did not adsorb Cr(VI). This was likely due to the higher sand content in this soil (loamy sand vs. silt loam, Table 2.1).

The Bt and Ap→Bt treatments reduced the same amount of Cr(VI) (not significant at $p \leq 0.05$). The increase in reduction from the Ap treatment was likely due to the higher Fe content of the Bt horizon soil material, suggesting that the Fe present in the Bt horizon could be acting as an electron shuttle to make Cr(VI) reduction by organic C more efficient (Brose and James, 2010). The Bt horizon soil material had the potential to

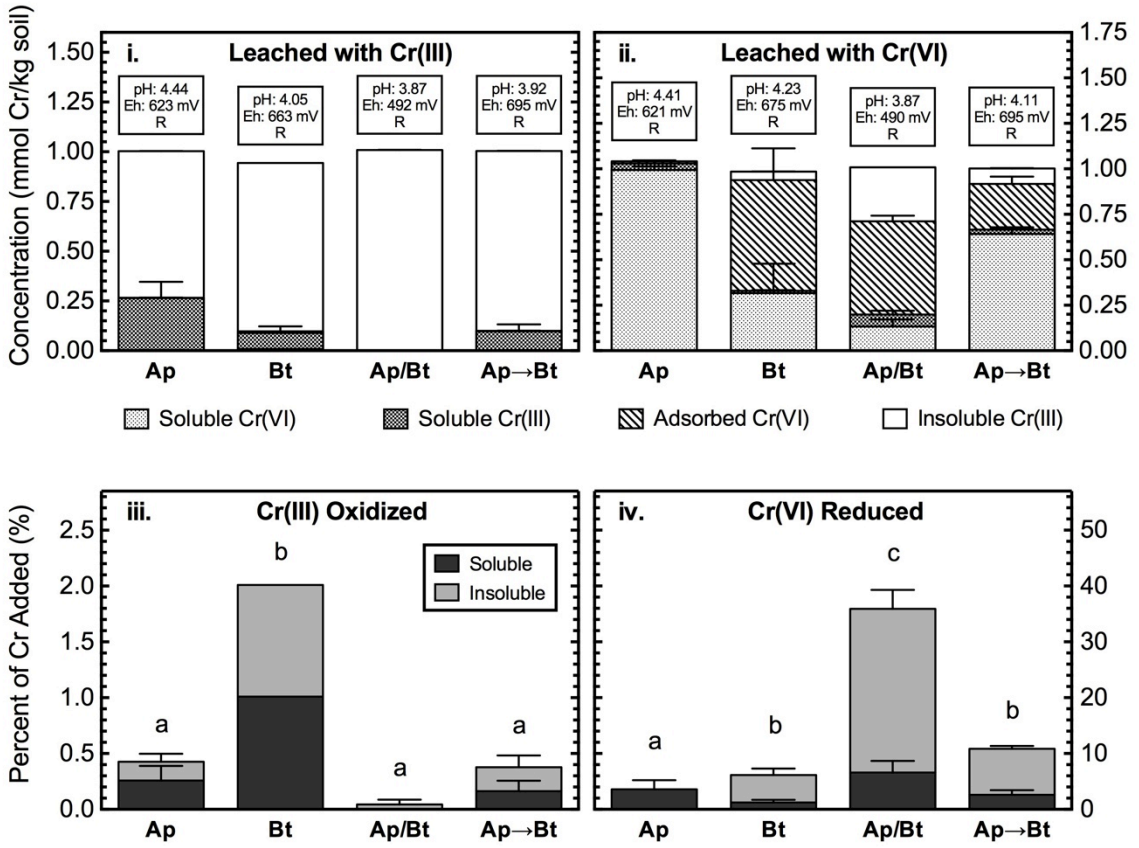

Figure 2.1 Chromium Speciation in Unicorn soil Ap and Bt horizons. Unicorn soil Ap and Bt horizons leached with **i.** soluble Cr(III) in the form of $Cr(NO_3)_3$ and **ii.** soluble Cr(VI) in the form of K_2CrO_4, where Ap is the Ap horizon alone, Bt is the Bt horizon alone, Ap/Bt is the Ap horizon on top of the Bt horizon, and Ap→Bt is the leachate from the Ap horizon alone leached through the Bt horizon alone. Potentiometric values reported above each bar, where O is reported when the combined Eh and pH values fall in the oxidizing zone of an Eh-pH plot for chromium species and R is reported when the combined Eh and pH values fall in the reducing zone of an Eh-pH plot for chromium species. Ordinary one-way ANOVA multiple comparison analysis of **iii.** total percent Cr(III) oxidized and **iv.** total percent Cr(VI) reduced using $p \leq 0.05$.

Table 2.1 Soil characterization data (continued on next page). Soil texture was determined by the particle size analysis method, color was determined using a Munsell® color book, pH_s was measured in a 1:10 soil:solution ratio with 0.01 M $CaCl_2$, and organic C was measured by a LECO® C-H-N analyzer. CBD Fe and Mn were determined by citrate-bicarbonate-dithionite extraction and Cr oxidized and reduced were measured using a procedure detailed in the methods section above.

Soil Horizon	Soil Texture (% sand, silt, clay)	Moist Color	pH_s	Eh (mV)	H_2O Content	Organic C	CBD Fe	CBD Mn	Cr Oxidized	Cr Reduced
					(g/kg)				(mmol/kg)	
Unicorn Ap	Loamy sand (74.8, 21.1, 4.1)	10YR 4/4	4.00	490	44	3.1	3.31	0.03	0.001	0.144
Unicorn Bt	Silt loam (29.8, 51.6, 18.6)	10YR 4/6	3.89	500	160	1.0	13.7	0.056	0.000	0.191
Glenelg Ap	Loam (36.6, 49.9, 13.5)	10YR 5/4	5.09	435	128	7.0	8.98	0.12	0.263	0.069
Glenelg Bt2	Clay loam (41.1, 25.3, 33.6)	7.5YR 4/6	5.69	422	225	1.2	27.3	0.062	0.006	0.089
Atsion O/A	NA*	5YR 2.5/1	2.39	530	170	116.8	0.42	0.003	0.000	1.00
Atsion Bh	Sand (88.0, 10.0, 2.0)	5YR 2.5/1	3.55	477	304	44.4	0.16	0.001	0.000	0.412

* NA: this value was unable to be determined due to the highly organic nature of the soil material.

Table 2.2 Soil characterization data (continued). Soil texture was determined by the particle size analysis method, color was determined using a Munsell® color book, pH_s was measured in a 1:10 soil:solution ratio with 0.01 M $CaCl_2$, and organic C was measured by a LECO® C-H-N analyzer. CBD Fe and Mn were determined by citrate-bicarbonate-dithionite extraction and Cr oxidized and reduced were measured using a procedure detailed in the methods section above.

Soil Horizon	Soil Texture (% sand, silt, clay)	Moist Color	pH_s	Eh (mV)	H_2O Content	Organic C	CBD Fe	CBD Mn	Cr Oxidized	Cr Reduced
					(g/kg)				(mmol/kg)	
Collington A	Loamy sand (83.2, 13.7, 3.1)	10YR 3/2	3.08	606	120	36.8	5.24	0.008	0.000	0.754
Collington Bt	Sandy clay loam (70.6, 5.0, 24.4)	10YR 3/6	3.37	607	200	1.7	24.3	0.035	0.000	0.244
Russett Ap	Sandy loam (57.6, 36.6, 5.8)	10YR 4/3	4.26	577	82	25.3	6.51	0.23	0.073	0.379
Russett Bt	Loam (40.4, 41.6, 18.0)	10YR 5/8	3.77	540	132	1.4	18.7	0.01	0.000	0.162
Jackland A/AB	Silt loam (34.5, 56.6, 8.9)	10YR 3/6	4.86	470	125	9.0	13.4	1.10	0.454	0.206
Jackland Bt	Clay loam (29.9, 36.7, 33.4)	10YR 5/6	5.14	460	229	4.0	18.5	0.96	0.490	0.164
Flickinger Ap	Loam (43.1, 47.1, 9.8)	10YR 3/3	6.46	397	212	30.0	13.1	1.66	0.540	0.105
Flickinger Bt2	Clay (28.5, 27.1, 44.4)	10YR 2/1	6.51	406	414	2.0	29.1	11.6	0.725	0.148

reduce 0.19 mmol of Cr(VI) per kg (Table 2.1), or 19% of the Cr(VI) added, but only reduced around 6% (Fig. 2.1(iv)), indicating, as above, that the contact time was insufficient for complete reduction to occur. The Ap/Bt interfacial treatment reduced 37% of the Cr(VI) added, which was over 20% more Cr(VI) than any other treatment ($p < 0.0001$) (Fig. 2.1(iv)). The amount of reduction observed was well above the potential Cr(VI) reduction for either horizon, which indicates that something is occurring across the interface to enhance Cr(VI) reduction. The increased reduction was not seen in the Ap→Bt "pseudo"-interfacial treatment, which suggests that the process may be dependent on the physical interaction of the two horizons, or, more specifically, the physical interaction of Fe(III)(hydr)oxides and organic C.

The Glenelg Ap horizon soil material contained 0.116 g/kg CBD extractable Mn, which is significantly higher than the amount of Mn detected in the previously discussed soil horizons (0.001 – 0.062 g/kg) (Table 2.1). This explains why more Cr(III) oxidation was observed than in the previous experiments (Fig. 2.2(i)). Even though there was no significant difference in Cr(III) oxidation across the four treatments (not significant at $p \leq 0.05$), those containing Ap horizon soil material oxidized 10% of the added Cr(III), while the Bt2 treatment, consistent with the Unicorn Bt treatment, only oxidized 2.3% of the added Cr(III) (Fig. 2.2(iii)).

When the Glenelg Ap and Bt2 horizon soil materials were leached with Cr(VI) (Fig. 2.2(ii)), the Ap, Bt2, and Ap→Bt2 treatments reduced less than 10% of the added Cr, which is consistent with the Cr(VI) reduction potential of the soil materials (Ap: 7% and Bt2: 9%, Table 2.1). The interfacial Ap/Bt2 treatment, however, reduced significantly more Cr(VI) ($p \leq 0.0003$): around 35% (Fig. 2.2(iv)). This supports the

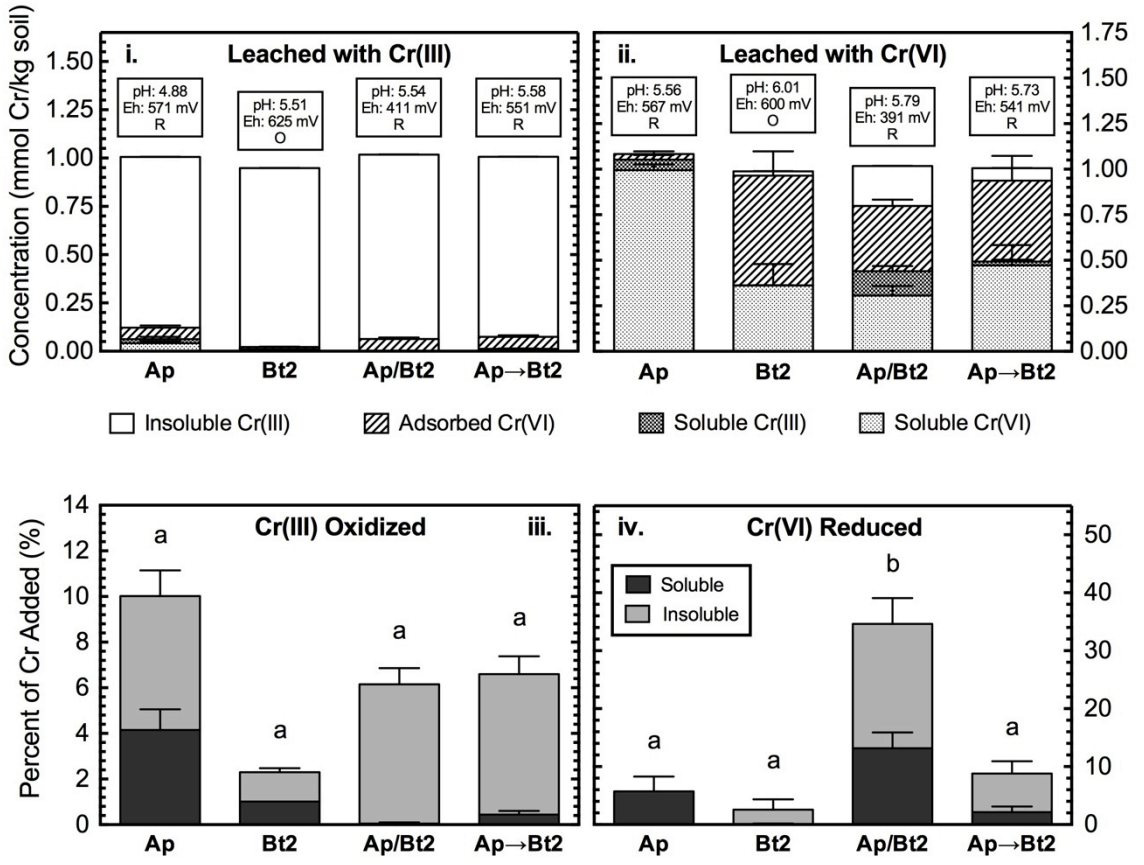

Figure 2.2 Chromium speciation in Glenelg soil Ap and Bt2 horizons. Glenelg soil Ap and Bt2 horizons leached with **i.** soluble Cr(III) in the form of $Cr(NO_3)_3$ and **ii.** soluble Cr(VI) in the form of K_2CrO_4, where Ap is the Ap horizon alone, Bt2 is the Bt2 horizon alone, Ap/Bt2 is the Ap horizon on top of the Bt2 horizon, and Ap→Bt2 is the leachate from the Ap horizon alone leached through the Bt2 horizon alone. Potentiometric values reported above each bar, where O is reported when the combined Eh and pH values fall in the oxidizing zone of an Eh-pH plot for chromium species and R is reported when the combined Eh and pH values fall in the reducing zone of an Eh-pH plot for chromium species. Ordinary one-way ANOVA multiple comparison analysis of **iii.** total percent Cr(III) oxidized and **iv.** total percent Cr(VI) reduced using $p \leq 0.05$.

evidence from the Unicorn experiment for the existence of an interfacial process which is enhancing Cr(VI) reduction.

As a Spodosol, the Atsion soil had many properties uncharacteristic of the other soils studied. The O/A horizon contained 117 g/kg organic C and the Bh horizon contained 44 g/kg organic C (Table 2.1). Both horizons contained significantly more C than any other soil horizon sampled, and in the Cr redox assessment the O/A horizon soil material reduced 100% of the added Cr(VI) while the Bh horizon soil material reduced 41% as a result of the high C content (Table 2.1). Very little oxidation was observed in the treatments with Cr(III) leached, and in those treatments nearly all of the Cr(III) was either adsorbed or precipitated (Fig. 2.3(i)). Figure 2.3(iii) shows a significant increase in the amount of Cr(III) oxidized by the Bh horizon compared to all of the other treatments ($p < 0.0001$); however, even the Bh horizon only oxidized around 2.2% of the added Cr(III), which is a very small amount. Due to the sandy nature of the Atsion soil horizons (Bh: 88% sand, Table 2.1) and the low surface area of sand, it is unlikely that much adsorption occurred. It is therefore more likely that the Cr(III) was precipitated. The pH values of the leachates from the Cr(III) soil treatments were between 3.37 and 3.88 (Fig. 2.3(i)), and were therefore too low for the precipitation of $Cr(OH)_3$, which occurs at or above pH 5.5 (Rai et al., 1987). Aluminum is known to inhibit surface-induced hydrolysis of Cr(III) at high pH values, and may be enhancing Cr(III) hydrolysis at lower pH values (Fendorf et al., 1993). Since Spodosols are known for their aluminum sesquioxide content, this is a plausible cause for the removal of Cr(III) from solution. In fact, a previous study from the same sampling location found 5.9 g/kg of ammonium-oxalate extractable Al in the Bh horizon (Condron, 1990).

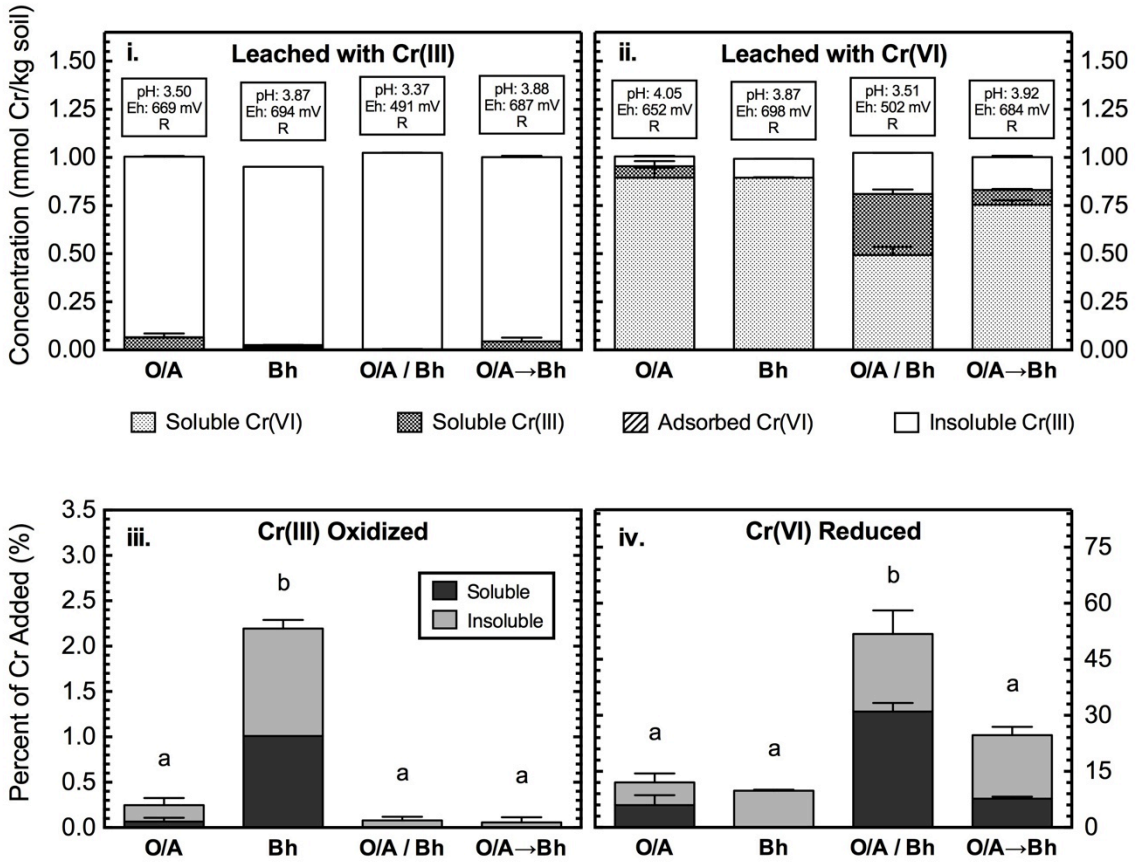

Figure 2.3 Chromium speciation in Atsion soil O/A and Bh horizons. Atsion soil O/A and Bh horizons leached with **i.** soluble Cr(III) in the form of $Cr(NO_3)_3$ and **ii.** soluble Cr(VI) in the form of K_2CrO_4, where O/A is the O/A horizon alone, Bh is the Bh horizon alone, O/A / Bh is the O/A horizon on top of the Bh horizon, and O/A→ Bh is the leachate from the O/A horizon alone leached through the Bh horizon alone. Potentiometric values reported above each bar, where O is reported when the combined Eh and pH values fall in the oxidizing zone of an Eh-pH plot for chromium species and R is reported when the combined Eh and pH values fall in the reducing zone of an Eh-pH plot for chromium species. Ordinary one-way ANOVA multiple comparison analysis of **iii.** total percent Cr(III) oxidized and **iv.** total percent Cr(VI) reduced using $p \leq 0.05$.

Contrary to what was expected from the Cr redox assessment and for a soil with such high organic C content, only a small amount of reduction was observed in the O/A, Bh and O/A→Bh treatments leached with Cr(VI) (Fig. 2.3(ii)). This was likely due to a combination of decreased contact time and complexation of organic C with Al, which renders the organic C less chemically reactive. The O/A / Bh interfacial treatment reduced around 54% of the added Cr(VI), which was significantly more than the other treatments ($p \leq 0.007$) (Fig. 2.3(iv)), indicating the occurrence of an interfacial process enhancing the reduction of Cr(VI). Similar to the Unicorn and Glenelg soil experiments described above, this significant increase in Cr(VI) reduction seems to be dependent on the physical interaction of the soil horizons.

II. Soils with High Fe(III)(hydr)oxide Contents

The Collington soil is known to contain glauconite, a mineral which contains structural Fe(II) under certain conditions. Since Fe(II) is a known reducing agent for Cr(VI), greater amounts of Cr(VI) reduction were expected than in similar non-glauconitic soils. This expectation was reaffirmed by the Cr redox assessment, according to which the A horizon material could potentially reduce 75% of the added Cr(VI) and the Bt horizon material could potentially reduce 24% of the added Cr(VI) (Table 2.2). However, as evidenced in Figs. 2.1(iv), 2.2(iv), and 2.4(iv), similar amounts of Cr(VI) reduction were observed in the Unicorn, Glenelg, and Collington soils. The most likely reasons for the lack of increased Cr(VI) reduction were the reduced contact time caused by leaching and the fact that the soil was aerated and therefore contained much less structural Fe(II) than an anaerobic glauconitic soil would (Fanning et al., 1989). The Collington A horizon soil material reduced less Cr(VI) than the A→Bt "pseudo"-

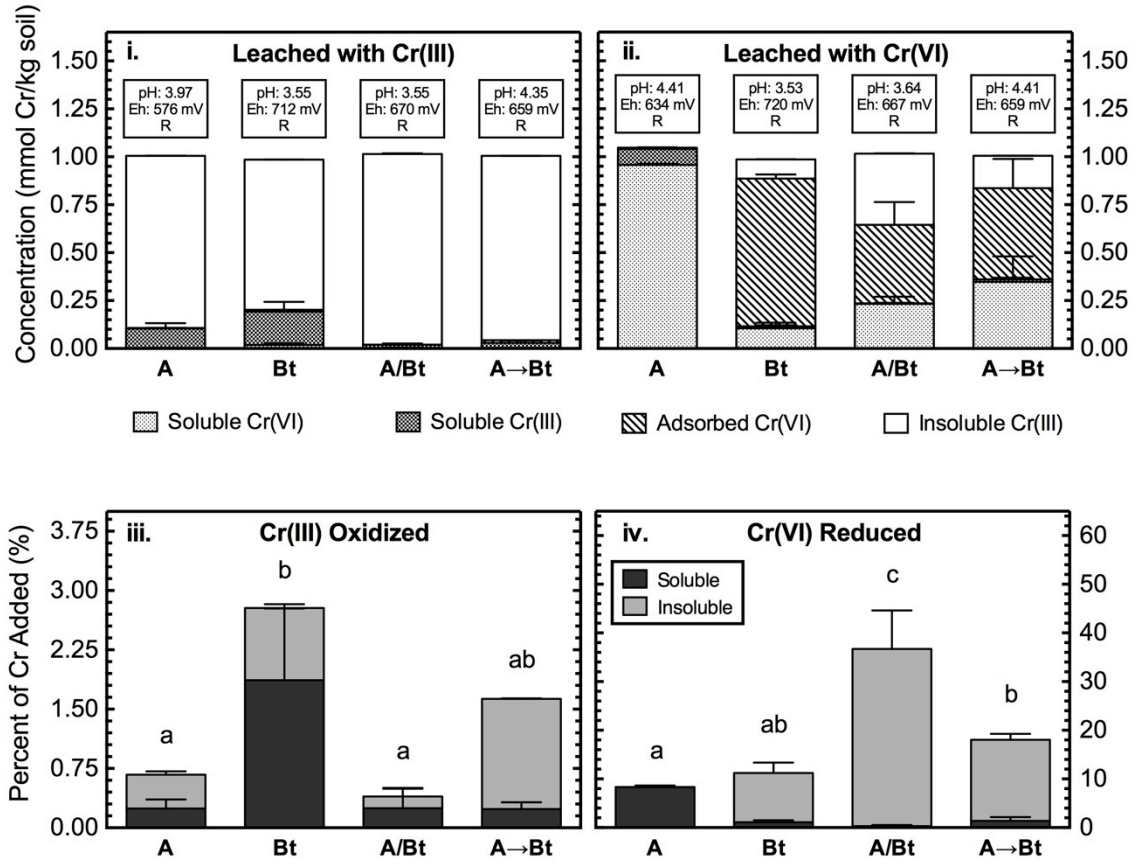

Figure 2.4 Chromium speciation in Collington soil A and Bt horizons. Collington soil A and Bt horizons leached with **i.** soluble Cr(III) in the form of $Cr(NO_3)_3$ and **ii.** soluble Cr(VI) in the form of K_2CrO_4, where A is the A horizon alone, Bt is the Bt horizon alone, A/Bt is the A horizon on top of the Bt horizon, and A→Bt is the leachate from the A horizon alone leached through the Bt horizon alone. Potentiometric values reported above each bar, where O is reported when the combined Eh and pH values fall in the oxidizing zone of an Eh-pH plot for chromium species and R is reported when the combined Eh and pH values fall in the reducing zone of an Eh-pH plot for chromium species. Ordinary one-way ANOVA multiple comparison analysis of **iii.** total percent Cr(III) oxidized and **iv.** total percent Cr(VI) reduced using $p \leq 0.05$.

interfacial treatment ($p = 0.04$) and didn't adsorb any Cr(VI) (Fig. 2.4(ii)). This was likely due to the coarser texture (31 g/kg clay) and lower concentration of CBD extractable Fe (5.2 g/kg) compared to the Bt horizon soil material (244 g/kg clay and 24.3 g/kg CBD Fe) (Table 2.2). The Bt treatment was not significantly different from the A or A→Bt treatment (not significant at $p \leq 0.05$) (Fig. 2.4(iv)). The interfacial A/Bt treatment reduced significantly more Cr(VI) than any other treatment ($p \leq 0.02$), indicating that an interfacial process is enhancing Cr(VI) reduction. No Cr(III) oxidation is visible in Fig. 2.4(i); however, due the small scale in Fig. 2.4(iii), differences in Cr(III) oxidized are visible. Although some of these differences were statistically significant, the low amounts of oxidation were approaching the detection limit for the method; therefore, any differences were likely not meaningful.

The Russett soil was notable for its high Fe(III)(hydr)oxide content, evident in the bright reddish orange color (Table 2.2) indicative of goethite and hematite (Soileau and McCracken, 1967). The Ap horizon had 6.5 g/kg Fe and 25.3 g/kg organic C while the Bt horizon had 18.7 g/kg Fe and 1.4 g/kg organic C (Table 2.2). Less than 1% of the Cr(III) added was oxidized by any of the treatments (Fig. 2.5(i) and 2.5(iii)), likely due to the low Mn(III,IV)(hydr)oxide content of both horizons (less than 0.23 g/kg, Table 2.2).

In the Ap, Bt, and Ap→Bt treatments leached with Cr(VI), a small amount of reduction was observed (6-10%, Figs. 2.5(ii) and 2.5(iv)). These numbers were well below the reduction potential of the materials (Ap: 38% and Bt: 16%, Table 2.2), indicating again that the contact time was not long enough for complete reduction to occur. The Bt treatment adsorbed more Cr(VI) than the Ap treatment, likely due to the

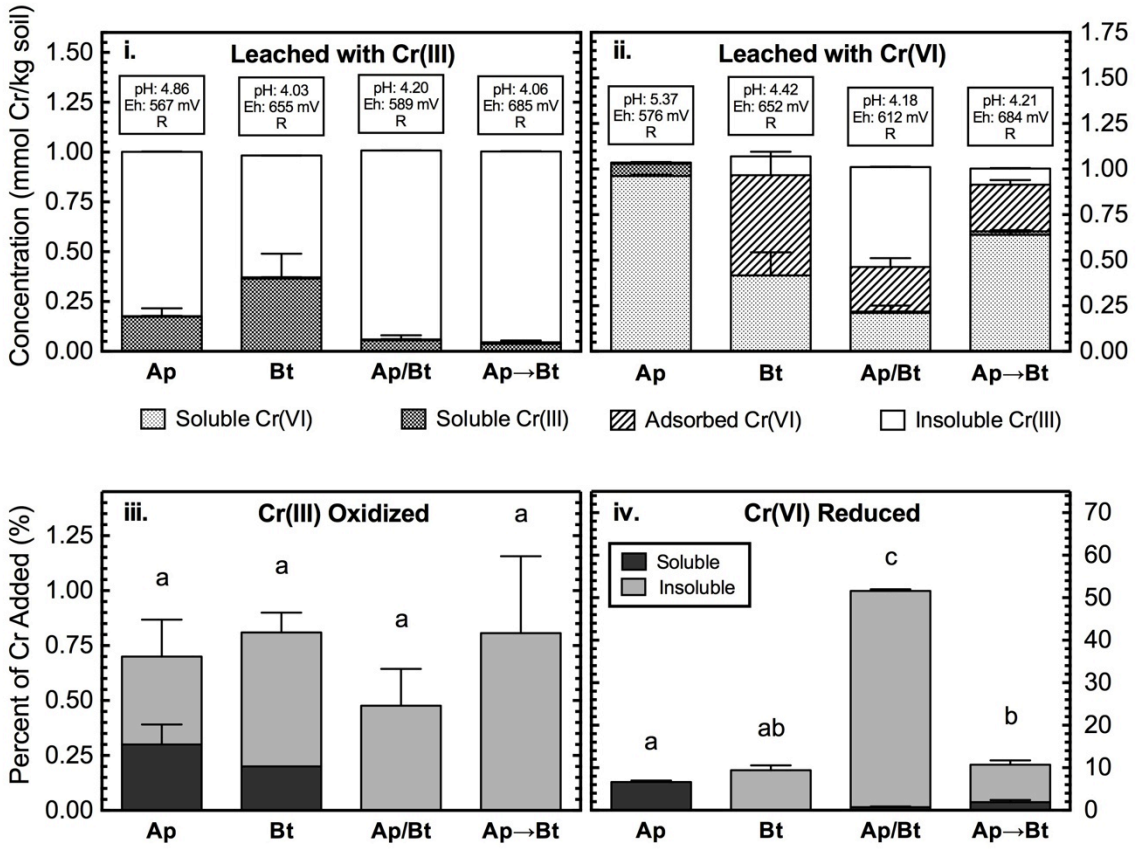

Figure 2.5 Chromium speciation in Russett soil Ap and Bt horizons. Russett soil Ap and Bt horizons leached with **i.** soluble Cr(III) in the form of $Cr(NO_3)_3$ and **ii.** soluble Cr(VI) in the form of K_2CrO_4, where Ap is the Ap horizon alone, Bt is the Bt horizon alone, Ap/Bt is the Ap horizon on top of the Bt horizon, and Ap→Bt is the leachate from the Ap horizon alone leached through the Bt horizon alone. Potentiometric values reported above each bar, where O is reported when the combined Eh and pH values fall in the oxidizing zone of an Eh-pH plot for chromium species and R is reported when the combined Eh and pH values fall in the reducing zone of an Eh-pH plot for chromium species. Ordinary one-way ANOVA multiple comparison analysis of **iii.** total percent Cr(III) oxidized and **iv.** total percent Cr(VI) reduced using $p \leq 0.05$.

increased amount of clay relative to the Ap horizon (180 g/kg clay compared to 58 g/kg, Table 2.2). The Ap/Bt interfacial treatment reduced significantly more Cr(VI) than any other treatment ($p < 0.0001$), including the Ap→Bt2 pseudo-interfacial treatment (Fig. 2.5(iv)), suggesting that an interfacial process relying on the physical interaction of two soil horizons might be assisting in the reduction of Cr.

III. Soils with High Mn(III,IV)(hydr)oxide Contents

The Jackland A/AB horizon soil material contained 1.1 g/kg CBD extractable Mn and the Bt horizon soil material contained 0.96 g/kg CBD extractable Mn (all previously discussed materials contained less than 0.23 g/kg CBD Mn) (Tables 2.1 and 2.2), so some oxidation of Cr(III) was expected. The Cr redox assessment indicated that the A/AB horizon material had the potential to oxidize 45% of the added Cr(III) and the Bt horizon material had the potential to oxidize 49% of the added Cr(III) (Table 2.2). Indeed, all of the treatments oxidized 16-20% of the added Cr(III), with no significant differences between treatments (not significant at $p \leq 0.05$) (Fig. 2.6(iii)). The decreased amount of Cr oxidation compared to the potentials was likely due to decreased contact time, similarly to what occurred with Cr reduction in the previously discussed soils. The lack of differences between the treatments was likely due to the similar Mn contents in the two soil horizon materials. The majority of the Cr(III) oxidized was adsorbed by the soil materials (Fig. 2.6(i)), likely due to the higher clay contents (A/AB: silt loam; Bt: clay loam, Table 2.2).

When Cr(VI) was leached, shown in Fig. 2.6(ii), the A/AB, Bt, and A/AB→Bt treatments exhibited the same amount of reduction (not significant at $p \leq 0.05$): around 10% (Fig. 2.1(iv)). Again, these numbers were well below the Cr(VI) reduction potentials

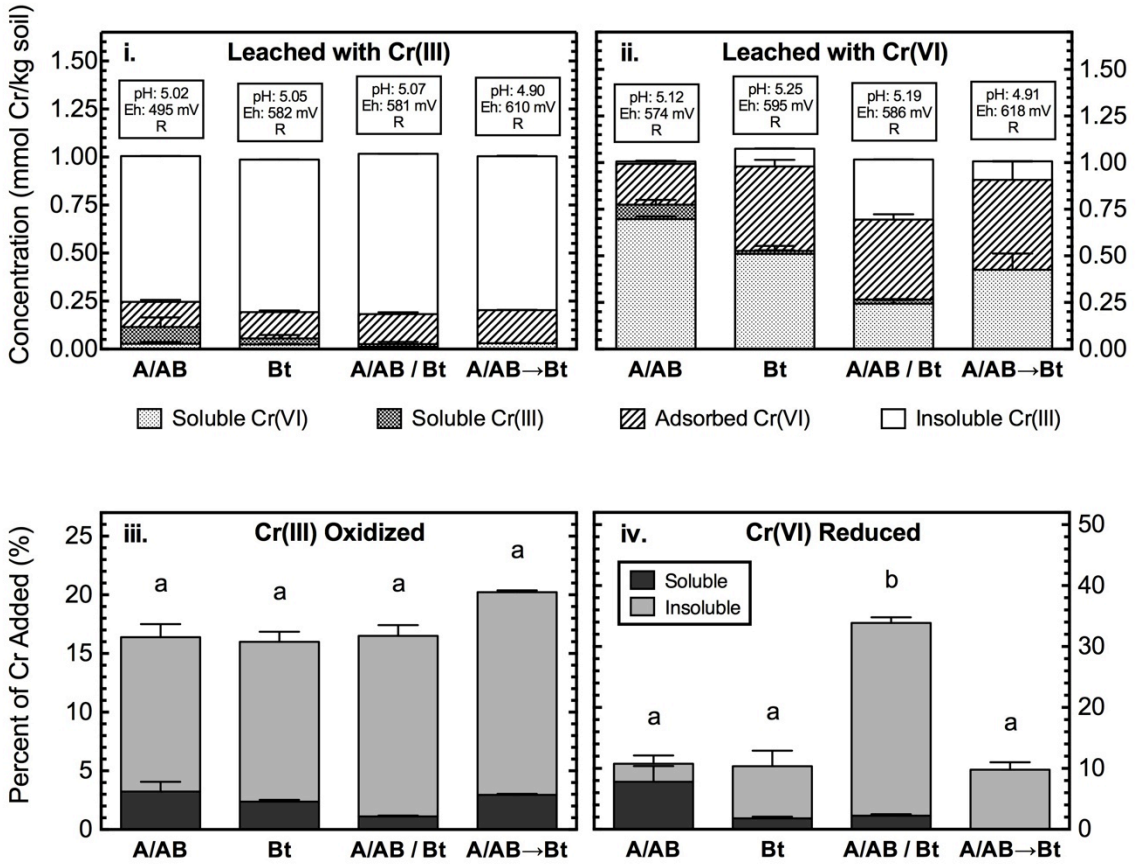

Figure 2.6 Chromium speciation in Jackland soil A/B and Bt horizons. Jackland soil A/AB and Bt horizons leached with **i.** soluble Cr(III) in the form of $Cr(NO_3)_3$ and **ii**. soluble Cr(VI) in the form of K_2CrO_4, where A/AB is the A/AB horizon alone, Bt is the Bt horizon alone, A/AB / Bt is the A/AB horizon on top of the Bt horizon, and A/AB→Bt is the leachate from the A/AB horizon alone leached through the Bt horizon alone. Potentiometric values reported above each bar, where O is reported when the combined Eh and pH values fall in the oxidizing zone of an Eh-pH plot for chromium species and R is reported when the combined Eh and pH values fall in the reducing zone of an Eh-pH plot for chromium species. Ordinary one-way ANOVA multiple comparison analysis of **iii.** total percent Cr(III) oxidized and **iv.** total percent Cr(VI) reduced using $p \leq 0.05$.

for the soil materials (A/AB: 21% and Bt: 16%, Table 2.2), suggesting that the contact time was not long enough for complete reduction. Consistent with the other soils in the study, less Cr(VI) adsorption was observed in the A/AB treatment than the other treatments, likely due to the lower clay content of the A/AB horizon soil material. The A/AB / Bt interfacial treatment reduced significantly more Cr(VI) than the other treatments ($p < 0.0001$) (Fig. 2.6(iv)), supporting the theory of an interfacial process enhancing Cr(VI) reduction.

The Flickinger soil was unique in its dramatically increasing Mn concentration with increasing depth. The Ap horizon contained 1.7 g/kg Mn and 30 g/kg organic C while the Bt2 horizon contained 11.6 g/kg Mn and 2 g/kg organic C (Table 2.2). Figs. 2.7(i) and 2.7(iii) show that the Bt2 horizon by itself oxidized twice as much Cr(III) as the Ap horizon ($p = 0.003$) and much of that oxidized Cr(III) was adsorbed as Cr(VI). Considering that there was nearly seven times more CBD-extractable Mn in the Bt2 horizon than in the Ap horizon, a higher percentage of Cr(III) oxidation was expected. In fact, according the the Cr oxidation potentials shown in Table 2.2, the Ap horizon had the potential to oxidize 54% of the added Cr(III) and the Bt2 horizon had the potential to oxidize 73% of the added Cr(III), while only 20% and 42% oxidation, respectively, was observed in Fig. 2.7(iii). While the difference between the observed data and the potentials was likely due to decreased contact time, the discrepancy between the increase in Mn concentration and increase in oxidation indicates that there is likely another process, such as precipitation of Cr(III), competing with oxidation (Fendorf et al., 1993). Figure 2.7(iii) suggests that the maximum amount of Cr(III) oxidation possible is around 40-45% of the total soluble Cr(III) added. The higher amount of adsorption of Cr(VI) by

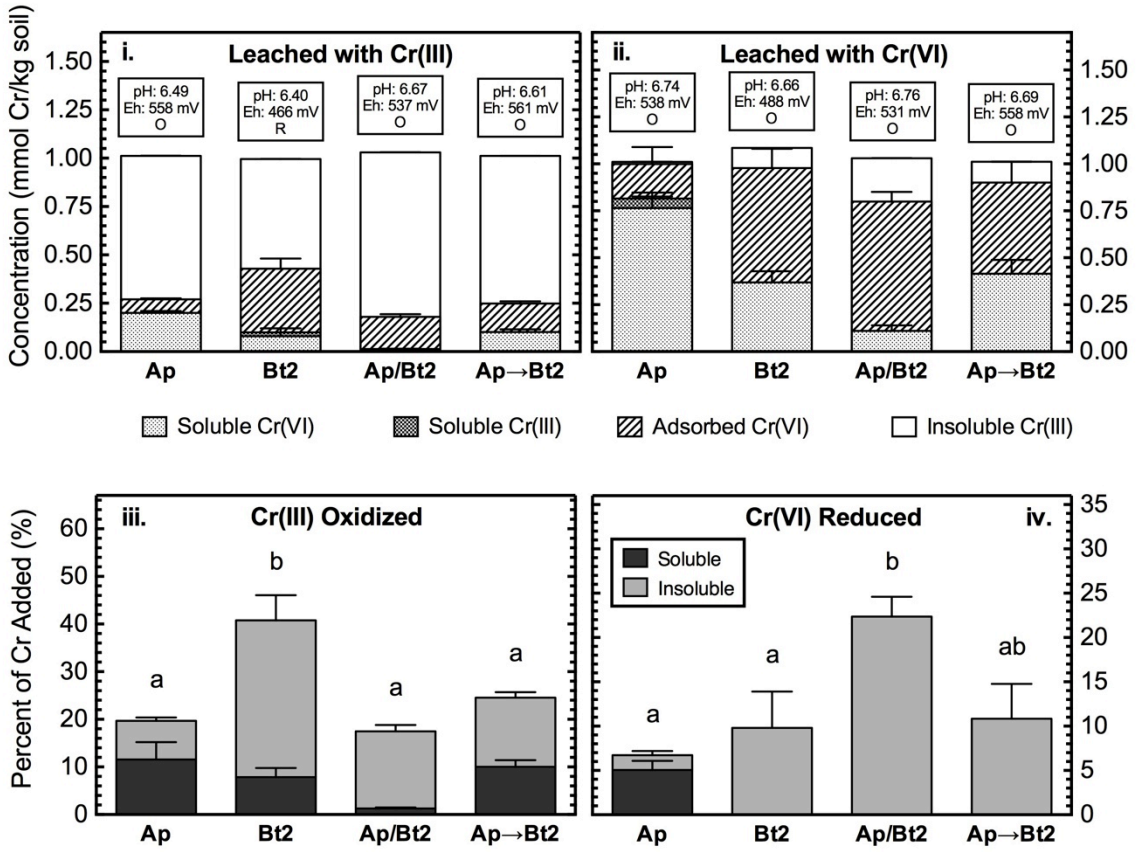

Figure 2.7 Chromium speciation in Flickinger soil Ap and Bt2 horizons. Flickinger soil Ap and Bt2 horizons leached with **i.** soluble Cr(III) in the form of $Cr(NO_3)_3$ and **ii.** soluble Cr(VI) in the form of K_2CrO_4, where Ap is the Ap horizon alone, Bt2 is the Bt2 horizon alone, Ap/Bt2 is the Ap horizon on top of the Bt2 horizon, and Ap→Bt2 is the leachate from the Ap horizon alone leached through the Bt2 horizon alone. Potentiometric values reported above each bar, where O is reported when the combined Eh and pH values fall in the oxidizing zone of an Eh-pH plot for chromium species and R is reported when the combined Eh and pH values fall in the reducing zone of an Eh-pH plot for chromium species. Ordinary one-way ANOVA multiple comparison analysis of **iii.** total percent Cr(III) oxidized and **iv.** total percent Cr(VI) reduced using $p \leq 0.05$.

the Bt2 horizon was likely due to the different textures of the horizons. The Ap horizon is a loam with 98 g/kg clay and the Bt2 horizon is a clay with 444 g/kg clay (Table 2.2), so the Bt2 horizon was able to adsorb more Cr(VI).

When Cr(III) was leached through the interfacial Ap/Bt2 treatment (Fig. 2.7(i)), much less Cr(III) was oxidized than by the Bt2 horizon on its own ($p = 0.004$). In fact, the interfacial treatment oxidized the same amount of Cr(III) as the Ap horizon (no significant difference at $p \leq 0.05$). This suggests that there could be an interfacial process occurring to keep the high levels of Mn, especially in the Bt2 horizon, from oxidizing Cr(III). The Ap→Bt2 pseudo-interfacial treatment with Cr(III) added resulted in similar amounts of oxidation as the Ap and the Ap/Bt2 treatments (not significant at $p \leq 0.05$), suggesting that the interfacial process occurring may not be restricted to the horizons being in physical contact with one another.

The Ap treatment leached with Cr(VI) was the only treatment in this suite to yield any soluble Cr(III) (Fig 2.7(ii)). The Ap horizon contained 30 g/kg organic C while the Bt2 horizon contained 2 g/kg (Table 2.2); therefore, this soluble Cr(III) was likely due to the formation of Cr(III)-organic acid complexes. The Ap and Bt2 treatments reduced the same amount of Cr(VI) (~8%, no significant difference at $p \leq 0.05$), while the Ap/Bt2 interfacial treatment reduced significantly more Cr(VI) (23%, $p \leq 0.05$) (Fig 2.7(iv)). This further supports the claim that an interfacial process is influencing Cr redox processes. The Ap→Bt2 treatment did not reduce a significantly different amount of Cr(VI) than any of the other treatments (not significant at $p \leq 0.05$) (Fig 2.7(iv)).

Summary and Conclusions

All seven soils, despite differences in physical characteristics such as texture, organic C content, and Fe(III) and Mn(III,IV) (hydr)oxide content, exhibited significant results regarding Cr redox in soil horizon interfaces. In accordance with low Mn concentrations, little to no Cr(III) oxidation was observed in any of the Unicorn or Glenelg soil treatments except the Glenelg Ap treatment, which contained the highest Mn concentration. Both soils' A and B horizons on their own reduced 3-6% of the total Cr(VI) added while the pseudo-interfacial treatments for both soils reduced 9-11% of the added Cr(VI) and the interfacial treatments reduced 35-37% of the Cr(VI). The increased Cr(VI) reduction in the interfacial treatments is a clear indication that soil horizon interfaces have a significant effect on Cr(VI) reduction. The Atsion soil, a Spodosol with high organic C in both horizons, exhibited low Cr(III) oxidation due to low Mn concentrations but reduced Cr(VI). The O/A and Bh horizon soil materials reduced 9-12% of the added Cr(VI), the pseudo-interfacial treatment reduced 24% of the Cr(VI) added, and the interfacial treatment reduced over 50% of the Cr(VI) added. This further supports the claim that horizon interfaces affect Cr(VI) reduction in soils.

The Collington soil did not oxidize noteworthy amounts of Cr(III) but did exhibit Cr(VI) reduction. The A and Bt horizon soil materials reduced 8 and 12% of the added Cr(VI), respectively. The pseudo-interfacial treatment reduced 18% of the Cr(VI) added, while the interfacial treatment reduced 38% of the Cr(VI). In a similar fashion, the Russet soil, which contained ferric Fe, did not oxidize any Cr(III); however, the Ap and Bt horizon soil materials reduced 6 and 9% of the added Cr(VI), respectively, the pseudo-interfacial treatment reduced 10% of the Cr(VI) added, and the interfacial treatment

reduced 52% of the Cr(VI). These Fe-dominant soils further demonstrate the profound effect interfaces have on Cr reduction.

The high Mn soils, Jackland and Flickinger, both oxidized Cr(III). All of the treatments for both soils oxidized between 16 and 24% of the added Cr(III) with the exception of the Flickinger Bt2 treatment, which oxidized over 40% of the added Cr(III). This was due to the extremely high Mn content of the Flickinger Bt2 horizon soil material, and it suggests that interfaces had little to no effect on Cr(III) oxidation. On the other hand, both soils also reduced Cr(VI). The A, B, and pseudo-interfacial treatments for both of the above soils all reduced between 7 and 11% of the added Cr(VI), while the Jackland interfacial treatment reduced 35% of the Cr(VI) added and the Flickinger interfacial treatment reduced 23% of the added Cr(VI). This is further evidence that interfaces affect Cr reduction, but not oxidation.

The effect of interfaces on Cr(VI) reduction combined with the lack of effect of interfaces on Cr(III) oxidation may suggest that the interfacial processes occurring are microbial. Microbial Cr(VI) reduction has been shown to be a common mechanism of Cr(VI) reduction in soils and is actively used in Cr(VI) remediation practices (Chaudhari et al., 2013; Field et al., 2013; Kim et al., 2014; Somenahally et al., 2013). Although soil microbes could be producing small amounts of reactive oxygen species such as superoxide which could oxidize both Mn(II) and Cr(III) (Tang et al., 2013; Tsu and Yang, 1996), the dominant Cr(III) oxidation mechanism in soils at common pH values are Mn(III,IV)(hydr)oxides. While these oxides can be produced by microorganisms, the actual mechanism of oxidation is abiotic, which would explain why Cr(III) oxidation was unaffected by interfaces (Murray and Tebo, 2007). A similar study comparing Cr(III)

oxidation and Cr(VI) reduction at interfaces from sampled soil materials before and after irradiation (to kill active microorganisms) would further elucidate the possible microbial mechanisms governing interfaces. Additionally, sampling the microbial communities in the different horizon soil materials would be useful in identifying the microorganisms potentially responsible for this interfacial phenomenon. These results indicate that interfaces have unique characteristics that may be enormously important regarding the cycling of chemicals, metals, and nutrients in soils. In general, much more research needs to be completed on soil interfaces of all types, including small-scale interfaces such as Fe(III) and Mn(III,IV) (hydr)oxide interfaces and large-scale interfaces such as boundaries between fill and original soil materials or contaminated material and soil.

CHAPTER 3

SURFACE SPECTROSCOPIC ANALYSIS OF MANGANESE(III,IV) (HYDR)OXIDE-CHROMIUM INTERACTIONS IN SYNTHETIC, FUNGAL, AND SOIL SYSTEMS

Introduction

As one of the most common global environmental contaminants, chromium (Cr) and its oxidation-reduction (redox) properties have been extensively studied in the past several decades. The oxidized, hexavalent form of chromium (Cr(VI)) is extremely toxic to all forms of life, including humans, animals, plants, and microorganisms, while reduced Cr in the trivalent form (Cr(III)) is an essential nutrient and, in general, not an environmental concern (Anderson, 1997). Additionally, in most of its forms, Cr(III) is insoluble, tightly bound to the soil surface, or strongly complexed with organic carbon (C) (James and Bartlett, 1983b; Kozuh et al., 1999), rendering it "safe" in terms of water quality concerns. On the other hand, Cr(VI) is extremely soluble and has a significantly decreased tendency to be sorbed by soils (Bartlett, 1991), making it a highly regulated element of concern in terrestrial environments.

The only oxidants of Cr(III) known to exist in soils at common pH values are manganese (Mn)(III,IV)(hydr)oxides. The following reaction describes the oxidation of Cr(III) to Cr(VI) in conjunction with the reduction of Mn(IV) to Mn(II):

$$Cr^{3+} + {}^{3}/_{2}\ MnO_2 + H_2O \rightarrow {CrO_4}^{2-} + {}^{3}/_{2}\ Mn^{2+} + 2\ H^{+}$$

In soils, Mn(III,IV)(hydr)oxides can exist in several different forms. Ferromanganese concretions can form as a result of soil wetting and drying and Mn coatings on soil particles can develop as a result of either dissolution of parent material (dolomite or

calcite marble) or Mn-oxidizing microorganisms. While Mn is commonly found in soils in low concentrations (0.01-0.2 g/kg), soils with extremely high Mn concentrations also exist. These manganiferous soils are formed from "Mn wad" a term for high-Mn parent material. While these soils are largely unstudied, one such soil found in Maryland, USA, was determined to be formed as a result of dolomite or calcite marble parent material with Fe and Mn impurities being dissolved over time, leaving behind high concentrations of Fe and Mn (169 g/kg Fe and 140 g/kg Mn) which oxidized when exposed to oxygen (Bourgault and Rabenhorst, 2011).

Other significant soil Mn(III,IV)(hydr)oxides are those created by bacteria and fungi. These biogenic oxides generally have smaller crystal sizes than their abiotic counterparts, and therefore are considered more reactive (Bargar et al., 2005; Santelli et al., 2011; Toner et al., 2005; Webb et al., 2005b). Several strains of Mn(II)-oxidizing bacteria have been examined and it has been determined that, in general, they first produce a poorly-ordered Mn(III,IV)(hydr)oxide similar to synthetic δ-MnO_2 which is ultimately transformed to one of several oxides including Ca-birnessite, Na-birnessite, feitknechtite, or todorokite depending on the solution chemistry (Feng et al., 2010; Mandernack et al., 1995; Villalobos et al., 2006; Webb et al., 2005b). Fungal oxidation of Mn(II) occurs at a slower rate than bacterial oxidation, and studies have shown that the originally formed poorly-ordered Mn(III,IV)(hydr)oxide similar to δ-MnO_2 does not transform as it does with bacterial Mn(III,IV)(hydr)oxides (Santelli et al., 2011). It is thought that different species of Mn(II)-oxidizing fungi utilize different pathways including enzymes, extracellular polymers, and production of reactive oxygen species,

which accounts for the production of structurally different Mn(III,IV)(hydr)oxides (Santelli et al., 2011).

Soil microorganisms are also capable of reducing Cr(VI). It is generally accepted that the process of chromate (CrO_4^{2-}) reduction is enzymatically mediated and facilitated through cell membranes or exopolymeric substances (EPS) (Dogan et al., 2011; Harish et al., 2012; Ozturk et al., 2012). The microbial chromate reduction reaction is as follows, where CRB denotes chromate-reducing bacteria:

$$CrO_4^{2-} + 8H^+ + 3e^- \xrightarrow{CRB} Cr^{3+} + 4H_2O \xrightarrow{pH\sim 7} Cr(OH)_3(s) + 3H^+ + 3H_2O$$

As Cr(VI) is toxic to biological cells, these chromate-reducing microorganisms have developed resistance to Cr(VI). A common mechanism of Cr(VI) resistance is to produce a Cr(VI)-reducing enzyme in the cytoplasm or cell membrane, while some yeast species have a thick cellular envelope with low permeability to Cr(VI) (Cervantes et al., 2001; Das and Guha, 2009; Ramirez-Diaz et al., 2008).

Other common mechanisms of Cr(VI) reduction include reduction by organic C and reduction by Fe(II) (Brose and James, 2013; Buerge and Hug, 1997; Dossing et al., 2011; Fendorf, 1995). The reduction of Cr(VI) and subsequent oxidation of organic C reaction is as follows, where CH_2O represents an empirical formula for many organic C compounds:

$$4\,CrO_4^{2-} + 3\,CH_2O + 20\,H^+ \rightarrow 4\,Cr^{3+} + 3\,CO_2 + 13\,H_2O$$

Following reduction, the cationic Cr(III) generally becomes complexed by organic acids. In soils, these complexes can either remain in solution, or can become sorbed to the soil surface (Cao et al., 2011; Puzon et al., 2005). Although complexation by organic acids slows the rate of Cr(III) oxidation by Mn(III,IV)(hydr)oxides, the complexes are resistant

to microbial degradation, and therefore can remain in soils for long periods of time (James and Bartlett, 1983b; Puzon et al., 2008). The following reaction represents the reduction of Cr(VI) along with the oxidation of Fe(II) to goethite, a common soil Fe(III)(hydr)oxide:

$$CrO_4^{2-} + 3\,Fe^{2+} + 2\,H_2O \rightarrow Cr^{3+} + 3\,FeO(OH) + H^+$$

Divalent Fe can be present either as an aqueous ion in anaerobic soils or structurally in such minerals as biotite, magnetite, or iron sulfides. Structural Fe(II) has been found to be slightly more effective than aqueous Fe^{2+} at reducing Cr(VI) (Jung et al., 2007; Loyaux-Lawniczak et al., 2001). A Fe(III)(hydr)oxide surface catalyzed mechanism has been proposed, where Fe(II) reduces the Cr(VI) with the Fe(III)(hydr)oxide acting as a catalyst and a facilitator of the surface precipitation of $Cr(OH)_3$ (Buerge and Hug, 1998).

Given the current knowledge of Cr(III) oxidation and Cr(VI) reduction in soils, especially with regard to Fe(III) and Mn(III,IV)(hydr)oxides, this study sought to comprehensively examine mineralogy changes of synthetic, microbial, and soil Fe(III) and Mn(III,IV) (hydr)oxides as a result of Cr redox reactions. To do this, a combination of quantitative column leaching experiments to measure Cr redox and X-ray absorbance spectroscopic (XAS) methods to qualitatively analyze the oxide structures was used. Due to the fine-grained, paracrystalline nature of Mn(III,IV)(hydr)oxides, crystal structure analysis by X-ray diffraction techniques is often not diagnostic for such fine paracrystalline minerals (Dixon and White, 2002). In this case, X-ray absorption near-edge structure (XANES) spectroscopy and extended X-ray absorption fine structure (EXAFS) spectroscopy were used to analyze the synthetic, microbial, and soil Fe(III) and

Mn(III,IV)(hydr)oxides before and after Cr(III) and Cr(VI) leaching to examine structural changes (Webb et al., 2005b).

This study will address the following two research questions: 1) how are Fe(III) and Mn(III,IV) (hydr)oxides from different origins (e.g. synthetic, soil, and fungal oxides) structurally different from each other? and 2) how do the structures of Fe(III) and Mn(III,IV) (hydr)oxides with different origins change as a result of oxidation or reduction of Cr? To accomplish this, a set of synthetic, fungal, and soil Fe(III) and Mn(III,IV) (hydr)oxides will be leached with soluble Cr(III) and Cr(VI) solutions. Chromium speciation will be analyzed spectrophotometrically and the solid (hydr)oxide samples will be analyzed by XAS techniques for structural information. The hypotheses for the study were that the oxides would have different mineralogy depending on their origin and that Mn oxide structures would change dramatically as a result of oxidation of Cr and reduction of Mn, but that Fe oxides would not change drastically due to their decreased direct involvement in Cr oxidation or reduction.

Methods

For this set of experiments, select sampled soil materials as well as synthetic Fe(III) and Mn(III,IV) (hydr)oxides were studied. Four different synthetic oxides were created using reagent-grade quartz sand as an inert substrate. The sand was first washed in acid by mixing 500 g of quartz sand in 5 L of 1 M HNO_3 and shaking in closed containers for 30 min every hour for 24 h in a reciprocating shaker. After shaking, the sand was separated from the acid by vacuum filtration, was washed 10 times with 500 mL of nanopure water over a vacuum filter, and was dried in the oven at 105 °C. An

Fe(III)(hydr)oxide-coated sand was synthesized by mixing 87.5 mL of 0.17 M $Fe(NO_3)_3$, 90 mL of 0.52 M NaOH, and 500 g of acid-washed sand and drying at 105 °C for 3 d with occasional stirring (Stahl and James, 1991a). Once the oxide-coated sand was dry, it was washed 10 times with nanopure water using vacuum filtration. A Mn(III,IV)(hydr)oxide-coated sand, was synthesized according to a similar procedure which involved mixing 77.5 mL of 0.5 M $MnCl_2$, 97.5 mL of 5.5 M NaOH, and 500 g of acid-washed sand and drying at 44 °C for 5 d with occasional stirring (Stahl and James, 1991b). The oxide-coated sand was washed 10 times with nanopure water once it was dry.

A Fe(III)/Mn(III,IV) mixed (hydr)oxide-coated sand was also synthesized by mixing 44 mL of 0.17 M $Fe(NO_3)_3$, 39 mL of 0.5 M $MnCl_2$, 48 mL of 5.5 M NaOH, 45 mL of 0.52 M NaOH, 75 mL of nanopure water, and 250 g of acid-washed quartz sand overnight in a beaker and drying in the oven at 38 °C for 6 days with occasional stirring (Herranz et al., 2006). The mixed oxide-coated sand was washed 10 times with nanopure water, lowering the pH to between 6 and 7. These oxides were characterized using a citrate-bicarbonate-dithionate (CBD) extraction (Loeppert and Inskeep, 1996) to quantify "free" Fe and Mn content of the coated sands and X-ray diffraction to determine the mineralogy of the oxides.

Two sampled soil horizons from Maryland were selected for this study due to their known Fe(III) and Mn(III,IV) (hydr)oxide properties, respectively. A soil with high Fe(III) oxide content was selected because of the ability of Fe(III) (hydr)oxides to sorb Cr(III) and Cr(VI). Samples from the Russett-Christiana complex mapping unit (coordinates: 39.012820, -76.854011) were similar to the Russett series (fine-loamy,

mixed, semiactive, mesic Aquic Hapludults), and were obtained for their high Fe(III) character. The Ap, AB, and Bt horizons were sampled on June 7, 2011. The Bt horizon was selected for this study because it had the highest concentration of Fe. A soil with high Mn content was desirable because of the ability of Mn(III,IV) (hydr)oxides to oxidize Cr(III) and sorb chromium. Samples from the Conestoga mapping unit (coordinates: 39.54805, -77.17803) were not similar to any known soil series, so they were designated 'Flickinger' after their location, as suggested by Bourgault (2008). The Ap, AB, Bt1, and Bt2 horizons were sampled on November 14, 2011. The soil horizon chosen for this experiment was Flickinger Bt2 because it contained the highest concentration of Mn.

The soil horizon samples were collected when the matric water potentials were approximately -33 kPa, respective matric water potentials for "field capacity" moisture. Approximately 8-12 L of soil material were brought back to the lab to be stored field-moist (while remaining aerobic) following sieving through a 4-mm polyethylene screen. The field moist, aerobic soil conditions were effected by double bagging each sieved soil horizon in 4-mil polyethylene bags, placing wet paper towels between bags, and storing them in closed 16 L polyethylene buckets with lids. The soils were not air-dried due to the severe and undesirable effects air-drying has on soil pH and Mn solubility (Bartlett and James, 1980; Perez et al., 2004).

Extensive soil characterization was performed on each soil horizon. The field-moist color and oven dry color were determined using the Munsell color book, and water content was determined by drying at 105 °C for 24 hours. Salt pH (pH_s) and redox potential (Eh) values were measured at a soil:solution ratio of 1:5 in 0.01 M $CaCl_2$ using

pH and platinum (Pt) combination electrodes with Ag/AgCl reference electrodes. Soil texture and particle size (% sand, % silt, and % clay) were determined by the pipette method (Gee and Bauder, 1986). Percent organic carbon and nitrogen for each horizon were determined in triplicate on a LECO CHN analyzer. Citrate-bicarbonate-dithionate extractable Fe and Mn were determined using the CBD method (Loeppert and Inskeep, 1996).

Additionally, a fungal Mn(III,IV)(hydr)oxide was selected for this study due to the fact that microbial Mn(III,IV)(hydr)oxides have been found to be a significant source of reactive Mn oxides in soil environments (Toner et al., 2006; Zhu et al., 2010). The fungal Mn(III,IV)(hydr)oxide was prepared according to the procedure detailed by Santelli et al. (2011). In brief, four species of fungi (*Plectosphaerella cucumerina DS2psM2a2*, *Pyrenochaeta* sp. DS3sAY3a, *Stagonospora* sp. SRC1lsM3a, and *Acremonium strictum* DS1bioAY4a) were grown in liquid HEPES-buffered (pH 7) AY media for several months. In order to obtain sufficient quantities of fungal oxide for MVE experimentation, all four fungal species were combined and concentrated by centrifugation (~2000 × g), decanting the supernatant liquid, and rinsing three times with nanopure water to remove any remaining soluble $MnCl_2$.

The seven materials described above (2 soil horizons, 4 synthetic oxides, 1 fungal oxide) were studied via column leaching experiments using a mechanical vacuum extractor (MVE). For each soil or synthetic oxide column replicate, a soil:solution ratio of 1:10 was used and for the fungal Mn(III,IV)(hydr)oxide, a soil:solution ratio of 1:1000 was used. All treatments were run with six replicates initially, except for in the case of the fungal Mn(III,IV)(hydr)oxide, where there was only enough sample volume to run

one sample. A sample of each initial material was also frozen at 0 °C at the time of MVE initialization for further analysis. For each replicate, a 50 mL MVE syringe barrel was prepped with a porous plastic spacer, 3 cm of synthetic polyester fiber stuffing, and a second plastic spacer. The barrels were then packed with 3.0 g of dry solid, or the field moist equivalent of 3.0 g, in the form of the sampled soils and synthetic oxides. In the case of the fungal oxide, the barrels were packed with the field moist equivalent of 0.03 g of dry mass. The barrels were then inserted into the MVE columns. Treatments in the form of 30 mL Cr(III) and Cr(VI) solutions were added to 50 mL syringe tubes corresponding to the appropriate samples. The Cr(III) solution was made up to be 2.6 mg Cr(III)/L (0.05 mM) by dissolving $Cr(NO_3)_3$ salt in 0.01 M KNO_3. Similarly, a 2.6 mg Cr(VI)/L (0.05 mM) solution was created using K_2CrO_4 salt. The background electrolyte, 0.01 M KNO_3 was utilized for these solutions to establish a consistent ionic strength in the samples without adding reactive compounds. The MVE allowed for the solutions to be leached through the solid materials at a fixed rate of 3.03 mL/hr. The leached solution was collected in a 50 mL syringe below each sample for further analysis. Following the completion of the leaching, three of the replicates for each treatment were removed from the MVE. The solid materials were transferred to centrifuge tubes and were washed twice with nanopure water using shaking and centrifugation to remove any residual soluble chromium. The solid materials were finally transferred to plastic sample vials and were frozen at -15 °C to be preserved for further analysis. The material preservation step was skipped for the fungal Mn(III,IV)(hydr)oxide samples due to small sample volume.

To analyze each treatment replicate, the collected leachates were centrifuged at ~26,000 × g for 20 min. This high speed was necessary to reduce the amount of colloids

in suspension, which can interfere with absorbance readings by flame atomic absorption spectroscopy (FAAS). Eh and pH were measured for each replicate. Next, 1:5 dilutions of the centrifuged filtrate were made by diluting 2 mL of sample to 10 mL using nanopure H_2O in test tubes. Additionally, 2 mL of the leftover Cr(III) and Cr(VI) solutions which were originally added to the replicates were diluted to 10 mL with nanopure water. This served as a measure to calculate the total amount of chromium added as well as to check the added solutions for possible errors. Seven Cr(VI) standards spanning from 0.005 to 1 mg/L were created from concentrated stock K_2CrO_4 solutions in nanopure water, and a blank containing 10 mL of nanopure water were created. Each sample and standard were vortexed for 15 seconds while 1 mL of 1,5-diphenylcarbazide reagent (DPC) was added (Bartlett and James, 1979). The test tubes developed color for 15 minutes before being analyzed colorimetrically on a flow-cell spectrophotometer at 540 nm. The absorbance readings of the samples were compared to a standard curve created using the standards and blank to quantify soluble Cr(VI).

To quantify total soluble Cr, approximately 8 mL of the centrifuged leachates were added to test tubes. These samples were not diluted so the Cr concentrations would be high enough for accurate detection, but were transferred to test tubes to reduce the chance of colloidal re-suspension in the process of transporting the samples. Five Cr standards spanning from 0.1 to 3 mg Cr/L were created from concentrated stock K_2CrO_4 solutions in 0.01 M KNO_3, and a blank containing 0.01 M KNO_3 will be created. The background of 0.01 M KNO_3 was necessary for these standards in order to make the matrix as close as possible to the samples because of strong matrix effects that occur when using FAAS. Additionally, approximately 8 mL of the leftover Cr(III) and Cr(VI)

solutions which were originally added to the replicates were added to test tubes to be analyzed to give the concentration of total chromium added to each replicate. Each sample and standard were analyzed using FAAS for Cr. The sample readings were compared to a standard curve in order to quantify total soluble chromium. Once total soluble chromium and soluble Cr(VI) were measured, soluble Cr(III) was calculated by subtracting soluble Cr(VI) from total soluble Cr.

To quantify sorbed Cr(VI), the remaining three replicates for each treatment were leached with phosphate buffer, where the PO_4^{2-} ions replaced CrO_4^{2-} ions on sorption sites. To quantitatively effect this, the 50 mL syringe barrels containing solid media were weighed following the initial chromium leaching in order to determine how much solution remained in the barrel. Once the barrels were replaced in the appropriate columns, 30 mL aliquots of 0.01 M phosphate buffer, which was made with a 1:1 molar ratio of K_2HPO_4 to KH_2PO_4 in nanopure water, were added and leached through the solid media. Once the leachates were collected, they were centrifuged at ~22,000 × g for 15 minutes. For the quantification of adsorbed Cr(VI), 1:5 dilutions of the supernatant liquid were made in test tubes with nanopure H2O, and the same seven Cr(VI) standards spanning from 0.005 mg/L to 1 mg/L and blank discussed above were created. Each test tube was vortexed for 15 seconds 1 mL of the DPC reagent was added. The test tubes were allowed to develop color for 15 minutes, and the absorbances were measured on a flow-cell spectrophotometer at 540 nm. The adsorbed Cr(VI) was quantified by comparing the sample absorbances to a standard curve. Once the adsorbed Cr(VI) was calculated, sorbed/precipitated Cr(III) was calculated by subtracting the measured soluble Cr(VI), soluble Cr(III), and sorbed Cr(VI) from the concentration of Cr added in the

original solution (James and Bartlett, 1983a). Following the phosphate leaching, the solid media were transferred to centrifuge tubes and were washed twice with nanopure water by shaking and centrifugation to remove any soluble chromium. The media were then transferred to plastic sample vials and frozen at 0 °C for further analysis.

The solid samples were also characterized using X-ray absorption spectroscopy (XAS) on beam line 11-2 at the Stanford Synchrotron Radiation Lightsource (SSRL), where Mn and Fe K-edge spectra were collected using a Si(2 2 0) double crystal monochromator and harmonic rejection mirror set at a cutoff energy of 9 keV. Wet, frozen samples for XAS analysis were thawed and loaded into Teflon sample holders and secured with Lexan windows and Kapton tape prior to analysis. A 100-element Ge detector with Cr X-ray filters was used to collect fluorescence data and 1-3 spectra scans were performed for each sample at 23 ± 2°C. Extended X-ray absorption fine structure (EXAFS) spectra were acquired from -200 to 1000 eV around the K-edge of the absorbing element (6539 eV for Mn, 7111 eV for Fe). To calibrate the energy, an elemental foil of the absorber (Mn) was placed between the 2^{nd} and 3^{rd} ionization chambers; spectra were calibrated to the inflection point of the elemental foil.

The SIXPACK software program described by Webb (2005) was used to analyze the sample spectra. Using this program, XAS scans were averaged, background-subtracted, normalized, and deglitched. The composition and structure of the Mn(III,IV)(hydr)oxides were determined using EXAFS spectroscopy (Bargar et al., 2005; Villalobos et al., 2003; Webb et al., 2005a; Webb et al., 2005b). Manganese K-edge EXAFS analysis was used to identify the natural and synthetic Mn(III,IV)(hydr)oxide minerals by comparison to a reference library of model Mn(III,IV)(hydr)oxide

compounds (Feng et al., 2010; Saratovsky et al., 2009; Villalobos et al., 2006; Webb et al., 2005a; Webb et al., 2005b). For EXAFS analysis, the **v**(**k**) spectra were **k**3-weighted and analyzed using a **k** range of 2–12 $Å^{-1}$.

Principal component analysis (PCA) was performed on the EXAFS spectra to establish the number of Mn(III,IV)(hydr)oxide components present in the samples. Target transformations were conducted using the following Mn model compound reference library to evaluate the fitness of each model compound to the overall data set: δ-MnO_2, hexagonal Na-birnessite ($Na^{+}_{0.31}(Mn^{4+}_{0.69}Mn^{3+}_{0.31})O_2 \bullet nH_2O$), triclinic Ca-birnessite, hexagonal acid birnessite ($H^{+}_{0.33}Mn^{3+}_{0.111}Mn^{2+}_{0.055}(Mn^{4+}_{0.722}Mn^{3+}_{0.11}*_{0.167})O_2 \bullet (H_2O)_{0.50}$, where * represents a layer of vacancies), groutite (α-MnOOH), feitknechtite (β-MnOOH), hausmannite (Mn_3O_4), synthetic todorokite ((Na, Ca, K)(Mg, Mn)$Mn_6O_{14} \bullet 5H_2O$), todorokite NMNH106238, Charro Redondo, Cuba, todorokite NMNH170286, Medford Quarry, Maryland, USA, Ca-buserite ($Ca_2Mn_{14}O_{27} \bullet 21H_2O$), Na-buserite (no accession number yet) ($Na_4Mn_{14}O_{27} \bullet 21H_2O$), rancieite NMNH160078, Paxton's Cave, Virginia, USA ($(Ca,Mn^{2+})Mn^{4+}_4O_9 \bullet 3H_2O$), pyrolusite ($\beta$-$MnO_2$), synthetic Mn_2O_3, aqueous $MnSO_4$, and aqueous $MnCl_2$.

Model compounds with SPOIL values <5 were used for subsequent linear least-squares combination fitting (LCF) of individual sample Mn EXAFS spectra, where SPOIL is a figure of merit used to determine the degree to which replacing an abstract component with the candidate would increase the fit error (Manceau et al., 2002). The SPOIL value is dimensionless, where <1.5 is excellent, 1.5–3 is good, 3–4.5 is fair, 4.5–6 is poor, and >6 is unacceptable (Malinowski, 1978). Linear least-squares combination fitting of the individual sample Mn EXAFS spectra was performed using the same

spectral reference library described above. Parameters for LCF were set as follows: binding energies were not allowed to float, a negative component contribution was prohibited, and components were not summed to 1.0. The goodness of fit was established by the minimization of the R-factor parameter (Newville, 2001).

Results and Discussion

I. Cr Leaching

Figure 3.1 shows that a significant amount of Cr(III) oxidation occurred in the Mn(III,IV)(hydr)oxide-coated sand (~41% of added Cr(III)) and that the oxidized species was mostly soluble Cr(VI) as opposed to adsorbed Cr(VI). As seen in Fig. 3.2(i), the total amount of Cr(III) oxidation was not significantly different from that of the mixed Fe(III)-Mn(III,IV)(hydr)oxide-coated sand or the high-Mn Flickinger soil material. However, there were significant differences in the amount of soluble vs. insoluble oxidation. The amount of Cr oxidized by the Mn(III,IV)(hydr)oxide-coated sand which remained as soluble Cr(VI) was significantly greater than for either the mixed Fe(III)-Mn(III,IV)(hydr)oxide-coated sand or the Flickinger Bt2 soil material ($p < 0.0001$), indicating that there was significantly less adsorption of newly oxidized Cr(VI). No reduction occurred when Cr(VI) was added to the Mn(III,IV)(hydr)oxide-coated sand (Fig. 3.2(ii)), which is consistent with the fact that potentiometric pH and Eh measurements for both treatments were in the oxidizing zone and no reducing agents were known to be present in the Mn(III,IV)(hydr)oxide-coated sand.

Figures 3.2(i) and 3.3 show that no oxidation occurred when Cr(III) was added to the Fe(III)(hydr)oxide-coated sand, which is consistent with the Eh-pH values being in

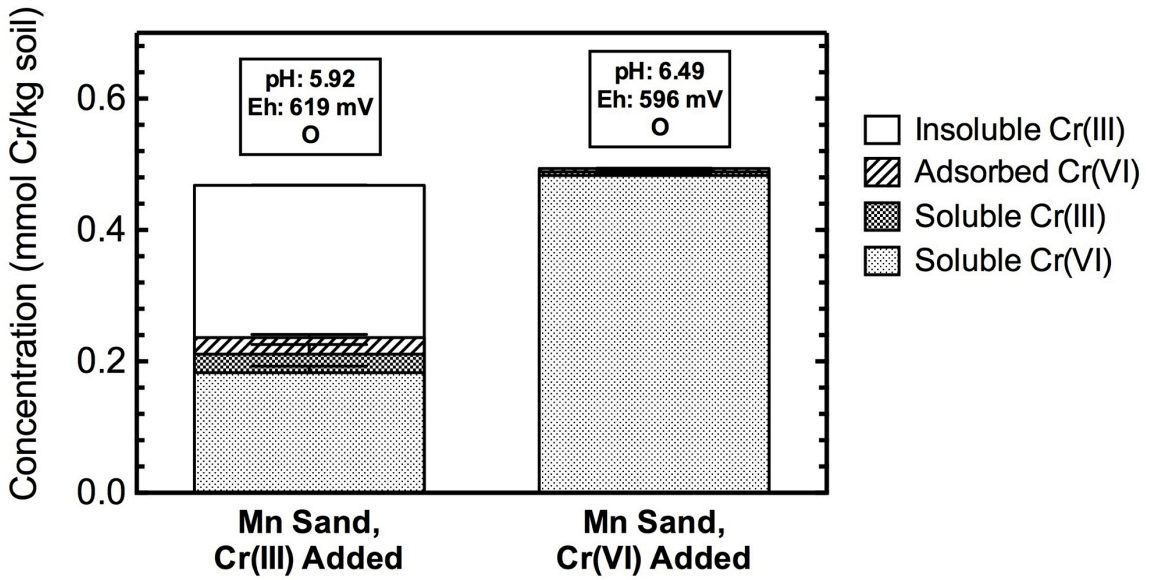

Figure 3.1 Chromium speciation in synthetic Mn(III,IV)(hydr)oxide-coated sand leached with soluble Cr. Mn(III,IV)(hydr)oxide-coated sand abbreviated as Mn Sand. Potentiometric values reported above each bar, where O is reported when the combined Eh and pH values fall in the oxidizing zone of an Eh-pH plot for chromium species and R is reported when the combined Eh and pH values fall in the reducing zone of an Eh-pH plot for chromium species.

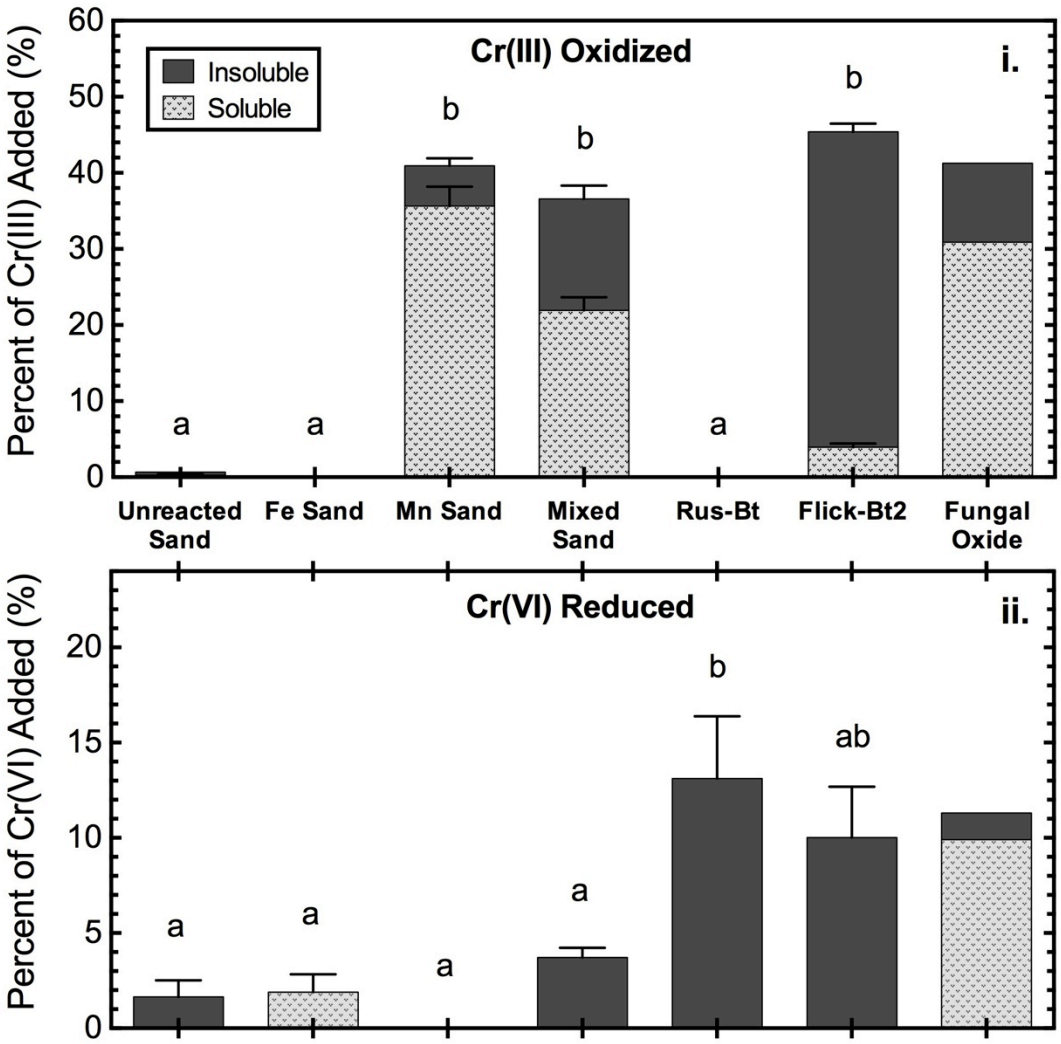

Figure 3.2 Repeated measures one-way ANOVA analysis. **i.** Percent Cr(III) oxidized and **ii.** percent Cr(VI) reduced by each soil/synthetic oxide material. Statistical analysis performed on total percent Cr(III) oxidized and total percent Cr(VI) reduced using $p \leq 0.05$. No analysis was performed using the fungal oxide data due to lack of sufficient replicates. Unreacted sand represents acid-washed reagent-grade sand with no Fe or Mn coating.

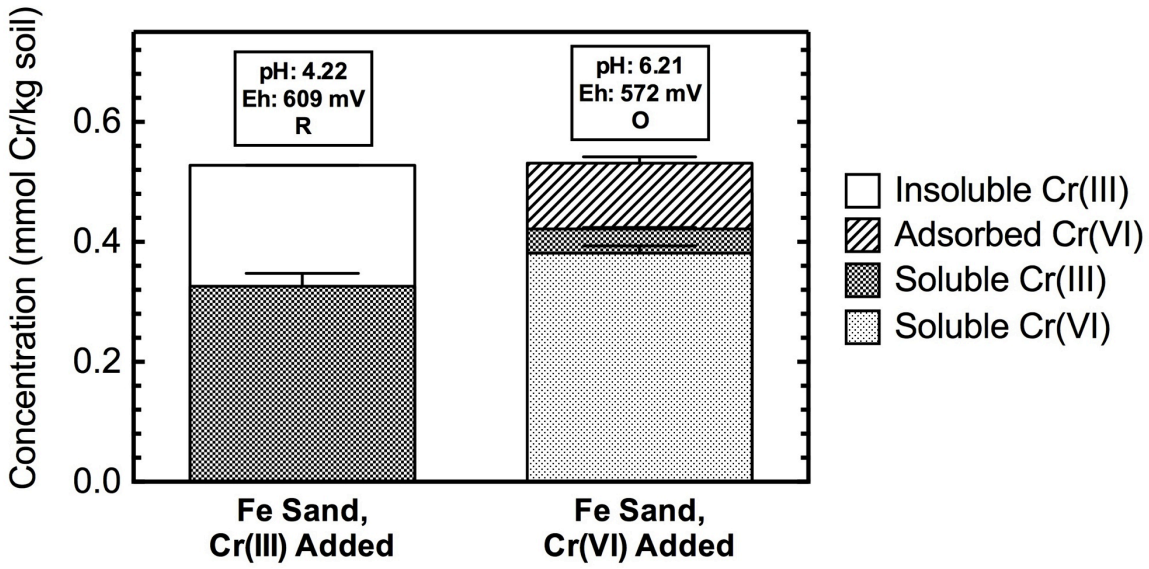

Figure 3.3 Chromium speciation in synthetic Fe(III)(hydr)oxide-coated sand leached with soluble Cr. Fe(III)(hydr)oxide-coated sand abbreviated as Fe Sand. Potentiometric values reported above each bar, where O is reported when the combined Eh and pH values fall in the oxidizing zone of an Eh-pH plot for chromium species and R is reported when the combined Eh and pH values fall in the reducing zone of an Eh-pH plot for chromium species.

the reducing zone and the lack of Cr(III) oxidizing agents. When Cr(VI) was added, a very small amount of reduction occurred (~2% of added Cr(VI)) but a more significant amount of the Cr(VI) (~20% of added Cr(VI)) was sorbed to the oxide surface. Interestingly, the potentiometric readings placed this treatment in the oxidizing zone, which was inconsistent with what was actually observed. This could indicate that Eh-pH data may not reflect the redox state governed by Fe chemistry and mineralogy of the soil. It also could indicate that Eh and pH may not have accurately reflected the surface properties of the Fe(III)(hydr)oxide-coated sands, which may have contained some Fe(II), a reducing agent for Cr(VI) (Loyaux-Lawniczak et al., 1999).

The mixed Fe(III)-Mn(III,IV)(hydr)oxide-coated sand (Fig. 3.4), behaved similarly to the Mn(III,IV)(hydr)oxide-coated sand, shown in Fig. 3.1, indicating that the Mn(III,IV)(hydr)oxide coatings may have influenced the oxide reactivity more than did the Fe(III)(hydr)oxide coatings. In fact, the two oxide-coated sand materials oxidized the same amount of total Cr (not significant at $p \leq 0.05$) (Fig. 3.2(i)). This is interesting because the mixed Fe(III)-Mn(III,IV)(hydr)oxide-coated sand had just over 41% more CBD-extractable Mn per dry mass (1.84 g/kg) than did the Mn(III,IV)(hydr)oxide-coated sand (1.3 g/kg) (Table 3.1), suggesting that the presence of Fe may have enhanced the ability of Mn(III,IV)(hydr)oxides to form on the sand surface (Davies and Morgan, 1989). However, this did not increase the amount of total chromium oxidation. When Cr(VI) was added, 3.7% (Fig. 3.2(ii)) was reduced to Cr(III), which may have been caused by the presence of small amounts of structural Fe(II). Similar to the Mn(III,IV)(hydr)oxide-coated sand, the Pt (Eh) and pH electrode measurements placed

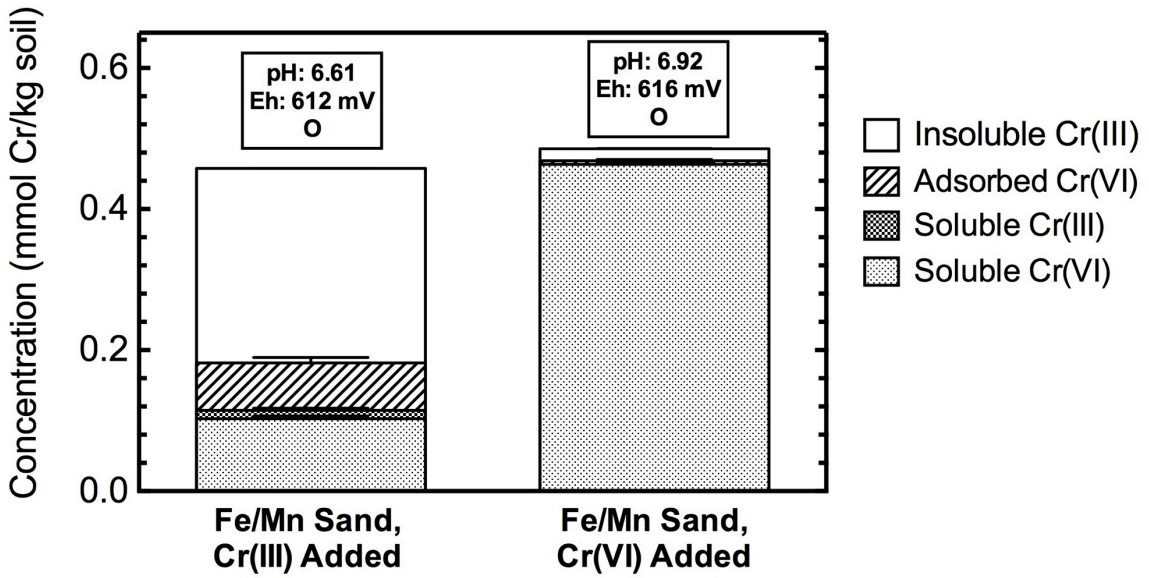

Figure 3.4 Chromium speciation in synthetic mixed Fe(III)-Mn(III,IV)(hydr)oxide-coated sand leached with soluble Cr. Mixed Fe(III)-Mn(III,IV)(hydr)oxide-coated sand abbreviated as Fe/Mn Sand. Potentiometric values reported above each bar, where O is reported when the combined Eh and pH values fall in the oxidizing zone of an Eh-pH plot for chromium species and R is reported when the combined Eh and pH values fall in the reducing zone of an Eh-pH plot for chromium species.

Table 3.1 Material characterization data. The pH_s was measured in a 1:10 soil:solution ratio with 0.01 M $CaCl_2$, the clay content was measured by the particle size analysis method, and organic C was measured by a LECO® C-H-N analyzer. CBD Fe and Mn were determined by citrate-bicarbonate-dithionite extraction and Cr oxidized was calculated from the Cr(III) leaching data.

	pH_s	Water Content	Clay Content	Organic C Content	CBD Fe Content	CBD Mn Content	Cr Oxidized (mmol Cr/g Mn)
		(g/kg)					
Mn(III,IV)(hydr)oxide-coated sand	6.13	NA	NA	NA	0.03	1.3	0.172
Fe(III)(hydr)oxide-coated sand	5.25	NA	NA	NA	1.09	0.0	NA
Mixed Fe(III)-Mn(III,IV)(hydr)oxide-coated sand	6.46	NA	NA	NA	0.8	1.84	0.093
Flickinger Bt2	6.51	414	444	2.0	29.1	11.6	0.019
Russet Bt	3.77	132	180	1.4	18.7	0.01	NA
Fungal Mn(III,IV) (hydr)oxide	~ 6-7*	14,344	NA	269	3.5	212	0.085

NA: Data unavailable due to the nature of the sample.
* More specific data unavailable due to lack of extra material.

both treatments in the oxidizing zone, which is consistent with the observed data for Cr(III) oxidation and Cr(VI) reduction by these oxides.

The Flickinger soil Bt2 horizon, which had an especially high concentration of Mn(III,IV)(hydr)oxides (11.6 g/kg, Table 3.1), predictably oxidized Cr(III). Interestingly, even though this soil material contained much more Mn than either the Mn(III,IV)(hydr)oxide-coated sand or the mixed Fe(III)-Mn(III,IV)(hydr)oxide-coated sand (Table 3.1), it oxidized the same amount of Cr(III) as did the two sands (not significant at $p \leq 0.05$) (Fig. 3.2(i)). This suggests that there is a maximum amount of Cr(III) that can be oxidized due to the competing process of precipitation of $Cr(OH)_3$, which occurs above pH 5.5 (Rai et al., 1987). Most of the newly-oxidized Cr(VI) was sorbed, as seen in Fig. 3.5, which is consisted with the theory of surface-induced oxidation beginning with the adsorption of Cr(III) to the Mn(III,IV)(hydr)oxide surface, followed by the oxidation of Cr(III) to Cr(VI) (Bartlett and James, 1979).

A previously demonstrated mechanism by Trebien et al. (2011) for the oxidation of Cr(III) by Mn(III,IV)(hydr)oxides included the following steps: 1) the formation of a Cr(III) complex on the Mn(III,IV)(hydr)oxide surface, 2) the transfer of electrons from Cr(III) to Mn(III or IV), 3) the formation of a Cr(VI) – Mn(II) complex, and 4) the release of Mn(II) and Cr(VI) into solution. However, in this study, the release of Cr(VI) into solution was not observed. A proposed mechanism for the oxidation of Cr(III) by this clay loam, high-Mn soil follows: Cr(III), which is cationic and added in a soluble form is adsorbed and hydrolyzed by the soil, likely due to the soil's high clay content and the negative charge due to high pH and isomorphous substitution in 2:1 clays. Once the Cr(III) is sorbed, it is in close contact with highly reactive, abundant paracrystalline

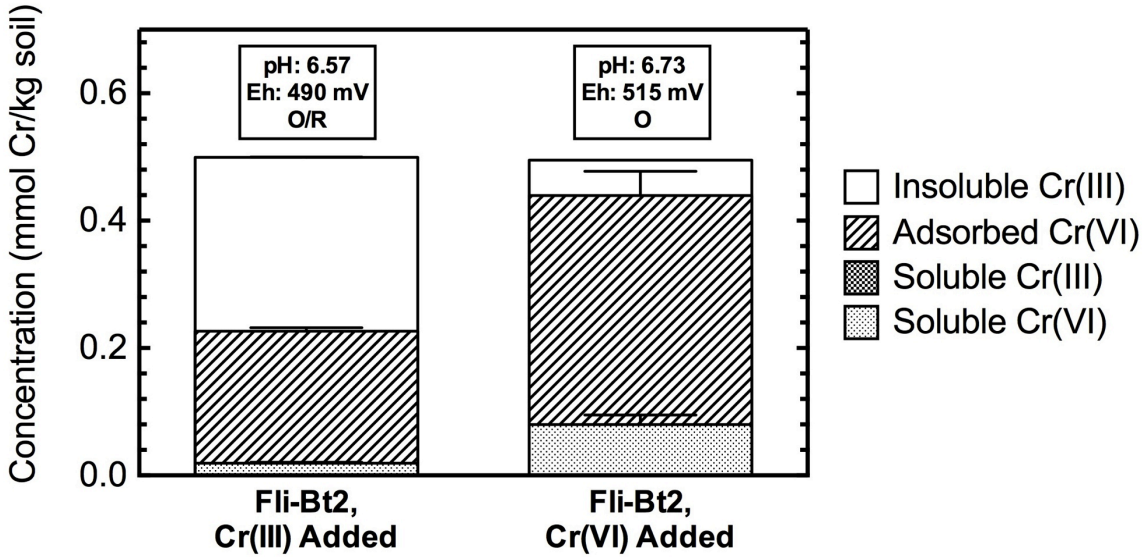

Figure 3.5 Chromium speciation in Flickinger Bt2 horizon soil material leached with soluble Cr. Flickinger Bt2 horizon soil material abbreviated as Fli-Bt2. Potentiometric values reported above each bar, where O is reported when the combined Eh and pH values fall in the oxidizing zone of an Eh-pH plot for chromium species and R is reported when the combined Eh and pH values fall in the reducing zone of an Eh-pH plot for chromium species.

Mn(III,IV)(hydr)oxides as coatings on other soil particles or as distinct nodules, which then oxidize the Cr(III). Instead of forming CrO_4^{2-} and releasing it into solution, the Cr(VI) could remain sorbed to the clay or Mn(III,IV)(hydr)oxide surface as an anion. These scenarios could cause the high percentage of oxidized, sorbed Cr(VI) observed.

There was a small amount of reduction in the Cr(VI) treatment. This may have been caused by small amounts of organic matter present in the soil, which have the capability of reducing Cr(VI) and forming soluble Cr(III)-organic C complexes (James and Bartlett, 1983a). Even though the Flickinger Bt2 soil horizon was sampled between 85 and 115 cm deep, there was still a measured 2.0 g organic C/kg soil present, which could be capable of Cr(VI) reduction. Also, even though the Cr(VI) was added in the form of soluble CrO_4^{2-}, a large amount of it adsorbed to the soil, likely due to the high concentrations of Fe(III)(hydr)oxides, possibly with net positive surface charge at low pH values (Arias et al., 1995). While CrO_4^{2-} adsorption is not as common as Cr(III) adsorption and precipitation by clayey soils, it is still possible, especially in low pH soils, due to pH-dependent charge. With a pH_s of 6.5, however, this soil doesn't qualify as having an extremely low pH. In terms of the potentiometric measurements, Eh and pH, the Cr(III) treatment yielded values on either side of the oxidation-reduction equilibrium line on the Eh-pH diagram (Appendix A), while the Cr(VI) treatment fell into the oxidizing zone, right above the oxidation-reduction line. The observed data suggested that both oxidation and reduction may occur, and values near the line support this.

Figures 3.2(i) and 3.6 demonstrate that the Russett Bt horizon, which has high concentrations of Fe(III)(hydr)oxides (Table 3.1), did not oxidize Cr(III). The soil material did, however, reduce a small amount of Cr(VI) (~13 % of added Cr(VI) (Fig.

3.2(ii)). Iron(II), which can be present in soils either structurally or as a result of anoxic soil conditions, reduces Cr(VI) (Buerge and Hug, 1997). In this soil, the free Fe was likely fully oxidized as Fe(III) with no associated Fe(II), evidenced by the reddish-orange color of the Fe(III)(hydr)oxides (10YR 6/6). Therefore, the small amount of reduction that did occur was likely due to either the small amount of organic C present (1.4 g/kg, Table 3.1) or structural Fe(II), potentially in the form of magnetite (Fe_3O_4), both of which are effective reducers of Cr(VI) (Dossing et al., 2011). Magnetite contains structural Fe(II) which does not oxidize in the presence of O_2, but would oxidize in the presence of adsorbed Cr(VI) (Jung et al., 2007). The potentiometric measurements placed both treatments in the reducing zone below the Cr(VI)/Cr(III) equilibrium line, which supports the lack of Cr(III) oxidation observed.

Regarding the fungal Mn(III,IV)(hydr)oxides, the scale of Fig. 3.7 is 100 times that of Figs. 3.1, 3.3, 3.4, 3.5 and 3.6. This is a result of the extremely high water content of the fungi (> 14 kg H_2O/kg) and associated Mn(III,IV)(hydr)oxides, as well as the highly reactive nature of the fungal Mn(III,IV)(hydr)oxides (212 g Mn/kg) (Table 3.1). Similar to the soil materials used, the fungal oxides were not dried due to the negative effects dehydration has on Mn(III,IV)(hydr)oxides; namely, drying over an extended period of time causes reduction of Mn(III,IV) to Mn(II) as well as collapsing of the layer structure (Post, 1999; Ross et al., 2001). Due to the high volume of biomass needed for redox tests with Cr(III) and Cr(VI), these treatments could not be replicated, resulting in the lack of error bars shown in Fig. 3.7. Since statistical analyses were not possible for these data, only general conclusions can be made. The fungal Mn(III,IV)(hydr)oxides oxidized approximately the same percentage of added Cr(III) as did the

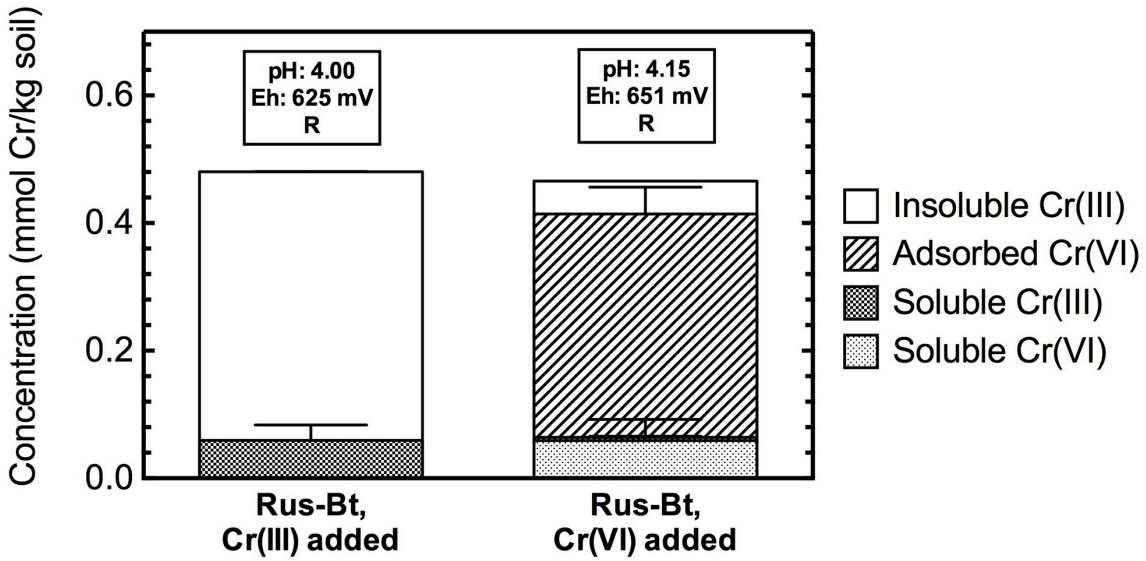

Figure 3.6 Chromium speciation in Russett Bt horizon soil material leached with soluble Cr. Russett Bt horizon soil material abbreviated as Rus-Bt. Potentiometric values reported above each bar, where O is reported when the combined Eh and pH values fall in the oxidizing zone of an Eh-pH plot for chromium species and R is reported when the combined Eh and pH values fall in the reducing zone of an Eh-pH plot for chromium species.

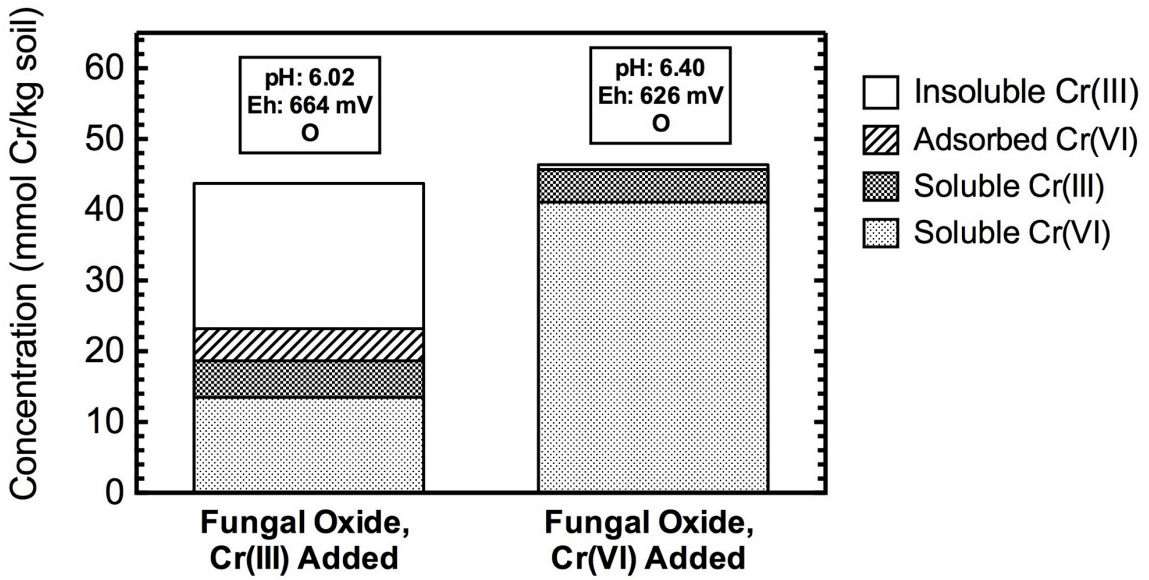

Figure 3.7 Chromium speciation in Mn(III,IV)(hydr)oxides produced by fungi leached with soluble Cr. Mn(III,IV)(hydr)oxides produced by fungi abbreviated as Fungal Oxides. Potentiometric values reported above each bar, where O is reported when the combined Eh and pH values fall in the oxidizing zone of an Eh-pH plot for chromium species and R is reported when the combined Eh and pH values fall in the reducing zone of an Eh-pH plot for chromium species.

Mn(III,IV)(hydr)oxide-coated sand. This is significant because 3.0 g of Mn(III,IV)(hydr)oxide-coated sand were used for those treatments, while only 0.032 g of fungal Mn(III,IV)(hydr)oxides were used. However, compared to the amount of Cr(III) oxidized to the amount of Mn(III,IV) present, the fungal Mn(III,IV)(hydr)oxides oxidized 0.085 mmol Cr/g Mn which was approximately the same as the mixed Fe(III)-Mn(III,IV)(hydr)oxide-coated sand (0.093 mmol Cr oxidized/g Mn) (Table 3.1). The Mn(III,IV)(hydr)oxide-coated sand oxidized 0.172 mmol Cr/g Mn and the Flickinger Bt2 soil material oxidized 0.019 mmol Cr/g Mn (Table 3.1), suggesting that the fungal oxide may not be more reactive than synthetic oxides, but it is more reactive than the Mn(III,IV)(hydr)oxides found in the natural soil. The following equation shows the generally accepted Cr(III) oxidation/Mn(IV) reduction reaction.

$$Cr^{3+} + {}^{3}/_{2}\ MnO_2 + H_2O \rightarrow {CrO_4}^{2-} + {}^{3}/_{2}\ Mn^{2+} + 2\ H^{+}$$

According to this equation, the molar ratio of Cr:Mn is 2:3. In this experiment, the molar ratios were much lower (ranging from 2:849 to 2:95), indicating that Cr(III) was the limiting reagent. Since the amount of Cr added to each treatment was kept constant, the differentiating factor was the concentration of free Mn(III,IV) incorporated into the oxide surfaces, which would be available for reduction by Cr(III). This is the same fraction of Mn that is measured using the CBD extraction method. In this study, even though the added Cr concentration was kept well below the optimal molar ratio, in no case was all of the Cr(III) oxidized. In fact, according to Fig. 3.2(i), there was not a statistically significant difference ($p > 0.05$) between the amount of Cr(III) oxidized by the Mn(III,IV)(hydr)oxide-coated sand, the mixed Fe(III)/Mn(III,IV)(hydr)oxide coated sand, or the Flickinger Bt2 horizon. Even though statistical tests were not possible for the

fungal Mn(III,IV)(hydr)oxide due to the impossibility of replication as a result of lack of material, it appears to be in the same range as the aforementioned materials, as well.

Regardless of the structural Mn content, Cr(III) oxidation appears to be at the maximum around 40-45% of added Cr(III). This could indicate that the practical Cr:Mn molar ratio may be much lower than Eqn. 3.1 suggests or that something besides stoichiometry is governing the oxidation of Cr(III). At pH levels above 5.5, Cr(III) precipitates as $Cr(OH)_3$ (Rai et al., 1987). All of the Mn-bearing materials studied had pH values above 5.9 for the Cr(III) treatments (Figs. 3.1, 3.4, 3.5, 3.7), indicating that Cr(III) precipitation was likely occurring simultaneously to Cr(III) oxidation. The fact that Cr(III) oxidation was maximized between 40-45% for each Mn-bearing material could suggest that the rate of oxidation is similar to or slightly slower than the rate of precipitation. Fendorf et al. (1992) showed that above pH 4, surface precipitation of $Cr(OH)_3$ inhibited Cr(III) oxidation by δ-MnO_2. Later studies of a variety of Mn(III,IV)(hydr)oxides concluded that Cr(III) oxidation rates vary depending on the amount of Mn(II) and Mn(III) present, specifically higher concentrations of Mn(II) and Mn(III) resulted in higher Cr(III) oxidation rates (Landrot et al., 2012).

The fungal Mn(III,IV)(hydr)oxide also reduced around 10% of the added Cr(VI) (Fig. 3.2(ii). This was likely caused by the high organic C content of the fungal mycelial biomass itself (269 g/kg, Table 3.1). Interestingly, most of the Cr(III) formed by reduction in the Cr(VI) treatment remained soluble, which is something not seen with any other material, and therefore is likely also related to the organic C-rich nature of the material. It is possible that soluble organic acid-Cr(III) complexes were formed so the Cr(III) did not have the opportunity to adsorb or precipitate as $Cr(OH)_3$. Nearly the same

percentage of Cr(III) remained soluble in both treatments, suggesting that the limit for soluble Cr(III) complexation was approximately 5% of the total chromium added.

II. Extended X-Ray Absorption Fine Structure (EXAFS)

Although material samples were collected after both Cr leaching and phosphate buffer leaching, no significant structural differences were expected, as phosphate leaching should have only desorbed anionic Cr(VI), and would not be expected to cause oxidation-reduction reactions or alter the Mn(III,IV)(hydr)oxide mineral structure. EXAFS analysis of the Mn(III,IV)(hydr)oxide-coated sand post-phosphate leaching (data not shown) confirmed the lack of structural changes from the post-Cr leaching samples, and therefore the decision was made to analyze only post-Cr leaching samples for the remaining materials. This allowed more of the allocated beam time to be dedicated to collecting higher quality data, rather than high quantities of lower quality data.

The Mn(III,IV)(hydr)oxide mineral structure of the Mn(III,IV)(hydr)oxide-coated sand was altered by Cr leaching (Fig. 3.8 and Table 3.2). Most of the differences in the spectra are visible in the 7-9.5 $Å^{-1}$ range (Fig. 3.8), which is one of the indicator ranges for Mn(III,IV)(hydr)oxides (Webb et al., 2005b). The unreacted sample does not have a visible dip in the data at 8.75 $Å^{-1}$ (Fig. 3.8(a)), therefore linear combination fitting of the data with a suite of layered and tunnel-structure Mn(III,IV)(hydr)oxide reference compounds determined that Na-buserite was the best component for the fit. A principle component analysis of all the collected EXAFS data (not shown) indicated that each sample contained, at most, two components. In each case, one-component and two-component fits were examined and a second component was incorporated if it noticeably

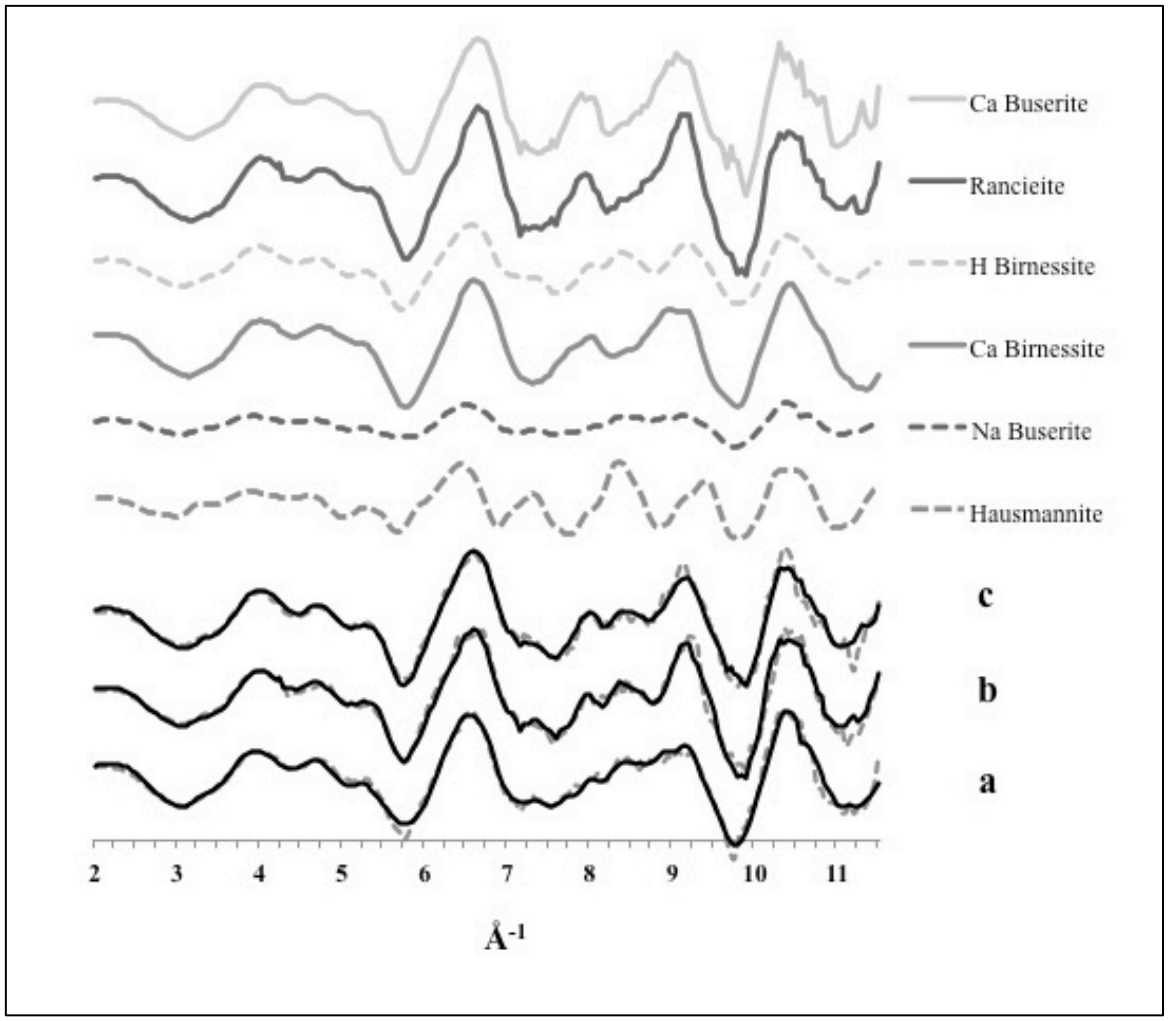

Figure 3.8 Mn(III,IV)(hydr)oxide-coated sand EXAFS data. The collected data for a) Mn(III,IV)(hydr)oxide-coated sand unreacted, b) Mn(III,IV)(hydr)oxide-coated sand leached with Cr(III), and c) Mn(III,IV)(hydr)oxide-coated sand leached with Cr(VI) in grey with the corresponding fits in black. The reference compounds detected in linear combination fitting analysis are shown above in grey.

Table 3.2 Mn(III,IV)(hydr)oxide-coated sand linear combination fitting data. Two-component least squares analyses with reduced chi-squared and R values showing the goodness of the fits. Note that the sum of the fractions may not equal 1.0, as the program settings prevent altering the fractions to conform to a sum of 1.0.

	Unreacted		Post-Cr(III)		Post-Cr(VI)	
Reduced χ^2	0.598		0.744		0.683	
R value	0.0443		0.0468		0.0498	
	ID	Fraction	ID	Fraction	ID	Fraction
Component 1	Na Buserite	2.1	Rancieite	0.69	Acid Birnessite	1.0
Component 2	Ca Birnessite	0.34	Hausmannite	0.60	Ca Buserite	0.37

improved the fit. In this case, Ca-birnessite, a type of birnessite which is triclinic and contains a small proportion of structural Mn(III) (Villalobos et al., 2006; Webb et al., 2005a), was incorporated into the fit as a secondary component due to the presence of strong peaks at 6.5 and 10.5 $Å^{-1}$.

Structurally, buserite ($Na_4Mn_{14}O_{27}•21H_2O$) is the hydrated form of birnessite ($Na_4Mn_{14}O_{27}•9H_2O$), both being layer-structured or "phyllomanganate" minerals containing sheets of predominantly edge-sharing $Mn^{4+}O_6$ octahedra with interlayer cations and water molecules. This means that the two have similar chemical structures, but the buserite contains more H_2O molecules in its interlayer, causing a larger distance between layers. Specifically, buserite has an average distance of 10 Å between layers while birnessite has about 7 Å between layers and once buserite dehydrates to birnessite, rehydration is not possible (Dixon and White, 2002). In this case, the unreacted Mn(III,IV)(hydr)oxide-coated sand was air dried in preparation, so hydrated buserite is unlikely, but, since birnessite and buserite are structurally similar, it is clear that the unreacted Mn(III,IV)(hydr)oxide-coated sand in its dry form is likely a birnessite-like layer structured phyllomanganate mineral with Mn(IV) as the dominant oxidation state (Schulze et al., 1995). The procedure for creating the Mn(III,IV)(hydr)oxide-coated sand included adding a high concentration of NaOH to $MnCl_2$, so the presence of Na^+ as a cation in the Mn(III,IV)(hydr)oxide mineral structure is logical and expected.

With the addition of Cr(III), the dip at 8.75 $Å^{-1}$ appeared along with a sharp peak at 9.25 $Å^{-1}$ (Fig. 3.8(b)), which altered the fit to a combination of rancieite and hausmannite (Table 3.2). Rancieite, $(Ca,Mn)Mn_4O_9•3H_2O$, is another layer structured mineral. The main structural difference between this mineral and birnessite is the

presence of different cations, specifically Ca^{2+} instead of Na^{+}, in the interlayer (McKenzie, 1989). Rancieite can contain small amounts of Mn(II), which could indicate reduction of Mn as a result of the Cr(III) oxidation observed in Fig. 3.1. When the Cr solutions were leached through the Mn(III,IV)(hydr)oxide-coated sand, the background electrolyte present was KNO_3, so it is possible that the Na^{+} present in the unreacted material was replaced by K^{+} in the Cr(III) and Cr(VI) samples. This could explain why the Cr(III) and Cr(VI) spectra in Fig. 3.8 appear very similar to each other, but different from the unreacted spectra. Hausmannite, the second component identified, was the only non-layer structured mineral detected for any of the Mn(III,IV)(hydr)oxide-coated sand samples. Hausmannite is a reduced oxide, meaning the Mn in the mineral structure has a valence of <4. Its formula is $Mn^{2+}(Mn^{3+})_2O_4$ and it has a tetragonal structure as opposed to the normal cubic spinel structure (McKenzie, 1989). As hausmannite contains mostly Mn(II) and Mn(III), this is further evidence of the reduction of Mn as a result of Cr oxidation.

While the data for the Mn(III,IV)(hydr)oxide-coated sand sample leached with Cr(VI) looks similar to the data for the sample leached with Cr(III) (Fig. 3.8), linear combination fitting with reference compounds shows that altering the components provides a better fit (Table 3.2). Geochemically, no Cr oxidation or reduction occurred (Fig. 3.1) so it was expected to look more similar to the unreacted material. The main component identified was acid birnessite, with the addition of Ca-buserite as a secondary component to strengthen the peak observed at 9.25 $Å^{-1}$ and the dip observed at 9.75 $Å^{-1}$ (Fig. 3.8(c)). Hexagonal acid birnessite contains more structural Mn vacancies than triclinic birnessite and, structurally, contains entirely Mn(IV) in the octahedral layer,

giving it a hexagonal symmetry, as opposed to triclinic birnessite, which contains significant amounts of structural Mn(III). These minerals, as mentioned above, are structurally similar so it is likely that the Cr(VI) treatment did little to change the fundamental structure of the Mn(III,IV)(hydr)oxides aside from replacing interlayer cations.

While the mixed Fe(III)-Mn(III,IV)(hydr)oxide-coated sand spectra were noisy, Fig. 3.9 makes it clear that there were some noticeable structural Mn differences between all three samples. The unreacted sample shows a very gradual peak from 7.5-9.5 $Å^{-1}$ (Fig. 3.9(a)). The Mn mineralogy of the unreacted mixed Fe(III)-Mn(III,IV)(hydr)oxide-coated sand identified by EXAFS was a mixture of layer-structured Na buserite and Na birnessite (Table 3.3), similar to the structure of the unreacted Mn(III,IV)(hydr)oxide-coated sand (Table 3.2).

The sample of mixed Fe(III)-Mn(III,IV)(hydr)oxide-coated sand leached with Cr(III) shows a very sharp peak at 8 $Å^{-1}$ and another peak from 8.75-9.5 $Å^{-1}$ (Fig. 3.9(b)). Linear combination fitting of the data (Table 3.3) shows that a mix of acid birnessite and groutite, an orthorhombic tunnel-structured polymorph of MnOOH, is the best fit for the oxide-coated sand leached with Cr(III) (Julien et al., 2004). The incorporation of a tunnel-structured Mn(III,IV)(hydr)oxide with dominantly Mn(III) into the fit indicates a significant change in mineralogy directly resulting from surface-induced Cr(III) oxidation, consistent with the mechanism proposed by Trebien et al. (2011). Also noteworthy is that the fit for the Cr(III) spectrum was not as good as it was for the other spectra (Fig. 3.9), mostly in the 7.75-8.75 $Å^{-1}$ range, even though groutite (α-MnOOH), which was the minor component, has similar peaks in that range. This could indicate that

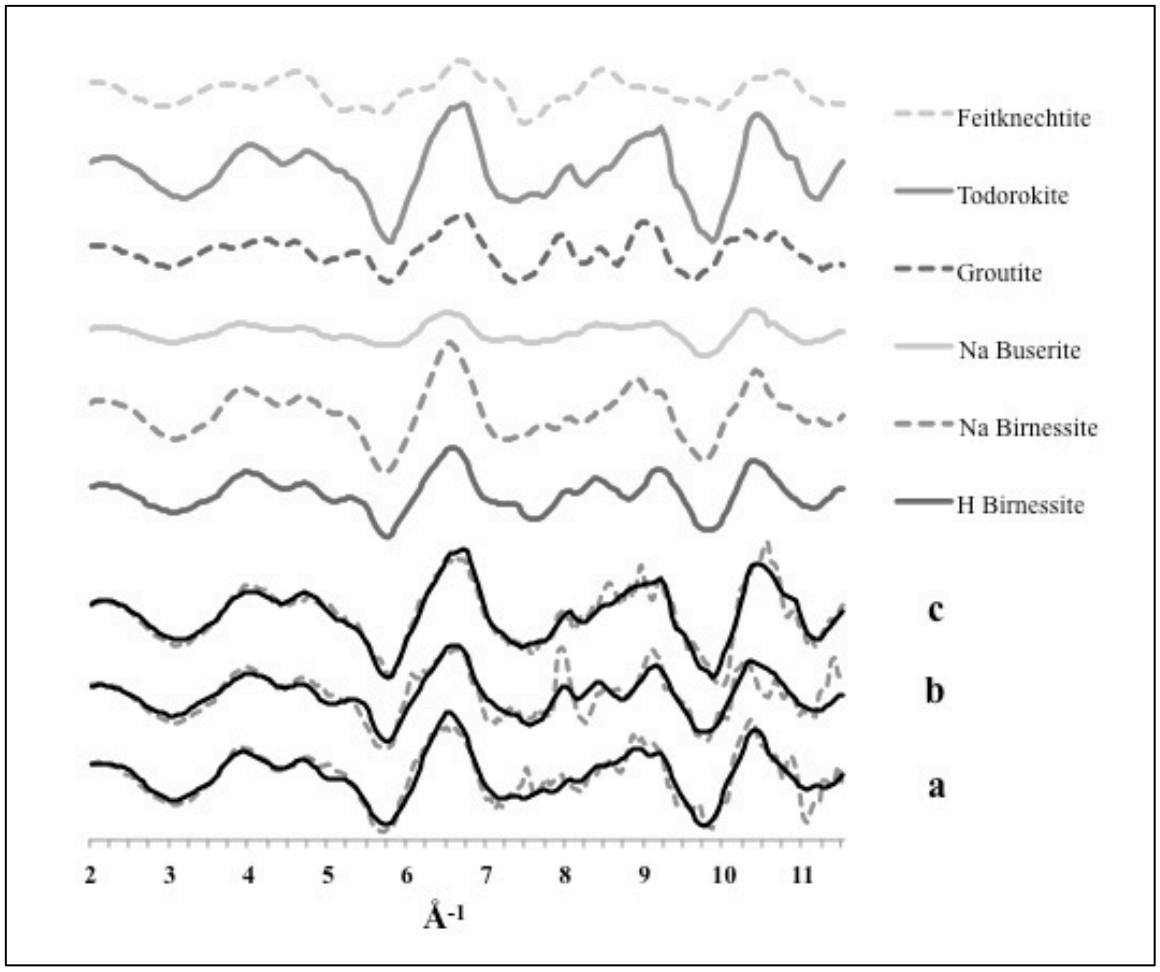

Figure 3.9 Mixed Fe(III)-Mn(III,IV)(hydr)oxide-coated sand EXAFS data. The collected data for a) mixed Fe(III)-Mn(III,IV)(hydr)oxide-coated sand unreacted, b) mixed Fe(III)-Mn(III,IV)(hydr)oxide-coated sand leached with Cr(III), and c) mixed Fe(III)-Mn(III,IV)(hydr)oxide-coated sand leached with Cr(VI) in grey with the corresponding fits in black. The reference compounds detected in linear combination fitting analysis are shown above in grey.

Table 3.3 Mixed Fe(III)-Mn(III,IV)(hydr)oxide-coated sand linear combination fitting data. Two-component least squares analyses with reduced chi-squared and R values showing the goodness of the fits. Note that the sum of the fractions may not equal 1.0, as the program settings prevent altering the fractions to conform to a sum of 1.0.

	Unreacted		Post-Cr(III)		Post-Cr(VI)	
Reduced χ^2	1.33		2.22		1.02	
R value	0.135		0.263		0.0754	
	ID	Fraction	ID	Fraction	ID	Fraction
Component 1	Na Buserite	0.91	Acid Birnessite	0.80	Todorokite	0.82
Component 2	Na Birnessite	0.63	Groutite	0.40	Feitknechtite	0.33

the surface interactions between Fe, Mn, and Cr are changing the mineralogy enough to deviate from the collected reference materials.

The mixed Fe(III)-Mn(III,IV)(hydr)oxide-coated sand sample leached with Cr(VI) shows a small peak at 8 $Å^{-1}$ and then a similar gradual peak to the unreacted sample (Fig. 3.9(c)). However, Table 3.3 shows that the best fitting components were todorokite and feitknechtite, two tunnel-structured Mn(III,IV)(hydr)oxide minerals. The true structure of todorokite is tunnels of 3x3 octahedra, although varying tunnel widths occur in nature so that tunnels with 3x4-3x9 octahedra are a more practical representation (McKenzie, 1989; Post, 1999). Feitknechtite, or β-MnOOH, is another polymorph of MnOOH, but the exact structure has not been reported (Luo et al., 1998; Post, 1999). It has been established as an intermediate phase in the oxidation of $Mn(OH)_2$ to birnessite, and contains Mn(III) (Elzinga, 2011), but in this case, Cr(VI) cannot be oxidized further, so this change did not accompany Cr(III) oxidation. This would suggest that the structural Mn changes were a result of the addition of K along with the Cr.

There were very few structural differences between the unreacted and Cr-leached samples of Flickinger Bt2 horizon soil material (Fig. 3.10 and Table 3.4). In fact, the differences were so few that the linear combination fitting picked the same two components for all three samples with slightly different fractions and statistical parameters. The main component identified in all three samples, δ-MnO_2, is a phyllomanganate with a relatively simple hexagonal structure due to the uniform oxidation state of Mn, IV+ (Villalobos et al., 2003). It is relatively similar in structure to hexagonal acid birnessite, and its natural counterpart is vernadite, indicating that the Mn(III,IV)(hydr)oxide present in this soil may belong to the vernadite family. Delta-

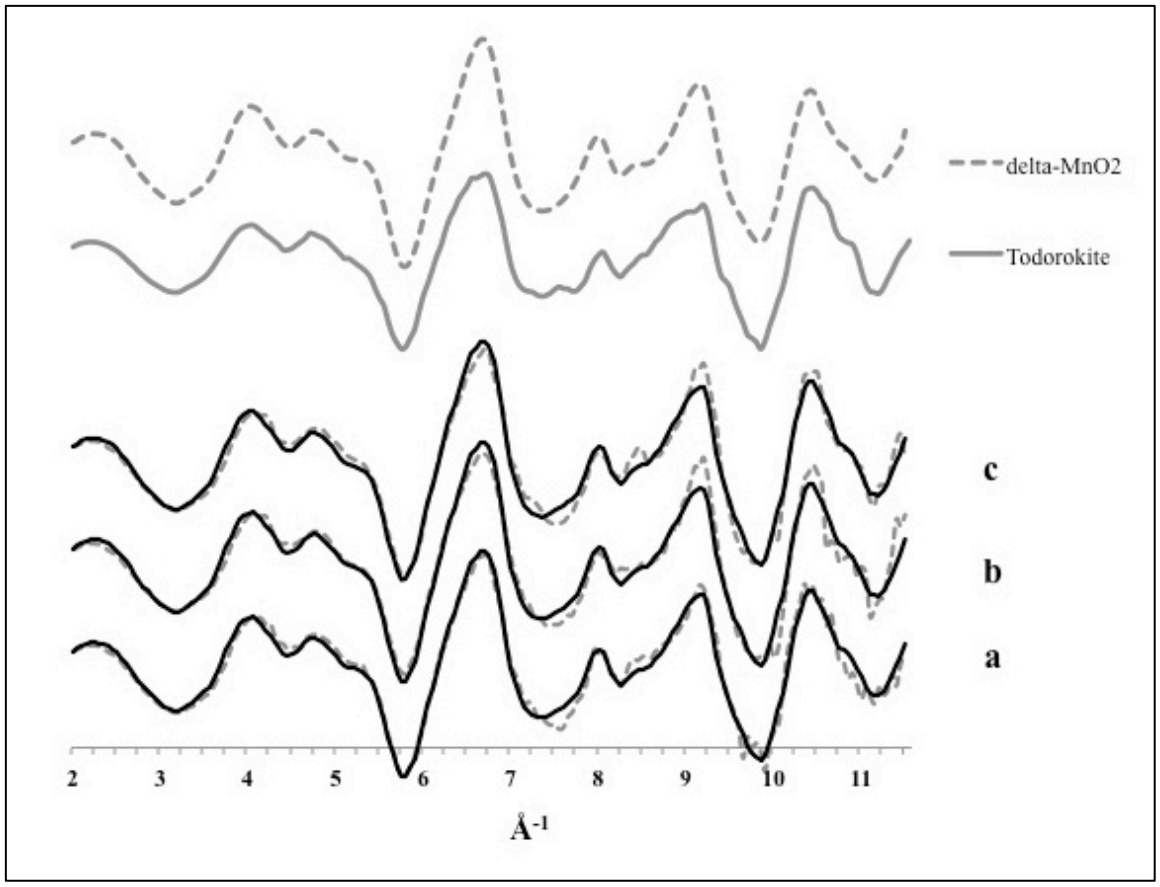

Figure 3.10 Flickinger Bt2 horizon EXAFS data. The collected data for a) Flickinger Bt2 unreacted, b) Flickinger Bt2 leached with Cr(III), and c) Flickinger Bt2 leached with Cr(VI) in grey with the corresponding fits in grey. The reference compounds detected in linear combination fitting analysis are shown above in grey.

Table 3.4 Flickinger Bt2 horizon linear combination fitting data. Two-component least squares analyses with reduced chi-squared and R values showing the goodness of the fits. Note that the sum of the fractions may not equal 1.0, as the program settings prevent altering the fractions to conform to a sum of 1.0.

	Unreacted		Post-Cr(III)		Post-Cr(VI)	
Reduced χ^2	0.596		1.08		0.792	
R value	0.0282		0.0444		0.0330	
	ID	Fraction	ID	Fraction	ID	Fraction
Component 1	∂-MnO_2	0.67	∂-MnO_2	0.71	∂-MnO_2	0.65
Component 2	Natural Todorokite	0.42	Natural Todorokite	0.46	Natural Todorokite	0.53

MnO_2 is a common biogenic Mn(III,IV)(hydr)oxide; however, the Mn(III,IV)(hydr)oxides in this soil were formed by dissolution of limestone parent material containing structural Fe(II) and Mn(II), which oxidize into Fe(III) and Mn(III,IV) (hydr)oxides upon exposure to O_2 (Bourgault and Rabenhorst, 2011). This does not exclude the possibility of microbial Mn redox cycling in the soils, but does suggest that δ-MnO_2 is a dominant Mn(III,IV)(hydr)oxide present in soils.

The secondary component in all three Flickinger Bt2 samples, todorokite, is a tunnel-structured Mn(III,IV)(hydr)oxide (discussed above), indicating that the Mn(III,IV)(hydr)oxides in the soil could naturally be more variable and less crystalline than the synthetic oxides. When compared to the synthetic oxide-coated sands, this soil exhibited far fewer structural differences with the addition of Cr. Geochemically, the soil material oxidized the same amount of Cr(III) as the synthetic oxide-coated sands (not significant at $p \leq 0.05$, Fig. 3.2(a)) so the lack of structural changes could indicate that some property of the soil, which is not present in the oxide-coated sands, may be resisting structural changes. It is possible that microbes present in the soil material are re-oxidizing Mn as it gets reduced by Cr, resulting in the lack of observed structural changes.

All three fungal Mn(III,IV)(hydr)oxide samples (Fig. 3.11) had the same major component, Ca-buserite, ($Ca_2Mn_{14}O_{27}$•$21H_2O$), which is the hydrated form of birnessite with Ca^{2+} as the charge balancing cation as opposed to Na^+, which was discussed above. The presence of Ca^{2+} renders the mineral more stable against dehydration to birnessite and usually accompanies a slight decrease in Mn oxidation state, relative to Na-birnessite (Post, 1999; Webb et al., 2005a). Even though the media used to grow the fungi contained more Na^+ than Ca^{2+}, Ca^{2+} has a stronger affinity for the Mn(III,IV)(hydr)oxide

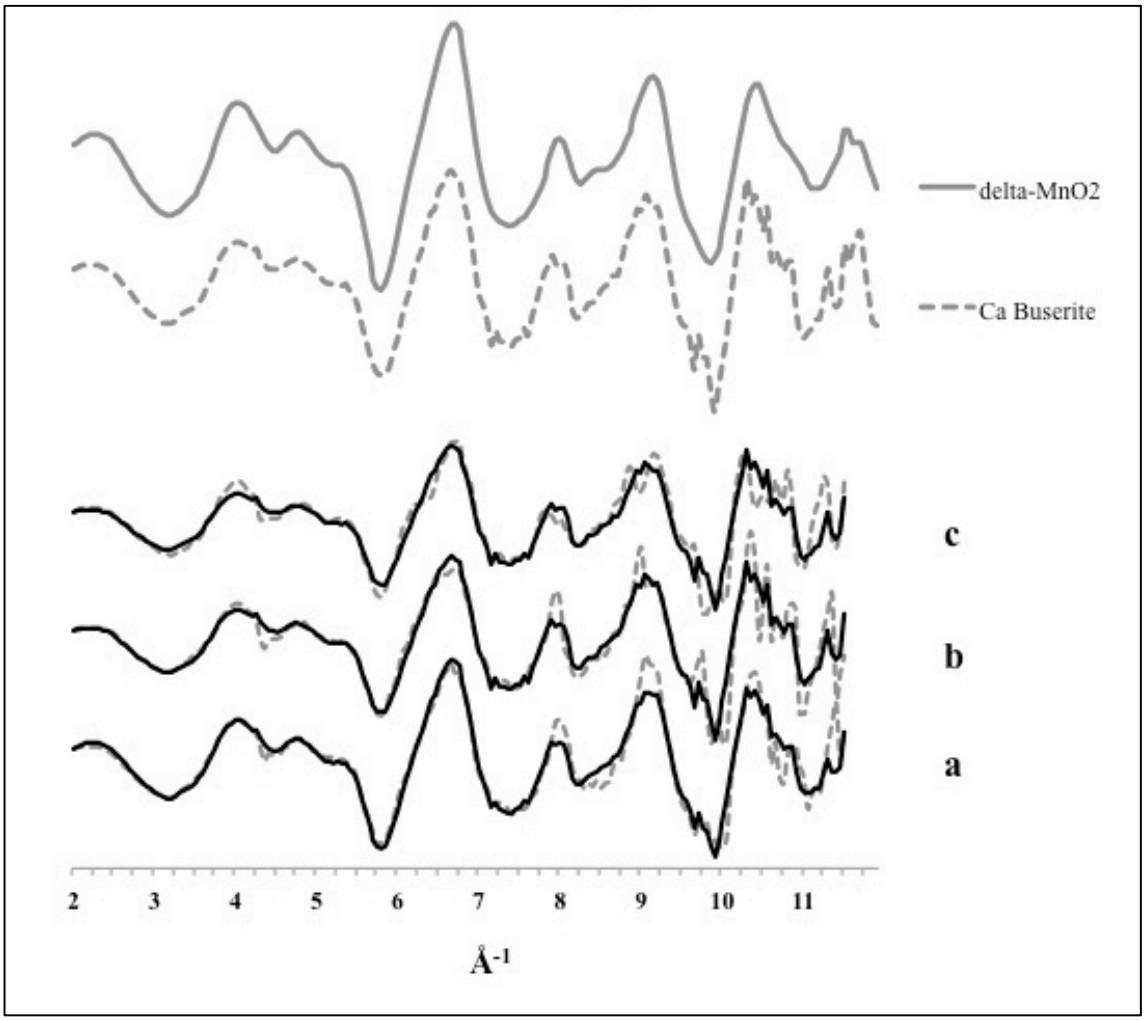

Figure 3.11 Fungal Mn(III,IV)(hydr)oxide EXAFS data. The collected data for a) fungal Mn(III,IV)(hydr)oxide unreacted, b) fungal Mn(III,IV)(hydr)oxide leached with Cr(III), and c) fungal Mn(III,IV)(hydr)oxide leached with Cr(VI) in grey with the corresponding fits in black. The reference compounds detected in linear combination fitting analysis are shown above in grey.

Table 3.5 Fungal Mn(III,IV)(hydr)oxide linear combination fitting data. One and two-component least squares analyses with reduced chi-squared and R values showing the goodness of the fits. Note that the sum of the fractions may not equal 1.0, as the program settings prevent altering the fractions to conform to a sum of 1.0.

	Unreacted		Post-Cr(III)		Post-Cr(VI)	
Reduced χ^2	1.02		1.49		1.26	
R value	0.0820		0.139		0.148	
	ID	Fraction	ID	Fraction	ID	Fraction
Component 1	Ca Buserite	0.52	Ca Buserite	0.77	Ca Buserite	0.68
Component 2	∂-MnO_2	0.31	--	--	--	--

surface, possibly leading to the formation of Ca-buserite (Webb et al., 2005a). As the fungi were grown in liquid media and were never dried prior to the experiment, the presence of hydrated buserite as opposed to dehydrated birnessite was expected. Both buserite and birnessite are layer-structured Mn(III,IV)(hydr)oxides with a higher degree of crystallinity than the oxides seen in the natural Flickinger soil material. The unreacted sample had a taller, sharper peak at 9 $Å^{-1}$ (Fig. 3.11(a)), allowing for a second component, δ-MnO2, to be detected in the fit (Table 3.5), which could suggest that the unreacted sample had a higher Mn oxidation state than the Cr-leached samples, as no second component was identified for either Cr-leached sample. Geochemically, significant Cr oxidation occurred when Cr(III) was leached, so a decrease in Mn oxidation state would be expected. The sample leached with Cr(VI) had a double peak in the 8.75-9.5 $Å^{-1}$ range, which was not fit by Ca buserite (Fig. 3.11(c) and Table 3.5). This feature was not present on any of the reference compounds, suggesting that there may have been a change in the Mn(III,IV)(hydr)oxide structure, perhaps resulting from the addition of K^+ along with Cr(VI), which cannot be identified using this reference library.

Summary and Conclusions

Despite vast differences in origin and mineralogy, all four of the Mn(III,IV)(hydr)oxides studied (including the Mn(III,IV)(hydr)oxide-coated sand, the mixed Fe(III)-Mn(III,IV)(hydr)oxide-coated sand, the Flickinger Bt2 horizon soil material, and the fungal Mn(III,IV)(hydr)oxide) oxidized the same amount of Cr(III): around 40%. As the different materials contained different amounts of Mn, measured by CBD extraction, this suggests that either some of the Mn(III,IV)(hydr)oxides were more efficient at oxidizing Cr(III) or that the amount of oxidation is limited by something other

than the amount of Mn present. The latter conclusion is supported by the fact that Cr should have been the limiting reagent in the reaction since Mn was added in excess, but in no case was all of the added Cr(III) oxidized. Significant reduction of Cr(VI) only occurred when organic C was present in the oxide material, i.e. the soil materials and fungal oxide.

Structural analysis of the Mn(III,IV)(hydr)oxides using EXAFS spectroscopy showed that the Mn(III,IV)(hydr)oxide-coated sand was originally a hexagonal birnessite-like phyllomanganate mineral, but was altered as a result of Cr(III) oxidation and Mn(IV) reduction to a combination of rancieite and hausmannite. The transformation from birnessite to hausmannite suggested a dramatic structural change from a layer-structured oxide to a tetragonal (non-layer structured) oxide. The unreacted mixed Fe(III)-Mn(III,IV)(hydr)oxide-coated sand was also a hexagonal birnessite-like phyllomanganate. As a result of the oxidation of Cr(III), Mn(IV) was reduced to Mn(III) and the (hydr)oxide took on some properties of tunnel-structured groutite. Leaching with Cr(VI) also structurally changed the (hydr)oxide to a combination of todorokite and feitknechtite, two tunnel-structured (hydr)oxides. This change did not accompany Cr oxidation or reduction, and therefore was brought about by leaching with K^+.

The Flickinger Bt2 horizon soil material was identified as a combination of hexagonal-structured δ-MnO_2, or vernadite, and tunnel-structured todorokite. There were no structural changes identified with the addition of Cr(III) or Cr(VI), indicating that the natural soil Mn(III,IV)(hydr)oxides are more variable than synthetic ones and that they have a greater capacity to resist structural change, perhaps due to continuous Mn redox cycling governed by the soil microbes. The fungal Mn(III,IV)(hydr)oxide was a

combination of Ca-buserite and δ-MnO_2 before the addition of Cr; after both Cr(III) and Cr(VI) were added, the oxides were identified as Ca-buserite, displaying a similar resistance to change as the soil Mn(III,IV)(hydr)oxide.

The contrast between the obvious structural changes displayed by the synthetic Mn(III,IV)(hydr)oxides and the natural Mn(III,IV)(hydr)oxides indicate a need to further study oxides found in nature. The propensity to undergo oxidation-reduction structural changes does not appear to be a function of the Mn(III,IV)(hydr)oxide mineral structure itself, although XANES analysis of the Mn oxidation state would shed more light on this. Further studies including XANES and EXAFS oxidation state and structural analyses of Fe and Cr (hydr)oxides are the next steps in elucidating mechanistic information on the processes occurring.

CHAPTER 4

OVERALL CONCLUSIONS

The research question addressed in Chapter 2, titled "Chromium Oxidation-Reduction Chemistry at Soil Horizon Interfaces Defined by Fe(III) and Mn(III,IV) (Hydr)oxides", was: how does oxidation-reduction of Cr change in mineralogically different soil horizons as affected by various types of interfacial conditions (e.g. defined by pH, Eh, organic matter content, and Fe(III) and Mn(III,IIV) (hydr)oxide mineral content)? The study attempted to answer this question by comparing Cr leaching experiments in simulated soil horizon interfaces to similar experiments in individual soil horizons. The results of the study for seven different soils were that soil horizon interfaces were more effective at reducing Cr(VI) than soil horizons on their own, but soil horizon interfaces did not have any effect on Cr(III) oxidation. Since Cr(VI) reduction in soils is, to a great extent, governed by microorganisms, while Cr(III) oxidation in soils is an abiotic process, these results are an indication that the processes enhancing Cr(VI) reduction without affecting Cr(III) oxidation at soil horizon interfaces are microbial.

As soil interfaces in general, including soil horizon interfaces, have been largely unstudied until this point, these results indicate a strong need to examine soil interfaces further. Specifically, to address the often large amounts of variation in the data which results from the variable nature of soils, especially when using field moist soil, a similar study with 6-12 replicates, as opposed to the 3 replicates used in this study, would provide a better idea of the true range represented by each soil. It would also allow for easier detection of possible outliers in the data. Additionally, as this study focused on

artificially created interfaces, a study comparing artificial interfaces to natural ones, by extracting intact soil columns from the field, would help to bridge the gap between laboratory experiments and realistic soil conditions.

To pinpoint the microbial processes that may be responsible for this interfacial phenomenon, a study comparing soil interfaces created by field-moist, sampled soils to interfaces constructed from soils which have been irradiated to make them microbially inactive would be useful. This would definitively prove the microbial nature of the interfacial processes occurring to affect Cr redox. Another study sampling the microbial communities of soils horizons individually and the microbial communities of a mix of the horizons, simulating an interface, would help elucidate the potential processes occurring.

To broaden the scope of these results, experiments studying other elements and compounds in soils would be beneficial. For example, studies of other toxic metals and their oxidation-reduction properties at soil horizon interfaces could bring the importance of studying these and other interfaces to the attention of a broad group of people. Additionally, studies on the immobilization of key soil ions at soil horizon interfaces compared to soil horizons on their own could shed light on key environmental issues such as the leaching of phosphate and sulfate from agricultural fields into groundwater.

The research questions addressed in chapter 3, titled "Surface Spectroscopic Analysis of Fe(III) and Manganese(III,IV) (Hydr)oxide-Chromium Interactions in Synthetic, Fungal, and Soil Systems", were: 1) how are Fe(III) and Mn(III,IV) (hydr)oxides from different origins (e.g. synthetic, soil, and fungal oxides) structurally different from each other? and 2) how do the structures of Fe(III) and Mn(III,IV) (hydr)oxides with different origins change as a result of oxidation or reduction of Cr? The

study attempted to address these questions by first leaching Cr(III) and Cr(VI) through each of the six materials and analyzing the Cr speciation. Then the Mn(III,IV)(hydr)oxide structures of the original materials as well as those leached with Cr(III) and Cr(VI) were analyzed using X-ray absorption spectroscopy. Despite the vast differences in their origins, the four Mn(III,IV)(hydr)oxide materials studied were primarily hexagonal, layer-structured phyllomanganate minerals. Upon leaching with Cr(III), both synthetic (hydr)oxide-coated sands demonstrated a structural change consistent with the reduction of Mn(IV), which occurred as a result of Cr(III) oxidation. The soil and fungal Mn(III,IV)(hydr)oxides, however, did not display the same structural change as a result of Cr(III) oxidation and Mn(IV) reduction.

One possible explanation for the lack of observable structural change in these natural Mn(III,IV)(hydr)oxides is that soil microbes in the case of the Flickinger soil or the fungal biomass in the case of the fungal oxides were able to re-oxidize Mn as it was reduced by Cr. This is highly probable for the fungal oxides, as the Mn(III,IV)(hydr)oxides were created by the fungi in the first place, so any newly created oxides would logically be of a similar structure to the original ones. The Mn(III,IV)(hydr)oxides in the Flickinger soil resulted from the weathering of parent material, but if newly-reduced Mn was re-oxidized by microbes, the structure may have been a similar enough phyllomanganate to avoid detection in small quantities. This would not have occurred in the synthetic (hydr)oxide samples because they did not contain a biotic component.

Additional studies to shed more light on the potential structural changes of natural Mn(III,IV)(hydr)oxides could include a similar study with higher Cr concentrations to see

if more Cr(III) oxidation and subsequent Mn(IV) reduction would occur, which could make Mn(III,IV)(hydr)oxide structural changes more distinct. Also, including Mn(III,IV)(hydr)oxide reference compounds with potassium as the interlayer cation in the reference library might yield more reliable results, as the Cr leaching also added a significant amount of potassium to the system. A study of the Fe and Cr mineralogy would also provide much more information on the structural effects of Cr(VI) reduction, and a XANES analysis of Mn, Fe, and Cr oxidation state would be able to quantify some of these structural changes. Finally, a study of the microbial community in high-Mn soil horizons would help to determine of microbial re-oxidation of Mn could be occurring.

Overall, these studies, together, reaffirm the need to further study soil interfaces, which occur at many scales and the microbiological processes governing metal oxidation and reduction at these interfaces. Future studies may want to focus on small-scale interfaces such as the interfaces between Fe and Mn in high-Mn soils as well as larger-scale interfaces such as those created by the disposal of waste on soils or the use of fill in construction and landscaping. Additionally, studies moving closer to field conditions would be beneficial. For example, as soluble Cr(III) is not generally present in soils in the form of a dissociated salt, leaching soluble Cr(III)-organic complexes would be a more realistic way to study the potential for soil and microbial Mn(III,IV)(hydr)oxides to oxidize Cr(III).

Appendix A

Eh-pH Diagrams

I. Chapter 2

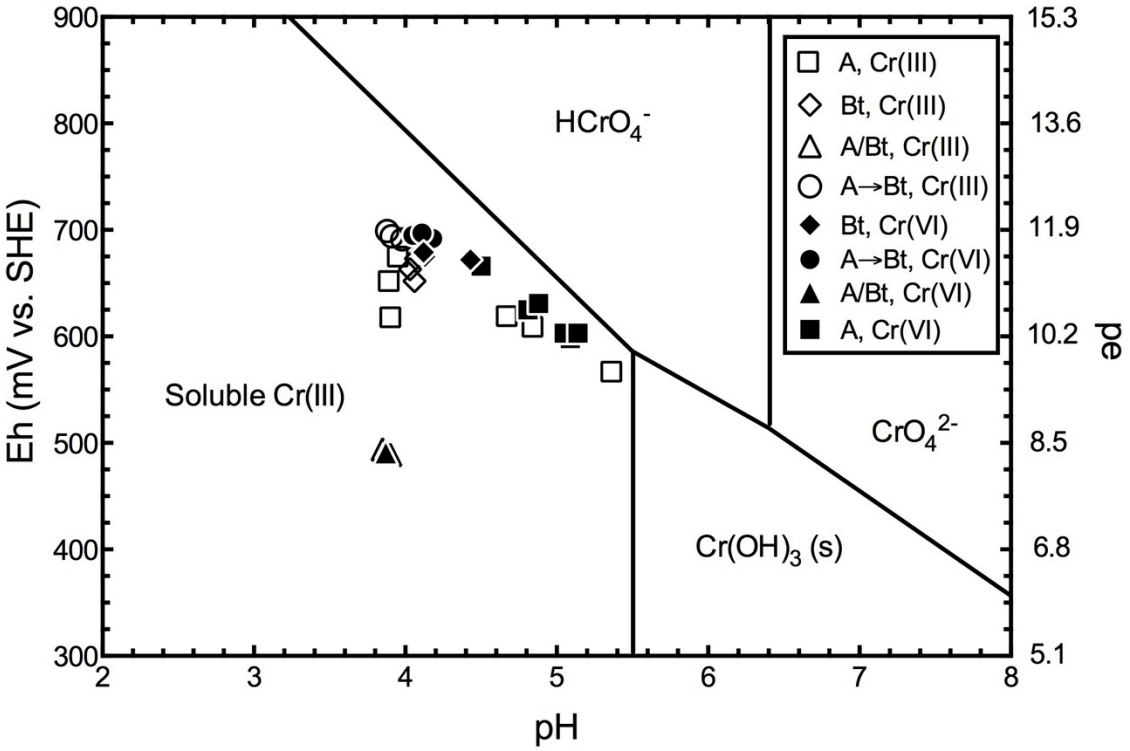

Figure A-1 Eh-pH diagram for Cr(III)-Cr(VI) redox and hydrolysis equilibria: Unicorn A and Bt horizon soil material leached with soluble Cr.

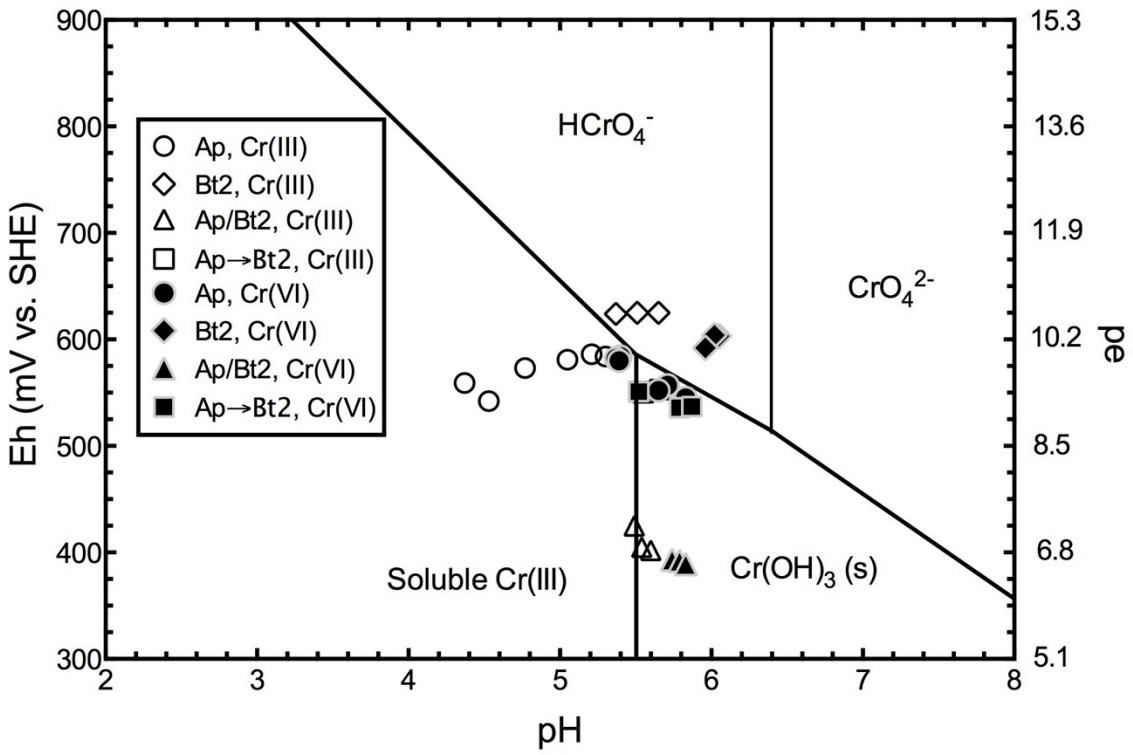

Figure A-2 Eh-pH diagram for Cr(III)-Cr(VI) redox and hydrolysis equilibria: Glenelg Ap and Bt2 horizon soil material leached with soluble Cr.

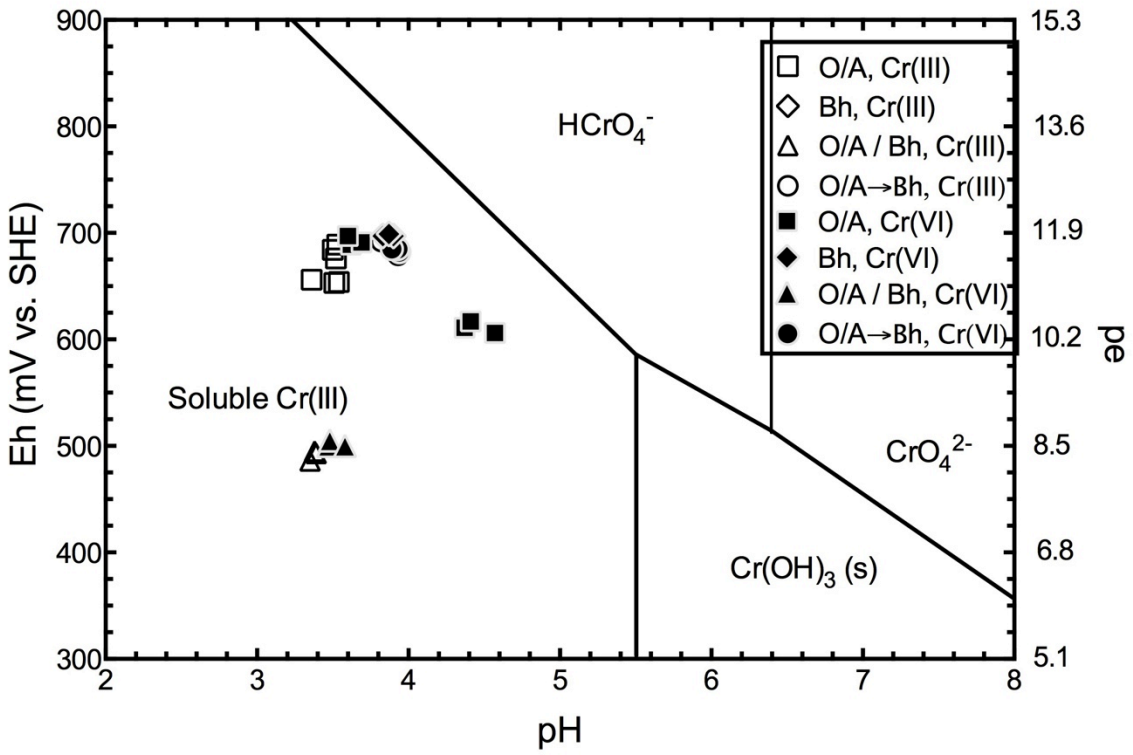

Figure A-3 Eh-pH diagram for Cr(III)-Cr(VI) redox and hydrolysis equilibria: Atsion O/A and Bh horizon soil material leached with soluble Cr.

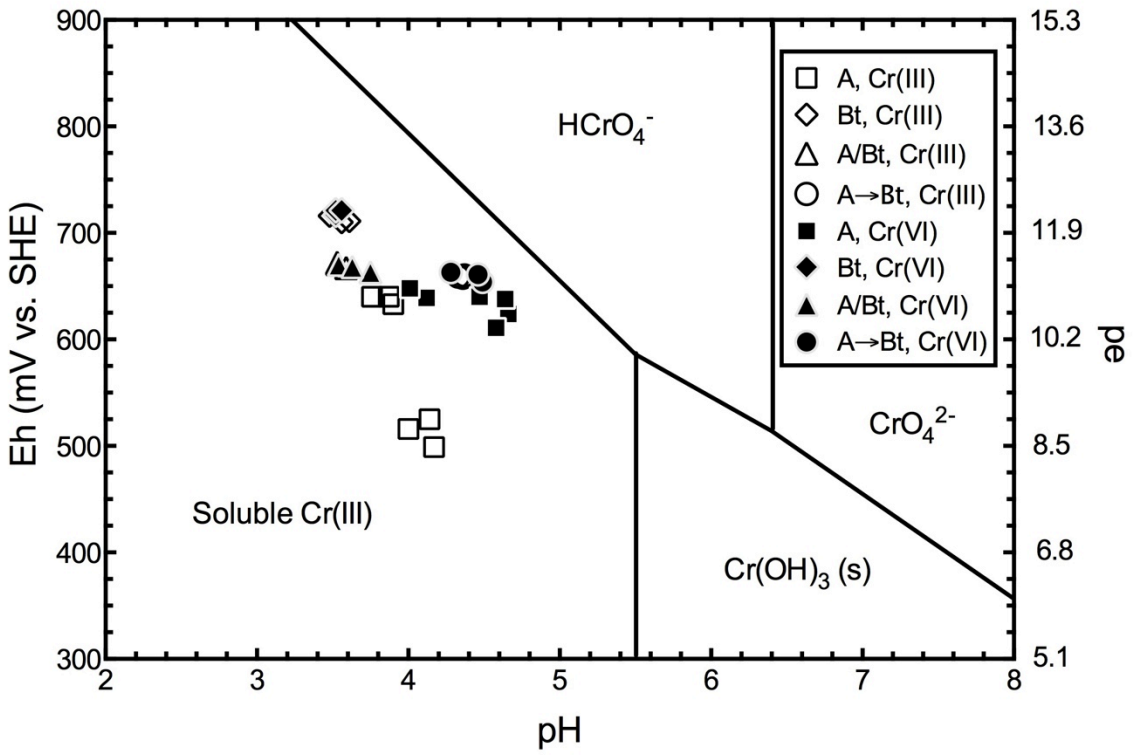

Figure A-4 Eh-pH diagram for Cr(III)-Cr(VI) redox and hydrolysis equilibria: Collington A and Bt horizon soil material leached with soluble Cr.

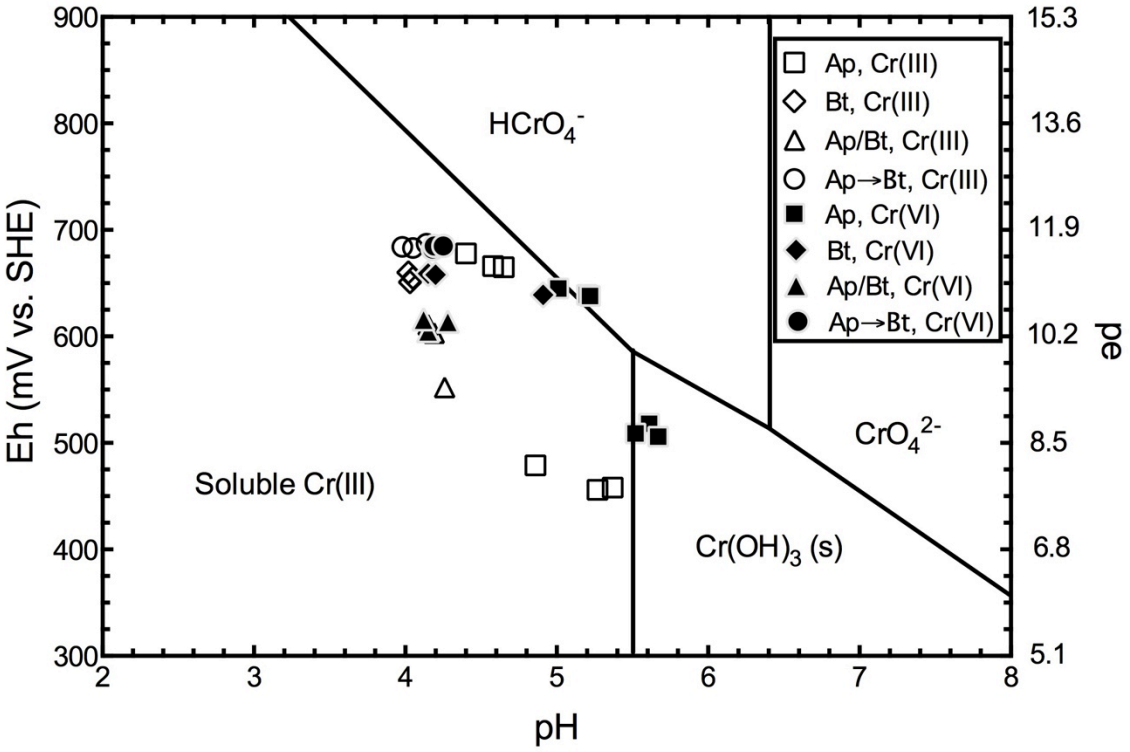

Figure A-5 Eh-pH diagram for Cr(III)-Cr(VI) redox and hydrolysis equilibria: Russett Ap and Bt horizon soil material leached with soluble Cr.

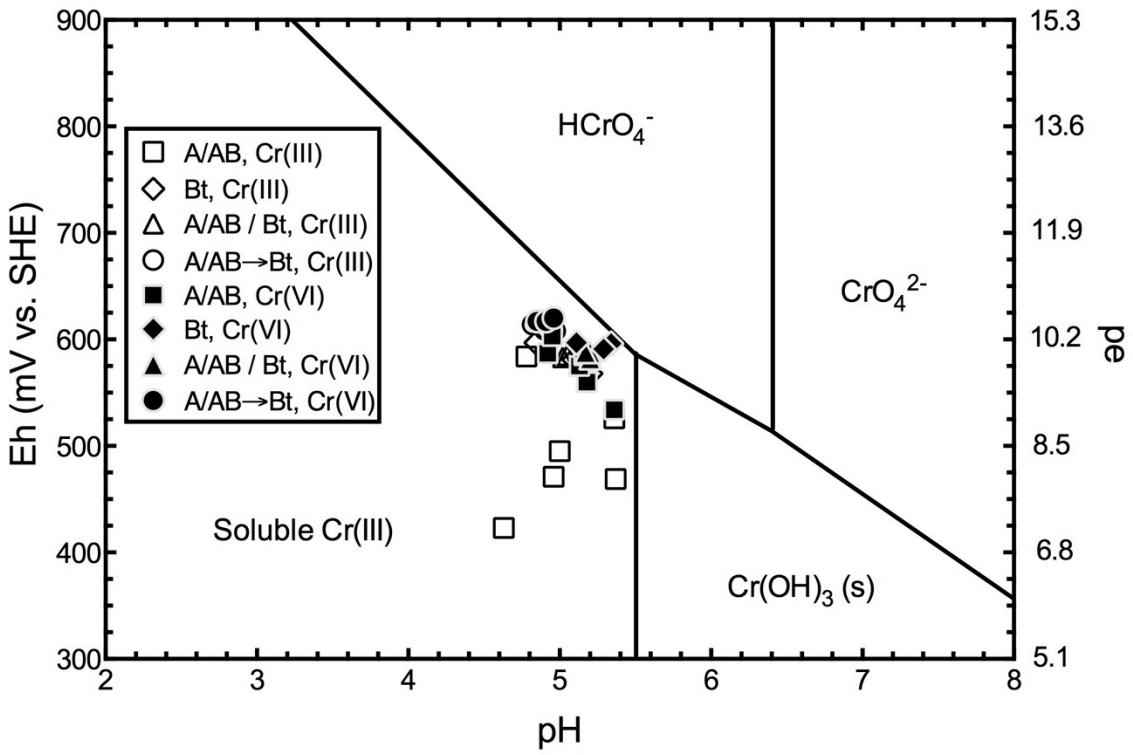

Figure A-6 Eh-pH diagram for Cr(III)-C(VI) redox and hydrolysis equilibria: Jackland A/AB and Bt horizon soil material leached with soluble Cr.

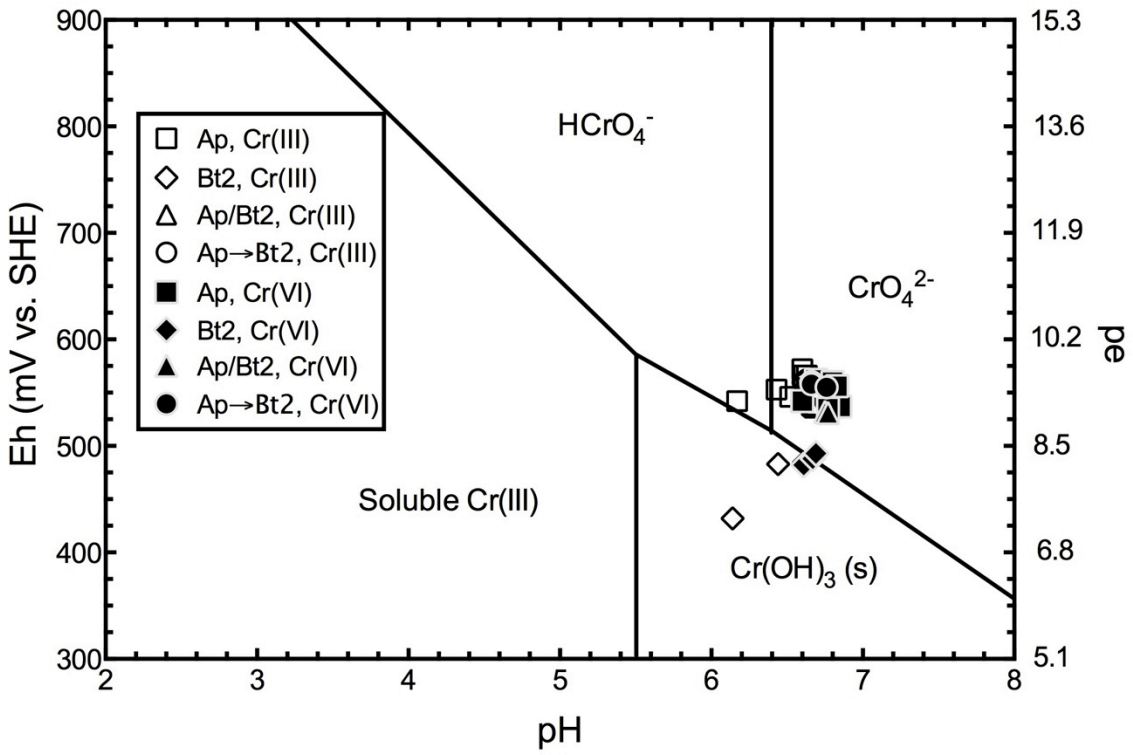

Figure A-7 Eh-pH diagram for Cr(III)-Cr(VI) redox and hydrolysis equilibria: Flickinger Ap and Bt2 horizon soil material leached with soluble Cr.

II. Chapter 3

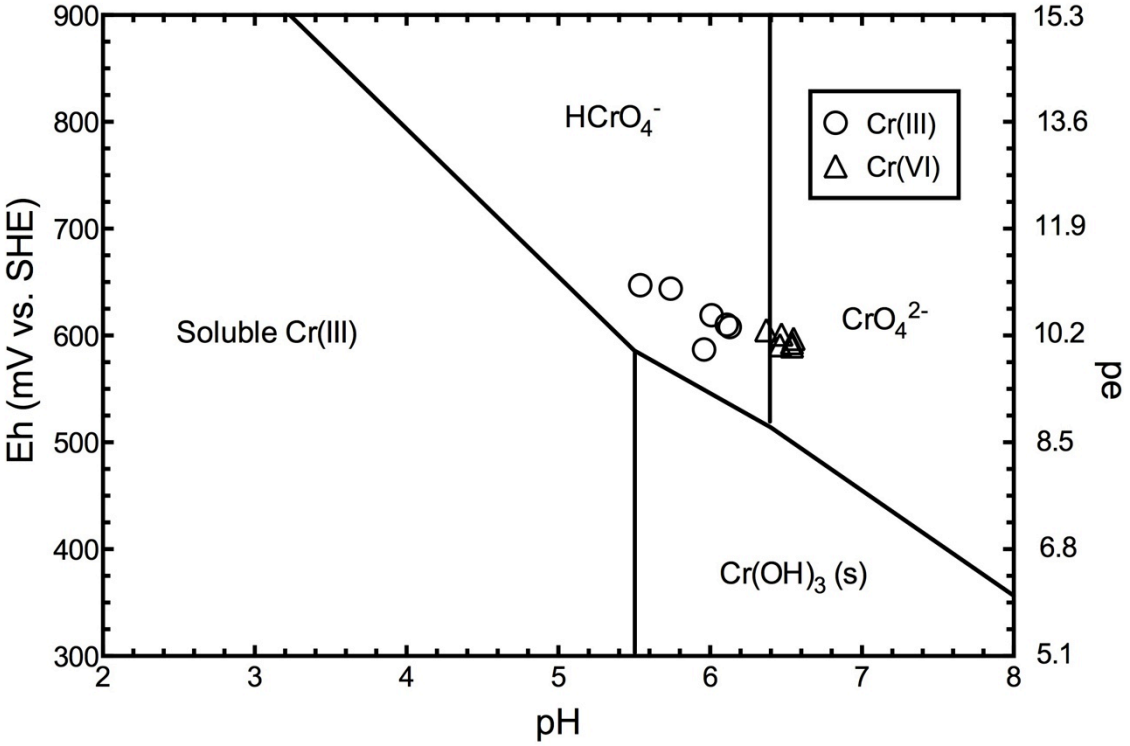

Figure A-8 Eh-pH diagram for Cr(III)-Cr(VI) redox and hydrolysis equilibria: Mn(III,IV)(hydr)oxide-coated sand leached with soluble Cr.

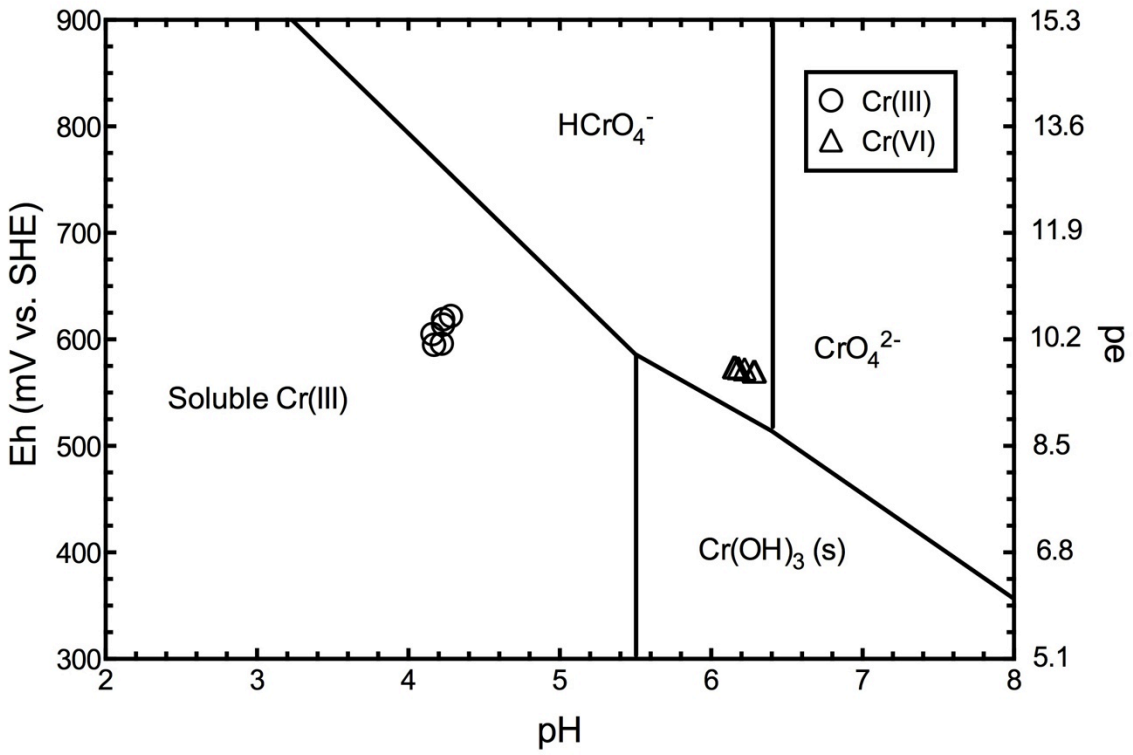

Figure A-9 Eh-pH diagram for Cr(III)-Cr(VI) redox and hydrolysis equilibria: Fe(III)(hydr)oxide-coated sand leached with soluble Cr.

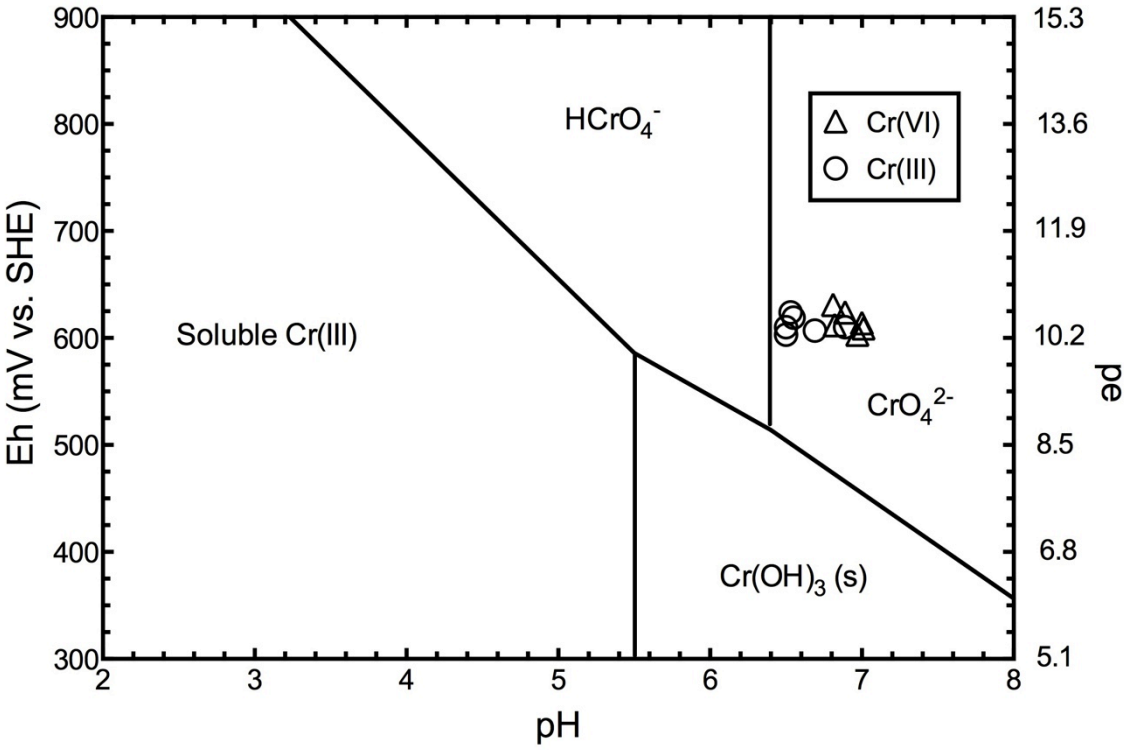

Figure A-10 Eh-pH diagram for Cr(III)-Cr(VI) redox and hydrolysis equilibria: Mixed Fe(III)-Mn(III,IV)(hydr)oxide-coated sand leached with soluble Cr.

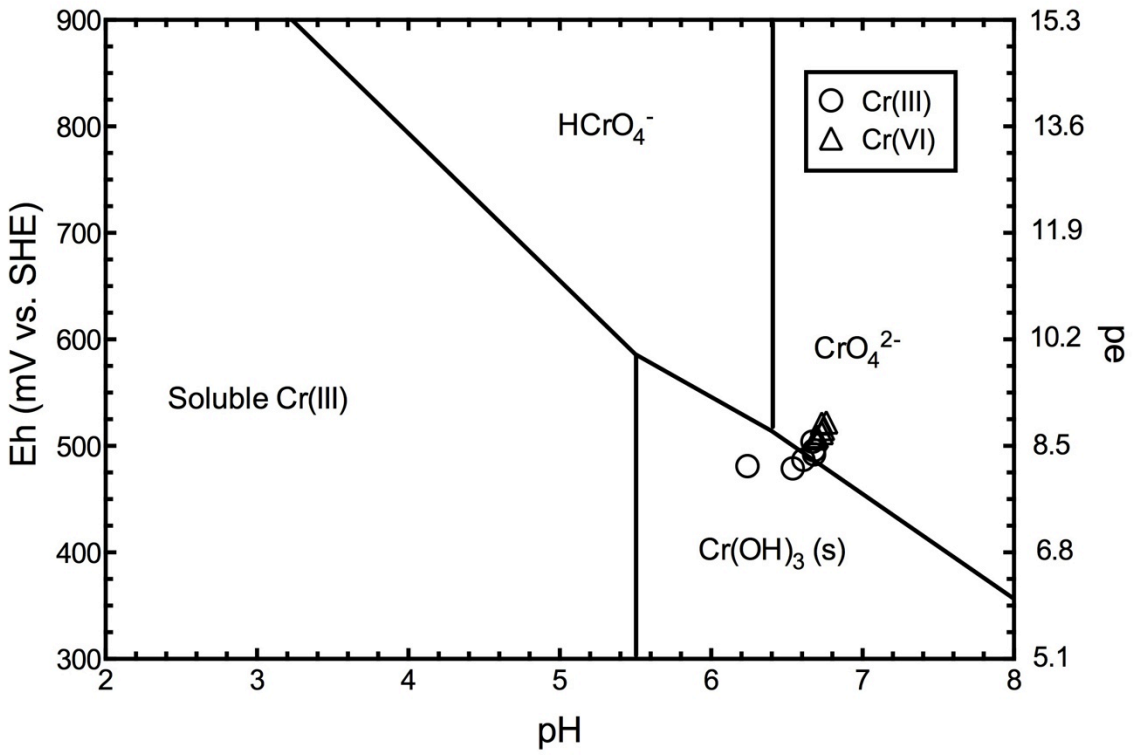

Figure A-11 Eh-pH diagram for Cr(III)-Cr(VI) redox and hydrolysis equilibria: Flickinger Bt2 horizon soil material leached with soluble Cr.

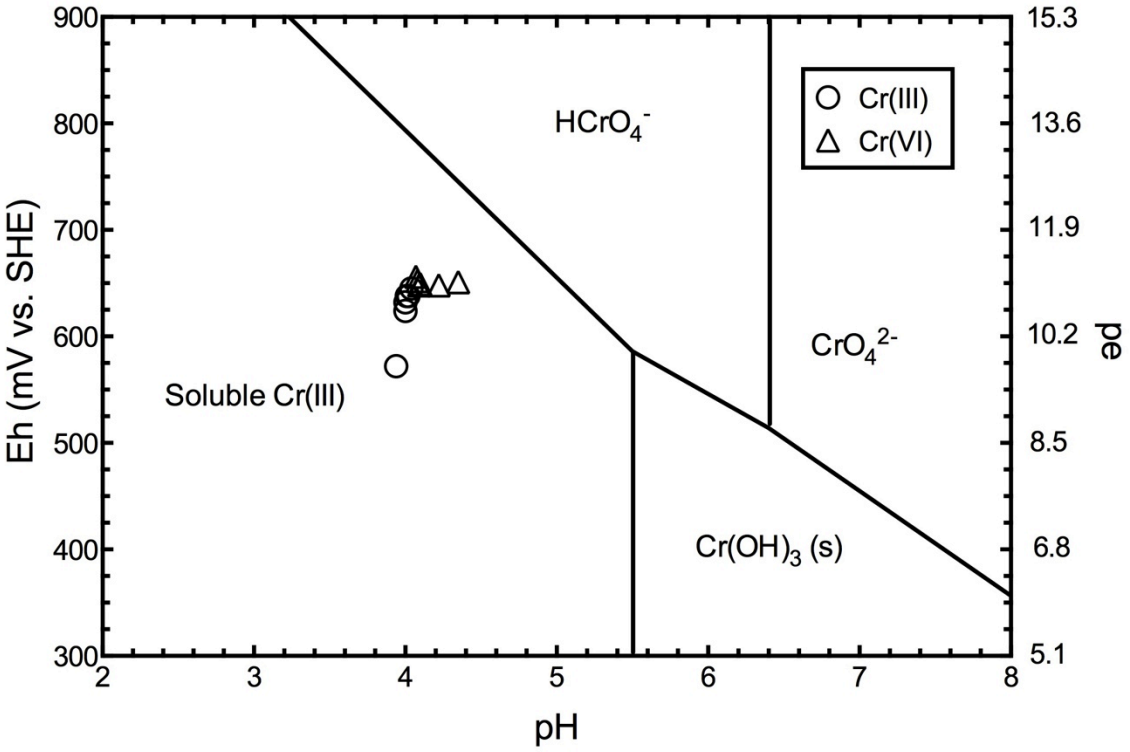

Figure A-12 Eh-pH diagram for Cr(III)-Cr(VI) redox and hydrolysis equilibria: Russett Bt horizon soil material leached with soluble Cr.

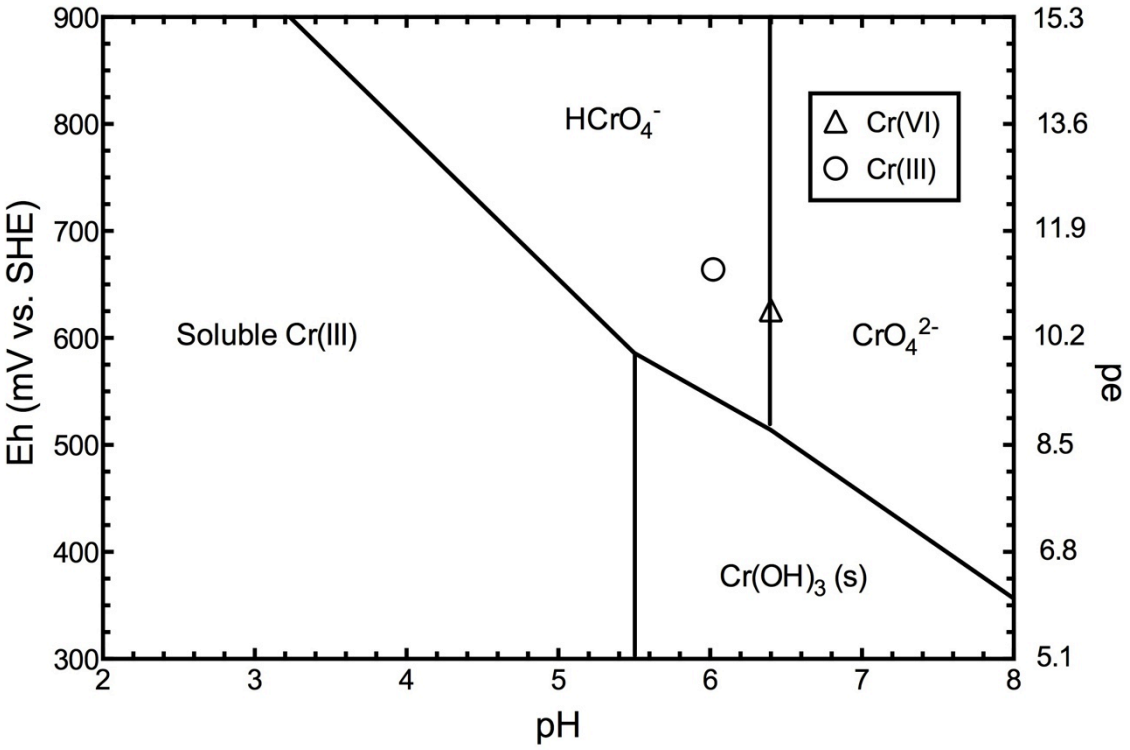

Figure A-13 Eh-pH diagram for Cr(III)-Cr(VI) redox and hydrolysis equilibria: Fungal Mn(III,IV)(hydr)oxides leached with soluble Cr.

Appendix B

Soil Sampling Photographs and GPS Data

I. Unicorn soil

Figure B-1 Unicorn soil Google Earth GPS image.

Figure B-2 Unicorn soil profile photograph.

II. Glenelg soil

Figure B-3 Glenelg soil Google Earth GPS image.

Figure B-4 Glenelg soil profile photograph.

III. Atsion soil

Figure B-5 Atsion soil Google Earth GPS image.

Figure B-6 Atsion soil profile photograph.

IV. Collington soil

Figure B-7 Collington soil Google Earth GPS image.

Figure B-8 Collington soil profile photograph.

V. Russett soil

Figure B-9 Russett soil Google Earth GPS image.

Figure B-10 Russett soil profile photograph.

VI. Jackland soil

Figure B-11 Jackland soil Google Earth GPS image.

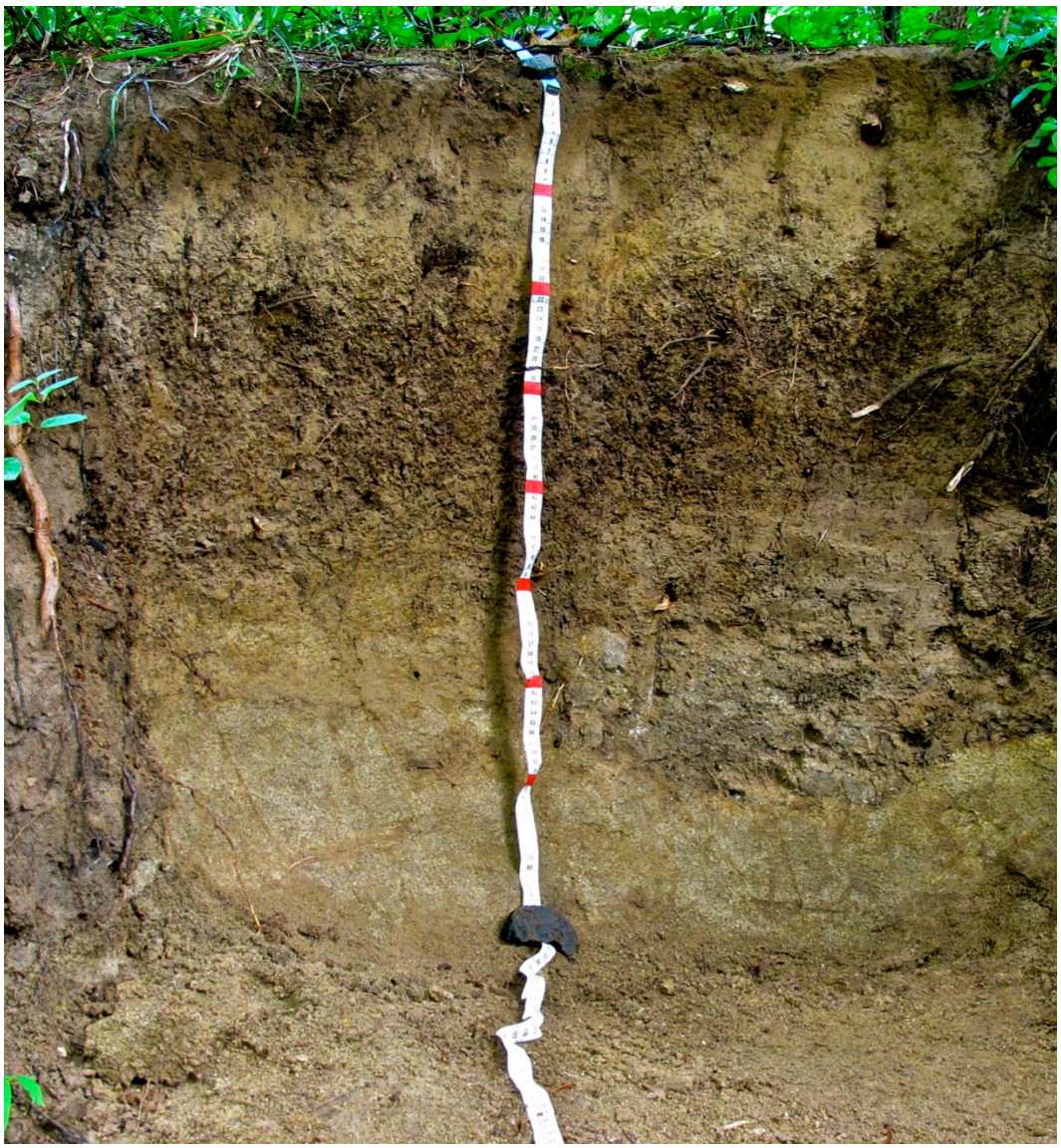

Figure B-12 Jackland soil profile photograph.

VII. Flickinger soil

Figure B-13 Flickinger soil Google Earth GPS image.

Figure B-14 Flickinger soil profile photograph.

Appendix C

Raw Cr speciation data

I. Chapter 2

Table C-1 Unicorn soil leached with $Cr(NO_3)_3$

							Cr Leaching				Phosphate Leaching			
Treatment	Ap Field Moist Mass (g)	Ap Dry Mass (g)	Bt Field Moist Mass (g)	Bt Dry Mass (g)	pH	Eh (mV)	Soluble Cr(VI) Abs.	Soluble Cr(VI) Conc. (mg/L)	Total Soluble Cr Abs.	Total Soluble Cr Conc. (mg/L)	Residual Liquid (mL)	De-sorbed Cr(VI) Abs.	De-sorbed Cr(VI) Conc. (mg/L)	Adsorbed Cr(VI) Conc. (mg/L)
Ap	2.091	2.001	NA	NA	5.36	567	0.002	0.01	0.006	0.09	3.655	0.002	0.01	0.01
Ap	2.090	2.000	NA	NA	4.84	609	0.001	0.005	0.016	0.24	3.161	0.001	0.01	0.005
Ap	2.090	2.000	NA	NA	4.67	619	0.003	0.02	0.064	1.0	1.585	0.001	0.005	0.005
Ap	2.082	1.992	NA	NA	3.9	618	0.001	0.00	0.022	0.35	1.208	0.002	0.002	0.002
Ap	2.092	2.002	NA	NA	3.89	652	0.001	0.00	0.074	1.2	1.856	0.001	0.00	0.00
Ap	2.087	1.997	NA	NA	3.95	675	0.002	0.002	0.072	1.2	1.394	0.002	0.002	0.002
Bt	NA	NA	2.324	2.003	4.06	652	0.000	0.02	0.008	0.1	2.529	0.000	0.02	0.02
Bt	NA	NA	2.323	2.003	4.03	663	0.000	0.02	0.025	0.40	1.971	0.000	0.02	0.02
Bt	NA	NA	2.322	2.002	4.07	673	0.000	0.02	0.010	0.16	2.984	0.000	0.02	0.02
Ap/Bt	2.082	1.994	2.327	2.006	3.87	492	0.000	0.00	0.003	0.00	4.842	0.000	0.00	0.00
Ap/Bt	2.092	2.004	2.319	1.999	3.85	494	0.000	0.00	0.002	0.00	4.902	0.001	0.00	0.003
Ap/Bt	2.094	2.006	2.322	2.002	3.9	489	0.000	0.00	0.002	0.00	4.787	0.000	0.00	0.00
Ap→Bt	2.082	1.992	1.161	1.001	3.98	691	0.002	0.002	0.007	0.1	1.269	0.002	0.002	0.006
Ap→Bt	2.092	2.002	1.167	1.006	3.91	694	0.002	0.002	0.026	0.41	0.829	0.002	0.002	0.002
Ap→Bt	2.087	1.997	1.160	1.000	3.88	699	0.003	0.009	0.015	0.23	0.937	0.003	0.009	0.01

Table C-2 Unicorn soil leached with K_2CrO_4

							Cr Leaching				Phosphate Leaching			
Treatment	Ap Field Moist Mass (g)	Ap Dry Mass (g)	Bt Field Moist Mass (g)	Bt Dry Mass (g)	pH	Eh (mV)	Soluble Cr(VI) Abs.	Soluble Cr(VI) Conc. (mg/L)	Total Soluble Cr Abs.	Total Soluble Cr Conc. (mg/L)	Residual Liquid (mL)	De-sorbed Cr(VI) Abs.	De-sorbed Cr(VI) Conc. (mg/L)	Adsorbed Cr(VI) Conc. (mg/L)
Ap	2.091	2.001	NA	NA	5.09	598	0.340	2.61	0.145	2.51	2.059	0.018	0.14	0.0084
Ap	2.094	2.004	NA	NA	5.05	603	0.356	2.73	0.149	2.59	2.021	0.018	0.14	0.0046
Ap	2.094	2.004	NA	NA	5.14	603	0.355	2.72	0.146	2.53	2.063	0.018	0.14	0.0022
Ap	2.086	1.996	NA	NA	4.81	625	0.350	2.50	0.151	2.70	0.901	0.014	0.088	0.034
Ap	2.089	1.999	NA	NA	4.88	631	0.338	2.42	0.147	2.62	0.783	0.018	0.12	0.072
Ap	2.095	2.005	NA	NA	4.5	666	0.351	2.51	0.149	2.66	1.175	0.022	0.15	0.076
Bt	NA	NA	2.320	2.000	4.13	675	0.063	0.46	0.030	0.48	1.642	0.258	1.90	1.96
Bt	NA	NA	2.325	2.004	4.12	679	0.045	0.34	0.022	0.36	1.941	0.276	2.04	2.12
Bt	NA	NA	2.318	1.998	4.43	672	0.225	1.65	0.109	1.70	2.150	0.098	0.71	0.66
Ap/Bt	2.091	2.003	2.324	2.003	3.87	489	0.040	0.55	0.041	0.83	6.251	0.105	0.125	1.25
Ap/Bt	2.086	1.998	2.324	2.003	3.87	490	0.021	0.28	0.022	0.41	5.796	0.123	0.149	1.49
Ap/Bt	2.082	1.994	2.324	2.003	3.87	491	0.016	0.21	0.018	0.32	7.041	0.120	0.141	1.41
Ap→Bt	2.086	1.996	1.158	0.998	4.05	695	0.207	1.48	0.090	1.5	1.651	0.121	0.857	0.874
Ap→Bt	2.089	1.999	1.156	0.997	4.18	692	0.252	1.80	0.111	1.91	3.591	0.088	0.62	0.55
Ap→Bt	2.095	2.005	1.161	1.001	4.11	697	0.236	1.68	0.102	1.74	0.784	0.086	0.61	0.72

Table C-3 Glenelg soil leached with $Cr(NO_3)_3$

Treatment	Ap Field Moist Mass (g)	Ap Dry Mass (g)	Bt2 Field Moist Mass (g)	Bt2 Dry Mass (g)	pH	Eh (mV)	Cr Leaching				Phosphate Leaching			
							Soluble Cr(VI) Abs.	Soluble Cr(VI) Conc. (mg/L)	Total Soluble Cr Abs.	Total Soluble Cr Conc. (mg/L)	Residual Liquid (mL)	De-sorbed Cr(VI) Abs.	De-sorbed Cr(VI) Conc. (mg/L)	Adsorbed Cr(VI) Conc. (mg/L)
Ap	2.261	2.001	NA	NA	5.05	581	0.026	0.20	0.009	0.1	2.498	0.026	0.20	0.20
Ap	2.265	2.004	NA	NA	5.21	586	0.016	0.12	0.007	0.1	3.984	0.030	0.23	0.24
Ap	2.260	2.000	NA	NA	5.3	584	0.019	0.14	0.008	0.1	3.382	0.028	0.21	0.22
Ap	2.254	1.998	NA	NA	4.53	542	0.007	0.03	0.008	0.1	1.651	0.016	0.098	0.10
Ap	2.252	1.996	NA	NA	4.37	559	0.013	0.077	0.009	0.1	1.456	0.016	0.098	0.099
Ap	2.262	2.005	NA	NA	4.77	573	0.013	0.077	0.017	0.26	1.837	0.012	0.069	0.069
Bt2	NA	NA	2.447	1.998	5.65	625	0.000	0.02	0.000	0.003	2.444	0.002	0.04	0.04
Bt2	NA	NA	2.449	1.999	5.37	624	0.000	0.02	0.000	0.003	1.911	0.000	0.02	0.02
Bt2	NA	NA	2.449	1.999	5.51	625	0.000	0.02	0.000	0.003	2.661	0.001	0.03	0.03
Ap/Bt2	2.254	1.998	2.454	2.003	5.49	425	0.000	0.00	0.002	0.00	5.697	0.011	0.13	0.13
Ap/Bt2	2.251	1.996	2.447	1.998	5.54	405	0.001	0.004	0.004	0.01	5.134	0.016	0.19	0.19
Ap/Bt2	2.252	1.996	2.448	1.998	5.6	402	0.000	0.00	0.002	0.00	6.331	0.015	0.17	0.17
Ap→Bt2	2.254	1.998	1.222	0.998	5.66	553	0.004	0.01	0.001	0.02	1.563	0.015	0.091	0.30
Ap→Bt2	2.252	1.996	1.220	0.996	5.55	550	0.005	0.02	0.003	0.05	1.305	0.010	0.055	0.26
Ap→Bt2	2.262	2.005	1.225	1.000	5.52	551	0.003	0.004	0.002	0.04	1.529	0.010	0.055	0.20

Table C-4 Glenelg soil leached with K_2CrO_4

Treatment	Ap Field Moist Mass (g)	Ap Dry Mass (g)	Bt2 Field Moist Mass (g)	Bt2 Dry Mass (g)	pH	Eh (mV)	Cr Leaching				Phosphate Leaching			
							Soluble Cr(VI) Abs.	Soluble Cr(VI) Conc. (mg/L)	Total Soluble Cr Abs.	Total Soluble Cr Conc. (mg/L)	Residual Liquid (mL)	De-sorbed Cr(VI) Abs.	De-sorbed Cr(VI) Conc. (mg/L)	Adsorbed Cr(VI) Conc. (mg/L)
Ap	2.260	2.000	NA	NA	5.40	584	0.365	2.80	0.156	2.73	2.205	0.018	0.14	0.00
Ap	2.260	2.000	NA	NA	5.37	582	0.356	2.73	0.155	2.71	1.501	0.013	0.097	0.00
Ap	2.264	2.004	NA	NA	5.39	580	0.353	2.70	0.156	2.73	1.842	0.015	0.11	0.00
Ap	2.256	2.000	NA	NA	5.71	557	0.319	2.33	0.167	2.69	2.025	0.043	0.29	0.19
Ap	2.256	2.000	NA	NA	5.65	552	0.336	2.46	0.166	2.67	1.560	0.037	0.25	0.16
Ap	2.264	2.007	NA	NA	5.83	545	0.328	2.40	0.167	2.69	2.350	0.039	0.27	0.14
Bt2	NA	NA	2.446	1.997	6.05	603	0.203	1.48	0.094	1.5	2.077	0.130	0.944	0.916
Bt2	NA	NA	2.453	2.002	6.02	604	0.119	0.864	0.050	0.80	2.542	0.224	1.64	1.69
Bt2	NA	NA	2.448	1.998	5.96	592	0.058	0.43	0.027	0.44	3.133	0.268	1.97	2.10
Ap/Bt2	2.258	2.002	2.453	2.002	5.74	393	0.039	0.53	0.037	0.74	5.462	0.097	1.2	1.1
Ap/Bt2	2.254	1.998	2.449	1.999	5.79	392	0.064	0.88	0.061	1.3	5.772	0.080	0.96	0.85
Ap/Bt2	2.254	1.998	2.446	1.997	5.83	389	0.071	0.98	0.068	1.4	4.482	0.075	0.93	0.83
Ap→Bt2	2.256	2.000	1.239	1.011	5.52	551	0.094	0.67	0.045	0.68	2.546	0.217	1.57	2.07
Ap→Bt2	2.256	2.000	1.226	1.001	5.79	536	0.223	1.61	0.110	1.71	2.826	0.097	0.69	0.88
Ap→Bt2	2.264	2.007	1.232	1.006	5.87	537	0.191	1.38	0.093	1.43	1.162	0.111	0.790	1.04

Table C-5 Atsion soil leached with $Cr(NO_3)_3$

Treatment	O/A Field Moist Mass (g)	O/A Dry Mass (g)	Bh Field Moist Mass (g)	Bh Dry Mass (g)	pH	Eh (mV)	Cr Leaching				Phosphate Leaching			
							Soluble Cr(VI) Abs.	Soluble Cr(VI) Conc. (mg/L)	Total Soluble Cr Abs.	Total Soluble Cr Conc. (mg/L)	Residual Liquid (mL)	De-sorbed Cr(VI) Abs.	De-sorbed Cr(VI) Conc. (mg/L)	Adsorbed Cr(VI) Conc. (mg/L)
O/A	2.340	2.000	NA	NA	3.36	656	0	0.00	0.003	0.04	2.413	0.002	0.01	0.01
O/A	2.341	2.001	NA	NA	3.54	654	0.001	0.005	0.003	0.04	2.730	0.001	0.005	0.005
O/A	2.343	2.003	NA	NA	3.51	653	0.001	0.005	0.006	0.09	5.541	0.001	0.005	0.005
O/A	2.332	1.993	NA	NA	3.52	676	0.000	0.00	0.025	0.38	2.346	0.002	0.00	0.00
O/A	2.388	2.041	NA	NA	3.50	684	0.000	0.00	0.014	0.21	2.236	0.002	0.00	0.00
O/A	2.352	2.010	NA	NA	3.53	689	0.001	0.00	0.015	0.23	2.723	0.003	0.004	0.004
Bh	NA	NA	2.608	2.000	3.90	690	0.000	0.02	0.002	0.04	2.031	0.001	0.03	0.03
Bh	NA	NA	2.608	2.000	3.85	695	0.000	0.02	0.002	0.04	1.821	0.001	0.03	0.03
Bh	NA	NA	2.606	1.998	3.85	696	0.000	0.02	0.003	0.05	2.191	0.000	0.02	0.02
O/A / Bh	2.338	1.998	2.606	1.998	3.35	486	0.000	0.00	0.004	0.01	8.846	0.001	0.00	0.003
O/A / Bh	2.335	1.996	2.608	2.000	3.39	493	0.000	0.00	0.004	0.01	7.228	0.000	0.00	0.00
O/A / Bh	2.344	2.003	2.605	1.998	3.38	495	0.000	0.00	0.003	0.00	8.830	0.001	0.00	0.003
O/A→Bh	2.332	1.993	1.308	1.003	3.82	692	0.000	0.00	0.014	0.21	2.521	0.000	0.00	0.00
O/A→Bh	2.388	2.041	1.305	1.001	3.89	691	0.000	0.00	0.004	0.07	1.656	0.002	0.00	0.00
O/A→Bh	2.352	2.010	1.298	0.995	3.93	679	0.000	0.00	0.003	0.05	1.456	0.001	0.00	0.004

Table C-6 Atsion soil leached with K_2CrO_4

Treatment	O/A Field Moist Mass (g)	O/A Dry Mass (g)	Bh Field Moist Mass (g)	Bh Dry Mass (g)	pH	Eh (mV)	Cr Leaching				Phosphate Leaching			
							Soluble Cr(VI) Abs.	Soluble Cr(VI) Conc. (mg/L)	Total Soluble Cr Abs.	Total Soluble Cr Conc. (mg/L)	Residual Liquid (mL)	De-sorbed Cr(VI) Abs.	De-sorbed Cr(VI) Conc. (mg/L)	Adsorbed Cr(VI) Conc. (mg/L)
O/A	2.344	2.003	NA	NA	4.37	611	0.349	2.67	0.133	2.28	2.267	0.011	0.082	0.00
O/A	2.341	2.001	NA	NA	4.41	617	0.301	2.31	0.120	2.04	4.835	0.006	0.04	0.00
O/A	2.342	2.002	NA	NA	4.57	606	0.349	2.67	0.120	2.04	2.516	0.006	0.04	0.00
O/A	2.349	2.008	NA	NA	3.62	689	0.279	2.03	0.147	2.34	1.775	0.007	0.03	0.00
O/A	2.333	1.994	NA	NA	3.69	691	0.308	2.25	0.158	2.53	2.293	0.011	0.062	0.00
O/A	2.386	2.039	NA	NA	3.60	697	0.266	1.93	0.143	2.27	3.887	0.017	0.11	0.00
Bh	NA	NA	2.604	1.997	3.83	697	0.309	2.29	0.146	2.25	1.782	0.011	0.10	0.00
Bh	NA	NA	2.606	1.998	3.90	697	0.307	2.28	0.146	2.25	2.381	0.012	0.11	0.00
Bh	NA	NA	2.605	1.998	3.87	699	0.310	2.30	0.144	2.22	2.522	0.014	0.12	0.00
O/A / Bh	2.34	2.000	2.607	1.999	3.47	500	0.078	1.1	0.084	1.8	6.452	0.002	0.02	0.00
O/A / Bh	2.335	1.996	2.61	2.002	3.48	505	0.097	1.3	0.104	2.22	6.302	0.006	0.06	0.00
O/A / Bh	2.336	1.997	2.607	1.999	3.58	500	0.104	1.44	0.109	2.33	6.389	0.009	0.10	0.00
O/A→Bh	2.349	2.008	1.311	1.005	3.94	682	0.258	1.87	0.130	2.05	1.071	0.008	0.04	0.00
O/A→Bh	2.333	1.994	1.316	1.009	3.93	685	0.284	2.07	0.143	2.27	1.609	0.012	0.069	0.00
O/A→Bh	2.386	2.039	1.315	1.008	3.89	685	0.261	1.90	0.134	2.12	1.886	0.016	0.098	0.00

Table C-7 Collington soil leached with $Cr(NO_3)_3$

Treatment	A Field Moist Mass (g)	A Dry Mass (g)	Bt Field Moist Mass (g)	Bt Dry Mass (g)	pH	Eh (mV)	Cr Leaching				Phosphate Leaching			
							Soluble Cr(VI) Abs.	Soluble Cr(VI) Conc. (mg/L)	Total Soluble Cr Abs.	Total Soluble Cr Conc. (mg/L)	Residual Liquid (mL)	De-sorbed Cr(VI) Abs.	De-sorbed Cr(VI) Conc. (mg/L)	Adsorbed Cr(VI) Conc. (mg/L)
A	2.237	1.997	NA	NA	3.76	640	0.000	0.00	0.013	0.16	2.038	0.003	0.02	0.02
A	2.246	2.005	NA	NA	3.90	633	0.001	0.00	0.013	0.16	1.287	0.002	0.009	0.009
A	2.243	2.002	NA	NA	3.87	640	0.000	0.00	0.039	0.51	1.375	0.002	0.009	0.009
A	2.243	2.002	NA	NA	4.17	499	0.001	0.02	0.017	0.22	1.004	0.000	0.01	0.01
A	2.244	2.003	NA	NA	4.14	525	0.000	0.01	0.007	0.09	1.789	0.000	0.01	0.01
A	2.241	2.000	NA	NA	4.00	516	0.000	0.01	0.037	0.48	2.731	0.000	0.01	0.01
Bt	NA	NA	2.404	2.003	3.56	710	0.010	0.093	0.042	0.67	2.020	0.000	0.02	0.02
Bt	NA	NA	2.401	2.001	3.61	711	0.000	0.02	0.038	0.61	2.318	0.000	0.02	0.025
Bt	NA	NA	2.402	2.002	3.48	716	0.000	0.02	0.013	0.21	3.345	0.000	0.02	0.025
A/Bt	2.239	1.999	2.418	2.015	3.53	672	0.000	0.00	0.003	0.04	3.243	0.002	0.009	0.01
A/Bt	2.257	2.015	2.398	1.998	3.53	671	0.000	0.00	0.012	0.15	3.761	0.001	0.002	0.002
A/Bt	2.243	2.002	2.392	1.993	3.59	667	0.007	0.04	0.008	0.1	3.646	0.001	0.002	0.000
A→Bt	2.243	2.002	1.206	1.005	4.36	658	-0.001	0.004	0.010	0.13	1.625	0.002	0.02	0.04
A→Bt	2.244	2.003	1.203	1.003	4.33	659	0.000	0.01	0.002	0.02	1.346	0.002	0.02	0.04
A→Bt	2.241	2.000	1.200	1.000	3.93	679	-0.001	0.004	0.007	0.09	1.452	0.002	0.02	0.04

Table C-8 Collington soil leached with K_2CrO_4

Treatment	A Field Moist Mass (g)	A Dry Mass (g)	Bt Field Moist Mass (g)	Bt Dry Mass (g)	pH	Eh (mV)	Cr Leaching				Phosphate Leaching			
							Soluble Cr(VI) Abs.	Soluble Cr(VI) Conc. (mg/L)	Total Soluble Cr Abs.	Total Soluble Cr Conc. (mg/L)	Residual Liquid (mL)	De-sorbed Cr(VI) Abs.	De-sorbed Cr(VI) Conc. (mg/L)	Adsorbed Cr(VI) Conc. (mg/L)
A	2.240	2.000	NA	NA	4.66	624	0.355	2.55	0.196	2.78	1.360	0.014	0.089	0.005
A	2.242	2.002	NA	NA	4.12	639	0.346	2.48	0.192	2.72	1.465	0.018	0.12	0.029
A	2.245	2.004	NA	NA	4.01	648	0.347	2.49	0.192	2.72	1.312	0.015	0.10	0.017
A	2.243	2.003	NA	NA	4.58	611	0.348	2.43	0.186	2.62	1.970	0.019	0.14	0.023
A	2.241	2.001	NA	NA	4.47	640	0.353	2.46	0.189	2.67	1.765	0.016	0.12	0.013
A	2.241	2.001	NA	NA	4.64	638	0.353	2.46	0.188	2.66	2.099	0.021	0.15	0.028
Bt	NA	NA	2.399	1.999	3.52	717	0.032	0.25	0.017	0.28	3.221	0.247	1.81	1.94
Bt	NA	NA	2.405	2.004	3.52	721	0.019	0.16	0.010	0.16	2.344	0.273	2.01	2.12
Bt	NA	NA	2.402	2.002	3.56	721	0.055	0.41	0.028	0.45	2.269	0.254	1.87	1.95
A/Bt	2.237	1.997	2.400	2.000	3.54	670	0.128	0.896	0.067	0.89	3.761	0.211	1.47	1.52
A/Bt	2.240	2.000	2.392	1.993	3.75	663	0.215	1.52	0.115	1.56	3.194	0.082	0.55	0.47
A/Bt	2.255	2.013	2.407	2.006	3.63	668	0.157	1.10	0.083	1.1	3.427	0.173	1.19	1.20
A→Bt	2.243	2.003	1.202	1.002	4.49	654	0.226	1.56	0.120	1.64	1.873	0.079	0.54	0.46
A→Bt	2.241	2.001	1.202	1.002	4.28	663	0.060	0.41	0.033	0.43	1.703	0.242	1.66	1.78
A→Bt	2.241	2.001	1.205	1.004	4.46	661	0.106	0.720	0.056	0.74	1.474	0.204	1.40	1.47

Table C-9 Russett soil leached with $Cr(NO_3)_3$

Treatment	Ap Field Moist Mass (g)	Ap Dry Mass (g)	Bt Field Moist Mass (g)	Bt Dry Mass (g)	pH	Eh (mV)	Cr Leaching				Phosphate Leaching			
							Soluble Cr(VI) Abs.	Soluble Cr(VI) Conc. (mg/L)	Total Soluble Cr Abs.	Total Soluble Cr Conc. (mg/L)	Residual Liquid (mL)	De-sorbed Cr(VI) Abs.	De-sorbed Cr(VI) Conc. (mg/L)	Adsorbed Cr(VI) Conc. (mg/L)
Ap	2.158	1.998	NA	NA	5.27	456	0.000	0.000	0.063	0.83	2.025	0.001	0.002	0.002
Ap	2.175	2.014	NA	NA	5.37	458	0.002	0.003	0.036	0.47	1.203	0.002	0.009	0.009
Ap	2.174	2.013	NA	NA	4.86	479	0.003	0.01	0.049	0.64	0.896	0.001	0.002	0.002
Ap	2.163	2.003	NA	NA	4.58	666	0.004	0.02	0.007	0.1	1.536	0.005	0.02	0.02
Ap	2.156	1.996	NA	NA	4.65	665	0.003	0.009	0.012	0.19	1.893	0.005	0.02	0.02
Ap	2.169	2.008	NA	NA	4.40	678	0.003	0.009	0.028	0.44	2.055	0.002	0.002	0.002
Bt	NA	NA	2.261	2.001	4.03	651	0.000	0.005	0.025	0.33	1.476	0.002	0.02	0.02
Bt	NA	NA	2.260	2.000	4.05	655	0.000	0.005	0.106	1.45	1.631	0.001	0.01	0.01
Bt	NA	NA	2.256	1.996	4.02	660	0.000	0.005	0.077	1.0	1.671	0.001	0.01	0.01
Ap/Bt	2.152	1.993	2.272	2.011	4.19	603	0.000	0.000	0.003	0.04	2.820	0.006	0.04	0.04
Ap/Bt	2.155	1.995	2.267	2.006	4.15	611	0.001	0.000	0.025	0.32	2.574	0.004	0.02	0.03
Ap/Bt	2.159	1.999	2.260	2.000	4.26	552	0.000	0.000	0.037	0.48	2.615	0.002	0.009	0.01
Ap→Bt	2.163	2.003	1.128	0.998	4.14	687	0.001	0.000	0.004	0.06	1.310	0.002	0.002	0.03
Ap→Bt	2.156	1.996	1.135	1.004	3.98	684	0.001	0.000	0.003	0.05	1.852	0.003	0.009	0.03
Ap→Bt	2.169	2.008	1.137	1.006	4.05	683	0.001	0.000	0.012	0.19	1.161	0.002	0.002	0.003

Table C-10 Russett soil leached with K_2CrO_4

Treatment	Ap Field Moist Mass (g)	Ap Dry Mass (g)	Bt Field Moist Mass (g)	Bt Dry Mass (g)	pH	Eh (mV)	Cr Leaching				Phosphate Leaching			
							Soluble Cr(VI) Abs.	Soluble Cr(VI) Conc. (mg/L)	Total Soluble Cr Abs.	Total Soluble Cr Conc. (mg/L)	Residual Liquid (mL)	De-sorbed Cr(VI) Abs.	De-sorbed Cr(VI) Conc. (mg/L)	Adsorbed Cr(VI) Conc. (mg/L)
Ap	2.161	2.001	NA	NA	5.61	518	0.355	2.54	0.194	2.75	0.915	0.010	0.062	0.0053
Ap	2.163	2.003	NA	NA	5.67	506	0.355	2.54	0.193	2.73	1.674	0.015	0.096	0.000
Ap	2.161	2.001	NA	NA	5.52	509	0.350	2.51	0.190	2.69	2.190	0.022	0.14	0.013
Ap	2.166	2.006	NA	NA	5.01	645	0.342	2.45	0.146	2.60	2.443	0.025	0.17	0.028
Ap	2.152	1.993	NA	NA	5.20	639	0.346	2.48	0.147	2.62	1.462	0.016	0.10	0.016
Ap	2.168	2.007	NA	NA	5.22	638	0.341	2.44	0.146	2.60	2.708	0.030	0.20	0.052
Bt	NA	NA	2.260	2.000	4.15	659	0.075	0.53	0.040	0.53	2.021	0.266	1.90	1.97
Bt	NA	NA	2.260	2.000	4.20	658	0.151	1.07	0.079	1.1	1.623	0.210	1.49	1.51
Bt	NA	NA	2.262	2.002	4.91	639	0.231	1.65	0.119	1.64	1.613	0.121	0.85	0.82
Ap/Bt	2.161	2.001	2.258	1.998	4.15	605	0.144	1.01	0.079	1.1	2.452	0.211	1.47	1.52
Ap/Bt	2.165	2.005	2.253	1.994	4.12	616	0.108	0.753	0.059	0.78	4.510	NA*	NA*	NA*
Ap/Bt	2.156	1.996	2.263	2.003	4.28	614	0.206	1.46	0.111	1.50	2.449	0.156	1.07	1.02
Ap→Bt	2.166	2.006	1.125	0.996	4.18	682	0.236	1.68	0.103	1.76	1.269	0.083	0.58	0.54
Ap→Bt	2.152	1.993	1.133	1.003	4.19	685	0.221	1.58	0.096	1.6	2.086	0.119	0.843	0.782
Ap→Bt	2.168	2.007	1.130	1.000	4.25	685	0.237	1.69	0.101	1.72	1.605	0.099	0.70	0.67

Table C-11 Jackland soil leached with $Cr(NO_3)_3$

Treatment	A/AB Field Moist Mass (g)	A/AB Dry Mass (g)	Bt Field Moist Mass (g)	Bt Dry Mass (g)	pH	Eh (mV)	Cr Leaching				Phosphate Leaching			
							Soluble Cr(VI) Abs.	Soluble Cr(VI) Conc. (mg/L)	Total Soluble Cr Abs.	Total Soluble Cr Conc. (mg/L)	Residual Liquid (mL)	De-sorbed Cr(VI) Abs.	De-sorbed Cr(VI) Conc. (mg/L)	Adsorbed Cr(VI) Conc. (mg/L)
A/AB	2.250	2.000	NA	NA	4.63	423	0.000	0.002	0.060	0.86	1.706	0.031	0.22	0.23
A/AB	2.253	2.003	NA	NA	4.96	471	0.007	0.05	0.021	0.29	1.709	0.042	0.29	0.30
A/AB	2.253	2.003	NA	NA	5.00	495	0.011	0.078	0.011	0.15	1.711	0.055	0.38	0.40
A/AB	2.243	1.994	NA	NA	5.37	469	0.017	0.11	0.011	0.16	2.100	0.053	0.36	0.37
A/AB	2.265	2.013	NA	NA	5.36	526	0.016	0.11	0.008	0.1	1.854	0.060	0.41	0.42
A/AB	2.256	2.005	NA	NA	4.78	584	0.022	0.15	0.020	0.30	2.064	0.050	0.34	0.35
Bt	NA	NA	2.461	2.001	5.21	568	0.008	0.06	0.007	0.1	2.752	0.052	0.37	0.39
Bt	NA	NA	2.457	1.998	5.09	581	0.007	0.05	0.017	0.23	2.309	0.042	0.30	0.31
Bt	NA	NA	2.461	2.001	4.84	597	0.009	0.07	0.008	0.1	7.112	0.044	0.31	0.35
A/AB / Bt	2.254	2.004	2.463	2.002	5.02	583	0.007	0.05	0.004	0.05	3.938	0.060	0.42	0.45
A/AB / Bt	2.254	2.004	2.461	2.001	5.13	576	0.008	0.06	0.007	0.09	3.037	0.050	0.35	0.37
A/AB / Bt	2.251	2.001	2.463	2.002	5.05	585	0.009	0.06	0.018	0.25	3.081	0.054	0.38	0.40
A/AB→Bt	2.243	1.994	1.219	0.991	4.90	609	0.011	0.074	0.005	0.07	1.664	0.012	0.081	0.45
A/AB→Bt	2.265	2.013	1.245	1.012	4.97	608	0.011	0.074	0.005	0.07	1.903	0.006	0.04	0.46
A/AB→Bt	2.256	2.005	1.236	1.005	4.82	614	0.012	0.081	0.005	0.07	1.385	0.014	0.095	0.44

Table C-12 Jackland soil leached with K_2CrO_4

Treatment	A/AB Field Moist Mass (g)	A/AB Dry Mass (g)	Bt Field Moist Mass (g)	Bt Dry Mass (g)	pH	Eh (mV)	Cr Leaching				Phosphate Leaching			
							Soluble Cr(VI) Abs.	Soluble Cr(VI) Conc. (mg/L)	Total Soluble Cr Abs.	Total Soluble Cr Conc. (mg/L)	Residual Liquid (mL)	De-sorbed Cr(VI) Abs.	De-sorbed Cr(VI) Conc. (mg/L)	Adsorbed Cr(VI) Conc. (mg/L)
A/AB	2.251	2.001	NA	NA	5.36	534	0.273	1.91	0.151	2.31	1.803	0.068	0.47	0.41
A/AB	2.252	2.002	NA	NA	5.18	560	0.246	1.72	0.135	2.04	2.237	0.089	0.62	0.56
A/AB	2.253	2.003	NA	NA	5.13	575	0.257	1.80	0.140	2.12	1.665	0.099	0.69	0.64
A/AB	2.245	1.996	NA	NA	4.92	587	0.246	1.67	0.105	1.69	2.389	0.114	0.774	0.720
A/AB	2.250	2.000	NA	NA	5.16	585	0.277	1.88	0.121	1.97	1.755	0.087	0.59	0.53
A/AB	2.248	1.998	NA	NA	4.95	603	0.269	1.83	0.118	1.92	2.536	0.092	0.62	0.55
Bt	NA	NA	2.459	1.999	5.11	597	0.175	1.24	0.095	1.3	2.253	0.187	1.32	1.33
Bt	NA	NA	2.459	1.999	5.34	596	0.165	1.17	0.089	1.21	2.071	0.169	1.19	1.20
Bt	NA	NA	2.465	2.004	5.29	591	0.215	1.53	0.116	1.59	2.081	0.147	1.04	1.01
A/AB / Bt	2.252	2.002	2.460	2.000	5.20	582	0.200	1.39	0.103	1.52	3.397	0.150	1.04	1.01
A/AB / Bt	2.250	2.000	2.464	2.003	5.20	588	0.152	1.06	0.079	1.1	3.237	0.179	1.25	1.26
A/AB / Bt	2.251	2.001	2.460	2.000	5.17	588	0.175	1.22	0.092	1.3	3.652	0.156	1.09	1.07
A/AB→Bt	2.245	1.996	1.226	0.997	4.85	617	0.120	0.815	0.044	0.67	2.868	0.126	0.856	1.58
A/AB→Bt	2.250	2.000	1.230	1.000	4.91	617	0.137	0.930	0.050	0.77	1.160	0.132	0.896	1.43
A/AB→Bt	2.248	1.998	1.223	0.994	4.96	620	0.225	1.53	0.090	1.4	1.216	0.040	0.27	0.74

Table C-13 Flickinger soil leached with $Cr(NO_3)_3$

Treatment	Ap Field Moist Mass (g)	Ap Dry Mass (g)	Bt2 Field Moist Mass (g)	Bt2 Dry Mass (g)	pH	Eh (mV)	Cr Leaching				Phosphate Leaching			
							Soluble Cr(VI) Abs.	Soluble Cr(VI) Conc. (mg/L)	Total Soluble Cr Abs.	Total Soluble Cr Conc. (mg/L)	Residual Liquid (mL)	De-sorbed Cr(VI) Abs.	De-sorbed Cr(VI) Conc. (mg/L)	Adsorbed Cr(VI) Conc. (mg/L)
Ap	2.422	2.002	NA	NA	6.43	553	0.011	0.078	0.012	0.16	2.263	0.034	0.24	0.25
Ap	2.421	2.001	NA	NA	6.52	546	0.012	0.085	0.011	0.15	2.497	0.039	0.27	0.28
Ap	2.422	2.002	NA	NA	6.17	542	0.015	0.11	0.019	0.26	1.687	0.029	0.20	0.21
Ap	2.416	1.997	NA	NA	6.60	572	0.068	0.46	0.028	0.42	2.554	0.028	0.19	0.17
Ap	2.415	1.996	NA	NA	6.61	566	0.079	0.54	0.030	0.45	1.993	0.027	0.18	0.17
Ap	2.419	1.999	NA	NA	6.63	566	0.079	0.54	0.032	0.48	2.560	0.034	0.23	0.21
Bt2	NA	NA	2.834	2.003	6.14	432	0.023	0.16	0.024	0.32	2.542	0.094	0.66	0.69
Bt2	NA	NA	2.831	2.001	6.44	483	0.042	0.30	0.021	0.28	3.148	0.101	0.709	0.742
Bt2	NA	NA	2.827	1.998	6.61	484	0.019	0.14	0.009	0.1	2.938	0.150	1.06	1.13
Ap/Bt2	2.422	2.002	2.831	2.001	6.66	538	0.012	0.085	0.005	0.07	5.891	0.051	0.35	0.39
Ap/Bt2	2.421	2.001	2.835	2.004	6.67	537	0.007	0.05	0.003	0.04	6.670	0.051	0.35	0.41
Ap/Bt2	2.423	2.002	2.833	2.002	6.68	536	0.008	0.06	0.004	0.05	6.230	0.064	0.44	0.50
Ap→Bt2	2.416	1.997	1.417	1.001	6.63	563	0.028	0.19	0.008	0.1	1.967	0.037	0.25	0.43
Ap→Bt2	2.415	1.996	1.415	1.000	6.60	560	0.040	0.27	0.014	0.21	3.062	0.026	0.18	0.33
Ap→Bt2	2.419	1.999	1.407	0.994	6.61	559	0.046	0.31	0.017	0.25	1.808	0.028	0.19	0.39

Table C-14 Flickinger soil leached with K_2CrO_4

Treatment	Ap Field Moist Mass (g)	Ap Dry Mass (g)	Bt2 Field Moist Mass (g)	Bt2 Dry Mass (g)	pH	Eh (mV)	Cr Leaching				Phosphate Leaching			
							Soluble Cr(VI) Abs.	Soluble Cr(VI) Conc. (mg/L)	Total Soluble Cr Abs.	Total Soluble Cr Conc. (mg/L)	Residual Liquid (mL)	De-sorbed Cr(VI) Abs.	De-sorbed Cr(VI) Conc. (mg/L)	Adsorbed Cr(VI) Conc. (mg/L)
Ap	2.424	2.003	NA	NA	6.60	542	0.276	1.93	0.143	2.17	2.122	0.067	0.47	0.39
Ap	2.424	2.003	NA	NA	6.85	537	0.185	1.29	0.092	1.3	2.653	0.175	1.22	1.21
Ap	2.420	2.000	NA	NA	6.77	535	0.202	1.41	0.104	1.54	2.046	0.172	1.20	1.19
Ap	2.425	2.004	NA	NA	6.69	562	0.349	2.37	0.152	2.54	2.225	0.023	0.16	0.033
Ap	2.417	1.998	NA	NA	6.80	560	0.359	2.44	0.151	2.52	1.966	0.021	0.14	0.029
Ap	2.412	1.993	NA	NA	6.83	556	0.350	2.38	0.149	2.48	2.442	0.024	0.16	0.027
Bt2	NA	NA	2.832	2.001	6.61	482	0.173	1.23	0.088	1.2	2.226	0.152	1.07	1.06
Bt2	NA	NA	2.828	1.999	6.67	488	0.125	0.882	0.062	0.83	2.871	0.237	1.69	1.75
Bt2	NA	NA	2.831	2.001	6.69	493	0.101	0.711	0.050	0.67	2.377	0.263	1.88	1.95
Ap/Bt2	2.422	2.002	2.835	2.004	6.77	531	0.102	0.708	0.045	0.63	6.492	0.213	1.49	1.61
Ap/Bt2	2.420	2.000	2.835	2.004	6.75	532	0.095	0.66	0.042	0.59	5.912	0.226	1.58	1.71
Ap/Bt2	2.423	2.002	2.830	2.000	6.77	531	0.037	0.26	0.015	0.21	6.535	0.258	1.80	2.06
Ap→Bt2	2.425	2.004	1.408	0.995	6.66	560	0.172	1.17	0.065	1.0	1.331	0.144	0.978	0.998
Ap→Bt2	2.417	1.998	1.426	1.008	6.66	558	0.103	0.699	0.035	0.53	1.369	0.258	1.75	1.85
Ap→Bt2	2.412	1.993	1.426	1.008	6.76	555	0.194	1.32	0.077	1.2	1.500	0.141	0.957	0.958

II. Chapter 3

Table C-15 Synthetic Fe(III) & Mn(III,IV) (hydr)oxide-coated sands

					Cr Leaching				Phosphate Leaching			
Material	Treatment	Dry Mass (g)	pH	Eh (mV)	Soluble Cr(VI) Abs.	Soluble Cr(VI) Conc. (mg/L)	Total Soluble Cr Abs.	Total Soluble Cr Conc. (mg/L)	Residual Liquid (mL)	De-sorbed Cr(VI) Abs.	De-sorbed Cr(VI) Conc. (mg/L)	Adsorbed Cr(VI) Conc. (mg/L)
Mn Sand	$Cr(NO_3)_3$	2.996	5.54	647	0.112	0.776	0.087	1.2	1.702	0.025	0.17	0.13
Mn Sand	$Cr(NO_3)_3$	2.999	5.74	644	0.121	0.839	0.077	1.1	2.130	0.020	0.13	0.084
Mn Sand	$Cr(NO_3)_3$	3.001	6.11	610	0.142	0.985	0.069	0.97	1.920	0.032	0.22	0.17
Mn Sand	K_2CrO_4	3.002	6.37	605	0.365	2.54	0.173	2.54	3.351	0.041	0.28	0.029
Mn Sand	K_2CrO_4	3.000	6.55	597	0.361	2.51	0.172	2.53	1.424	0.021	0.14	0.029
Mn Sand	K_2CrO_4	3.002	6.47	601	0.361	2.51	0.173	2.54	1.497	0.021	0.14	0.023
Fe Sand	$Cr(NO_3)_3$	3.003	4.23	614	0.000	0.00	0.102	1.60	1.190	0.000	0.00	0.00
Fe Sand	$Cr(NO_3)_3$	2.999	4.23	619	0.000	0.00	0.139	2.18	1.244	0.000	0.00	0.00
Fe Sand	$Cr(NO_3)_3$	2.996	4.28	622	0.000	0.00	0.096	1.51	0.991	0.000	0.00	0.00
Fe Sand	K_2CrO_4	3.003	6.22	572	0.305	2.02	0.142	2.23	0.980	0.079	0.53	0.48
Fe Sand	K_2CrO_4	2.996	6.28	570	0.277	1.83	0.128	2.01	2.008	0.100	0.66	0.59
Fe Sand	K_2CrO_4	3.005	6.29	570	0.274	1.81	0.128	2.01	1.157	0.105	0.70	0.66
Fe/Mn Sand	$Cr(NO_3)_3$	3.004	6.69	607	0.096	0.59	0.055	0.63	1.901	0.068	0.41	0.40
Fe/Mn Sand	$Cr(NO_3)_3$	3.005	6.50	610	0.074	0.45	0.051	0.58	2.620	0.048	0.28	0.27
Fe/Mn Sand	$Cr(NO_3)_3$	3.004	6.53	624	0.087	0.53	0.051	0.58	1.424	0.065	0.39	0.38
Fe/Mn Sand	K_2CrO_4	3.003	7.00	614	0.372	2.45	0.185	2.27	2.205	0.031	0.18	0.0081
Fe/Mn Sand	K_2CrO_4	2.998	6.89	624	0.363	2.39	0.181	2.22	1.781	0.030	0.17	0.037
Fe/Mn Sand	K_2CrO_4	3.005	6.81	631	0.362	2.38	0.183	2.25	1.120	0.022	0.12	0.035

Table C-16 Natural soil and fungal Fe(III) & Mn(III,IV) (hydr)oxides

						Cr Leaching				Phosphate Leaching			
Material	Treatment	Wet Mass (g)	Dry Mass (g)	pH	Eh (mV)	Soluble Cr(VI) Abs.	Soluble Cr(VI) Conc. (mg/L)	Total Soluble Cr Abs.	Total Soluble Cr Conc. (mg/L)	Residual Liquid (mL)	De-sorbed Cr(VI) Abs.	De-sorbed Cr(VI) Conc. (mg/L)	Adsorbed Cr(VI) Conc. (mg/L)
Flickinger Bt2	$Cr(NO_3)_3$	4.240	2.999	6.68	492	0.016	0.10	0.007	0.09	3.575	0.139	0.948	1.05
Flickinger Bt2	$Cr(NO_3)_3$	4.240	2.999	6.68	496	0.018	0.12	0.008	0.1	3.303	0.140	0.955	1.05
Flickinger Bt2	$Cr(NO_3)_3$	4.241	2.999	6.67	504	0.012	0.075	0.005	0.07	3.655	0.149	1.02	1.13
Flickinger Bt2	K_2CrO_4	4.240	2.999	6.74	516	0.051	0.34	0.023	0.27	3.612	0.276	1.91	2.10
Flickinger Bt2	K_2CrO_4	4.243	3.001	6.73	521	0.034	0.23	0.014	0.17	3.584	0.266	1.84	2.03
Flickinger Bt2	K_2CrO_4	4.243	3.001	6.76	522	0.107	0.726	0.055	0.64	3.647	0.203	1.40	1.48
Russett Bt	$Cr(NO_3)_3$	3.400	3.004	4.01	638	0.000	0.00	0.016	0.19	4.183	0.000	0.00	0.00
Russett Bt	$Cr(NO_3)_3$	3.394	2.998	4.02	638	0.000	0.00	0.007	0.09	2.389	0.000	0.00	0.00
Russett Bt	$Cr(NO_3)_3$	3.392	2.996	4.04	645	0.000	0.00	0.057	0.67	1.816	0.000	0.00	0.00
Russett Bt	K_2CrO_4	3.394	2.998	4.08	652	0.000	0.00	0.003	0.05	1.699	0.248	1.84	1.95
Russett Bt	K_2CrO_4	3.394	2.998	4.07	656	0.008	0.05	0.007	0.09	2.085	0.266	1.98	2.11
Russett Bt	K_2CrO_4	3.395	2.999	4.35	651	0.108	0.791	0.066	0.77	1.719	0.185	1.37	1.40
Fungal Oxide	$Cr(NO_3)_3$	0.457	0.032	6.02	664	0.119	0.736	0.087	1.02	1.586	0.047	0.28	0.25
Fungal Oxide	K_2CrO_4	0.457	0.032	6.4	626	0.342	2.24	0.201	2.49	1.907	0.024	0.13	0.00

References

Anderson R.A. (1997) Chromium as an essential nutrient for humans. Regulatory Toxicology and Pharmacology 26:S35-S41. DOI: 10.1006/rtph.1997.1136.

Aoki T., Munemori M. (1982) Recovery of chromium(VI) from wastewaters with iron(III) hydroxide .1. Adsorption mechanism of chromium(VI) on iron(III) hydroxide. Water Research 16:793-796. DOI: 10.1016/0043-1354(82)90006-9.

Arias M., Barral M.T., Diazfierros F. (1995) Effects of iron and aluminum-oxides on the colloidal and surface-properties of kaolin. Clays and Clay Minerals 43:406-416. DOI: 10.1346/ccmn.1995.0430403.

Bahaa-eldin E.A.R., Yusoff I., Rahim S.A., Zuhairi W.Y.W., Ghani M.R.A. (2011) Tracing subsurface migration of contaminants from an abandoned municipal landfill. Environmental Earth Sciences 63:1043-1055. DOI: 10.1007/s12665-010-0780-3.

Bargar J.R., Webb S.M., Tebo B.M. (2005) EXAFS, XANES and in-situ SR-XRD characterization of biogenic manganese oxides produced in sea water. Physica Scripta T115:888-890.

Bartlett R., James B. (1979) Behavior of chromium in soils 3. Oxidation, Journal of Environmental Quality. pp. 31-35.

Bartlett R., James B. (1980) Studying dried, stored soil samples - Some pitfalls. Soil Science Society of America Journal 44:721-724.

Bartlett R.J. (1991) Chromium cycling in soils and water - Links, gaps, and methods. Environmental Health Perspectives 92:17-24. DOI: 10.2307/3431133.

Blanchard M., Morin G., Lazzeri M., Balan E. (2010) First-principles study of the structural and isotopic properties of Al- and OH-bearing hematite. Geochimica Et Cosmochimica Acta 74:3948-3962. DOI: 10.1016/j.gca.2010.04.018.

Bongoua-Devisme A.J., Cebron A., Kassin K.E., Yoro G.R., Mustin C., Berthelin J. (2013) Microbial communities involved in Fe reduction and mobility during soil organic matter (SOM) mineralization in two contrasted paddy soils. Geomicrobiology Journal 30:347-361. DOI: 10.1080/01490451.2012.688928.

Bourgault R.R. (2008) Multi-scale pedologic investigation of manganiferous soils in the Maryland Piedmont, Environmental Science and Technology, University of Maryland, College Park, College Park, MD. pp. 262.

Bourgault R.R., Rabenhorst M.C. (2011) Genesis and characterization of manganiferous soils in the Eastern Piedmont, USA. Geoderma 165:84-94. DOI: 10.1016/j.geoderma.2011.07.008.

Brose D.A., James B.R. (2010) Oxidation-Reduction Transformations of Chromium in Aerobic Soils and the Role of Electron-Shuttling Quinones. Environmental Science & Technology 44:9438-9444. DOI: 10.1021/es101859b.

Brose D.A., James B.R. (2013) Hexavalent chromium reduction by tartaric acid and isopropyl alcohol in Mid-Atlantic soils and the role of Mn(III,IV)(hydr)oxides. Environmental Science & Technology 47:12985-12991. DOI: 10.1021/es401903s.

Buerge I.J., Hug S.J. (1997) Kinetics and pH dependence of chromium(VI) reduction by iron(II). Environmental Science & Technology 31:1426-1432. DOI: 10.1021/es960672i.

Buerge I.J., Hug S.J. (1998) Influence of organic ligands on chromium(VI) reduction by iron(II). Environmental Science & Technology 32:2092-2099. DOI: 10.1021/es970932b.

Camargo F.A.O., Bento F.M., Okeke B.C., Frankenberger W.T. (2003) Chromate reduction by chromium-resistant bacteria isolated from soils contaminated with dichromate. Journal of Environmental Quality 32:1228-1233.

Camprubi A., Canet C., Rodriguez-Diaz A.A., Prol-Ledesma R.M., Blanco-Florido D., Villanueva R.E., Lopez-Sanchez A. (2008) Geology ore deposits and hydrothermal venting in Bahia Concepcion, Baja California Sur, Mexico. Island Arc 17:6-25. DOI: 10.1111/j.1440-1738.2007.00586.x.

Cao X.H., Guo J., Mao J.D., Lan Y.Q. (2011) Adsorption and mobility of Cr(III)-organic acid complexes in soils. Journal of Hazardous Materials 192:1533-1538. DOI: 10.1016/j.jhazmat.2011.06.076.

Cervantes C., Campos-Garcia J., Devars S., Gutierrez-Corona F., Loza-Tavera H., Torres-Guzman J.C., Moreno-Sanchez R. (2001) Interactions of chromium with microorganisms and plants. Fems Microbiology Reviews 25:335-347. DOI: 10.1111/j.1574-6976.2001.tb00581.x.

Chang H.S., Singer J.H., Seaman J.C. (2012) In situ chromium(VI) reduction using iron(II) solutions: Modeling dynamic geochemical gradients. Vadose Zone Journal 11. DOI: 10.2136/vzj2011.0172.

Chaudhari A.U., Tapase S.R., Markad V.L., Kodam K.M. (2013) Simultaneous decolorization of reactive Orange M2R dye and reduction of chromate by Lysinibacillus sp KMK-A. Journal of Hazardous Materials 262:580-588. DOI: 10.1016/j.jhazmat.2013.09.006.

Chen J.M., Hao O.J. (1998) Microbial chromium (VI) reduction. Critical Reviews in Environmental Science and Technology 28:219-251. DOI: 10.1080/10643389891254214.

Chen N., Lan Y.Q., Wang B., Mao J.D. (2013) Reduction of Cr(VI) by organic acids in the presence of Al(III). Journal of Hazardous Materials 260:150-156. DOI: 10.1016/j.jhazmat.2013.05.010.

Cheng R.H., Borca C.N., Pilet N., Xu B., Yuan L., Doudin B., Liou S.H., Dowben P.A. (2002) Oxidation of metals at the chromium oxide interface. Applied Physics Letters 81:2109-2111. DOI: 10.1063/1.1506942.

Choppala G., Bolan N., Lamb D., Kunhikrishnan A. (2013) Comparative sorption and mobility of Cr(III) and Cr(VI) species in a range of soils: Implications to bioavailability. Water Air and Soil Pollution 224. DOI: 1699

10.1007/s11270-013-1699-6.

Cifuentes F.R., Lindemann W.C., Barton L.L. (1996) Chromium sorption and reduction in soil with implications to bioremediation. Soil Science 161:233-241. DOI: 10.1097/00010694-199604000-00004.

Condron M.A. (1990) Soils with spodic characteristics on the Eastern Shore of Maryland, University of Maryland, College Park. pp. 115.

Contreras E.M., Orozco A.M.F., Zaritzky N.E. (2011) Biological Cr(VI) removal coupled with biomass growth, biomass decay, and multiple substrate limitation. Water Research 45:3034-3046. DOI: 10.1016/j.watres.2011.03.011.

Cornell R.M., Giovanoli R. (1985) Effect of solution conditions on the proportion and morphology of goethite formed from ferrihydrite. Clays and Clay Minerals 33:424-432. DOI: 10.1346/ccmn.1985.0330508.

Cui H.J., Liu X.W., Tan W.F., Feng X.H., Liu F., Ruan H.D. (2008) Influence of Mn(III) availability on the phase transformation from layered buserite to tunnel-structured todorokite. Clays and Clay Minerals 56:397-403. DOI: 10.1346/ccmn.2008.0560401.

Cygan R.T., Post J.E., Heaney P.J., Kubicki J.D. (2012) Molecular models of birnessite and related hydrated layered minerals. American Mineralogist 97:1505-1514. DOI: 10.2138/am.2012.3957.

D'Amore D.V., Stewart S.R., Huddleston J.H. (2004) Saturation, reduction, and the formation of iron-manganese concretions in the Jackson-Frazier Wetland, Oregon. Soil Science Society of America Journal 68:1012-1022.

Das S.K., Guha A.K. (2009) Biosorption of hexavalent chromium by Termitomyces clypeatus biomass: Kinetics and transmission electron microscopic study. Journal of Hazardous Materials 167:685-691. DOI: 10.1016/j.jhazmat.2009.01.037.

Davies S.H.R., Morgan J.J. (1989) Manganese(II) oxidation-kinetics on metal-oxide surfaces. Journal of Colloid and Interface Science 129:63-77. DOI: 10.1016/0021-9797(89)90416-5.

Deng Y.W., Stjernstrom M., Banwart S. (1996) Accumulation and remobilization of aqueous chromium(VI) at iron oxide surfaces: Application of a thin-film continuous flow-through reactor. Journal of Contaminant Hydrology 21:141-151. DOI: 10.1016/0169-7722(95)00039-9.

Dixon J.B., White G.N. (2002) Manganese oxides, in: J. B. Dixon and D. G. Schulze (Eds.), Soil Mineralogy with Environmental Applications, Soil Science Society of America, Madison, WI. pp. 367-.

Dogan N.M., Kantar C., Gulcan S., Dodge C.J., Yimaz B.C., Mazmanci M.A. (2011) Chromium(VI) bioremoval by Pseudomonas bacteria: Role of microbial exudates for natural attenuation and biotreatment of Cr(VI) contamination. Environmental Science & Technology 45:2278-2285. DOI: 10.1021/es102095t.

Dossing L.N., Dideriksen K., Stipp S.L.S., Frei R. (2011) Reduction of hexavalent chromium by ferrous iron: A process of chromium isotope fractionation and its relevance to natural environments. Chemical Geology 285:157-166. DOI: 10.1016/j.chemgeo.2011.04.005.

Dotro G., Larsen D., Palazolo P. (2011) Preliminary evaluation of biological and physical-chemical chromium removal mechanisms in gravel media used in constructed wetlands. Water Air and Soil Pollution 215:507-515. DOI: 10.1007/s11270-010-0495-9.

Dowding C.E., Fey M.V. (2007) Morphological, chemical and mineralogical properties of some manganese-rich oxisols derived from dolomite in Mpumalanga province, South Africa. Geoderma 141:23-33. DOI: 10.1016/j.geoderma.2007.04.024.

Elzinga E.J. (2011) Reductive transformation of birnessite by aqueous Mn(II). Environmental Science & Technology 45:6366-6372. DOI: 10.1021/es2013038.

Emerson D., Field E.K., Chertkov O., Davenport K.W., Goodwin L., Munk C., Nolan M., Woyke T. (2013) Comparative genomics of freshwater Fe-oxidizing bacteria: implications for physiology, ecology, and systematics. Frontiers in Microbiology 4:17. DOI: 10.3389/fmicb.2013.00254.

Fageria N.K., Stone L.F. (2006) Physical, chemical, and biological changes in the rhizosphere and nutrient availability. Journal of Plant Nutrition 29:1327-1356. DOI: 10.1080/01904160600767682.

Fanning D.S., Rabenhorst M.C., May L., Wagner D.P. (1989) Oxidation-state of iron in glauconite from oxidized and reduced zones of soil-geologic columns. Clays and Clay Minerals 37:59-64.

Fendorf S., Wielinga B.W., Hansel C.M. (2000) Chromium transformations in natural environments: The role of biological and abiological processes in chromium(VI) reduction. International Geology Review 42:691-701. DOI: 10.1080/00206810009465107.

Fendorf S.E. (1995) Surface-reactions of chromium in soils and waters. Geoderma 67:55-71. DOI: 10.1016/0016-7061(94)00062-f.

Fendorf S.E., Fendorf M., Sparks D.L., Gronsky R. (1992) Inhibitory mechanisms of Cr(III) oxidation by delta-MnO2. Journal of Colloid and Interface Science 153:37-54. DOI: 10.1016/0021-9797(92)90296-x.

Fendorf S.E., Zasoski R.J. (1992) Chromium(III) oxidation by delta-MnO2 .1. Characterization. Environmental Science & Technology 26:79-85. DOI: 10.1021/es00025a006.

Fendorf S.E., Zasoski R.J., Burau R.G. (1993) Competing metal-ion influences on chromium(III) oxidation by birnessite. Soil Science Society of America Journal 57:1508-1515.

Feng X.H., Zhai L.M., Tan W.F., Liu F., He J.Z. (2007) Adsorption and redox reactions of heavy metals on synthesized Mn oxide minerals. Environmental Pollution 147:366-373. DOI: 10.1016/j.envpol.2006.05.028.

Feng X.H., Zhu M.Q., Ginder-Vogel M., Ni C.Y., Parikh S.J., Sparks D.L. (2010) Formation of nano-crystalline todorokite from biogenic Mn oxides. Geochimica Et Cosmochimica Acta 74:3232-3245. DOI: 10.1016/j.gca.2010.03.005.

Field E.K., Gerlach R., Viamajala S., Jennings L.K., Peyton B.M., Apel W.A. (2013) Hexavalent chromium reduction by Cellulomonas sp strain ES6: the influence of carbon source, iron minerals, and electron shuttling compounds. Biodegradation 24:437-450. DOI: 10.1007/s10532-012-9600-7.

Filimonova L.G., Sivtsov A.V., Trubkin N.V. (2010) Manganese oxides and associated minerals as constituents of dispersed mineralization of metasomatic rocks in the Dukat ore field. Geology of Ore Deposits 52:322-333. DOI: 10.1134/s1075701510040069.

Fujimoto C.K., Sherman G.D. (1948) Behavior of manganese in the soil and the manganese cycle. Soil Science 66:131-145. DOI: 10.1097/00010694-194808000-00006.

Gasparatos D., Tarenidis D., Haidouti C., Oikonomou G. (2005) Microscopic structure of soil Fe-Mn nodules: environmental implication. Environmental Chemistry Letters 2:175-178. DOI: 10.1007/s10311-004-0092-5.

Gee G.W., Bauder J.W. (1986) Particle-size analysis, in: A. Klute (Ed.), Methods of Soil Analysis Part 1 - Physical and Mineralogical Methods, Soil Science Society of America, Inc., Madison, WI. pp. 383-411.

Grangeon S., Lanson B., Miyata N., Tani Y., Manceau A. (2010) Structure of nanocrystalline phyllomanganates produced by freshwater fungi. American Mineralogist 95:1608-1616. DOI: 10.2138/am.2010.3516.

Hansen D.J., McGuire J.T., Mohanty B.P. (2011) Enhanced biogeochemical cycling and subsequent reduction of hydraulic conductivity associated with soil-layer interfaces in the vadose zone. Journal of Environmental Quality 40:1941-1954. DOI: 10.2134/jeq2011.0112.

Harish R., Samuel J., Mishra R., Chandrasekaran N., Mukherjee A. (2012) Bio-reduction of Cr(VI) by exopolysaccharides (EPS) from indigenous bacterial species of Sukinda chromite mine, India. Biodegradation 23:487-496. DOI: 10.1007/s10532-011-9527-4.

Herranz T., Rojas S., Ojeda M., Perez-Alonso F.J., Terreros P., Pirota K., Fierro J.L.G. (2006) Synthesis, structural features, and reactivity of Fe-Mn mixed oxides prepared by microemulsion. Chemistry of Materials 18:2364-2375. DOI: 10.1021/cm052568i.

James B.R., Bartlett R.J. (1983a) Behavior of chromium in soils: VII. Adsorption and reduction of hexavalent forms. J. Environ. Qual. 12:177-181. DOI: 10.2134/jeq1983.00472425001200020005x.

James B.R., Bartlett R.J. (1983b) Behavior of chromium in soils. VI. Interactions between oxidation-reduction and organic complexation. J. Environ. Qual. 12:173-176. DOI: 10.2134/jeq1983.00472425001200020004x.

Jardine P.M., Mehlhorn T.L., Bailey W.B., Brooks S.C., Fendorf S., Gentry R.W., Phelps T.J., Saiers J.E. (2011) Geochemical processes governing the fate and transport of chromium(III) and chromium(VI) in soils. Vadose Zone Journal 10:1058-1070. DOI: 10.2136/vzj2010.0102.

Jardine P.M., Stewart M.A., Barnett M.O., Basta N.T., Brooks S.C., Fendorf S., Mehlhorn T.L. (2013) Influence of soil geochemical and physical properties on chromium(VI) sorption and bioaccessibility. Environmental Science & Technology 47:11241-11248. DOI: 10.1021/es401611h.

Jeon B.H., Dempsey B.A., Burgos W.D. (2003) Kinetics and mechanisms for reactions of Fe(II) with iron(III) oxides. Environmental Science & Technology 37:3309-3315. DOI: 10.1021/es025900p.

Jien S.H., Hseu Z.Y., Chen Z.S. (2010) Hydropedological implications of ferromanganiferous nodules in rice-growing plinthitic Ultisols under different moisture regimes. Soil Science Society of America Journal 74:880-891. DOI: 10.2136/sssaj2009.0020.

Julien C.M., Massot M., Poinsignon C. (2004) Lattice vibrations of manganese oxides - Part 1. Periodic structures. Spectrochimica Acta Part a-Molecular and Biomolecular Spectroscopy 60:689-700. DOI: 10.1016/s1386-1425(03)00279-8.

Jung Y., Choi J., Lee W. (2007) Spectroscopic investigation of magnetite surface for the reduction of hexavalent chromium. Chemosphere 68:1968-1975. DOI: 10.1016/j.chemosphere.2007.02.028.

Kantar C., Demir A., Koleli N. (2014) Effect of exopolymeric substances on the kinetics of sorption and desorption of trivalent chromium in soil. Chemical Papers 68:112-120. DOI: 10.2478/s11696-013-0427-4.

Kim I.S., Ekpeghere K.I., Ha S.Y., Kim B.S., Song B., Kim J.T., Kim H.G., Koh S.C. (2014) Full-scale biological treatment of tannery wastewater using the novel microbial consortium BM-S-1. Journal of Environmental Science and Health Part a-Toxic/Hazardous Substances & Environmental Engineering 49:355-364. DOI: 10.1080/10934529.2014.846707.

Komarek M., Vanek A., Ettler V. (2013) Chemical stabilization of metals and arsenic in contaminated soils using oxides - A review. Environmental Pollution 172:9-22. DOI: 10.1016/j.envpol.2012.07.045.

Kozuh N., Stupar J., Gorenc B. (1999) Reduction and oxidation processes of chromium in soils. Environmental Science & Technology 34:112-119. DOI: 10.1021/es981162m.

Kwon K.D., Refson K., Sposito G. (2013) Understanding the trends in transition metal sorption by vacancy sites in birnessite. Geochimica Et Cosmochimica Acta 101:222-232. DOI: 10.1016/j.gca.2012.08.038.

Landrot G., Ginder-Vogel M., Livi K., Fitts J.P., Sparks D.L. (2012) Chromium(III) oxidation by three poorly-crystalline manganese(IV) oxides. 1. Chromium(III)-oxidizing capacity. Environmental Science & Technology 46:11594-11600. DOI: 10.1021/es302383y.

Lanson B., Drits V.A., Silvester E., Manceau A. (2000) Structure of H-exchanged hexagonal birnessite and its mechanism of formation from Na-rich monoclinic buserite at low pH. American Mineralogist 85:826-838.

Leita L., Margon A., Sinicco T., Mondini C. (2011) Glucose promotes the reduction of hexavalent chromium in soil. Geoderma 164:122-127. DOI: 10.1016/j.geoderma.2011.05.013.

Liu H.B., Chen T.H., Qing C.S., Xie Q.Q., Frost R.L. (2013) Confirmation of the assignment of vibrations of goethite: An ATR and IES study of goethite structure. Spectrochimica Acta Part a-Molecular and Biomolecular Spectroscopy 116:154-159. DOI: 10.1016/j.saa.2013.06.102.

Loeppert R.H., Inskeep W.P. (1996) Iron, in: D. L. Sparks (Ed.), Methods of Soil Analysis Part 3 - Chemical Methods, Soil Science Society of America, Inc., Madison, WI. pp. 639-664.

Loyaux-Lawniczak S., Lecomte P., Ehrhardt J.-J. (2001) Behavior of hexavalent chromium in a polluted groundwater: Redox processes and immobilization in soils. Environmental Science & Technology 35:1350-1357. DOI: 10.1021/es001073l.

Loyaux-Lawniczak S., Refait P., Lecomte P., Ehrhardt J.J., Genin J.M.R. (1999) The reduction of chromate ions by Fe(II) layered hydroxides. Hydrology and Earth System Sciences 3:593-599.

Luo J., Huang A.M., Park S.H., Suib S.L., O'Young C.L. (1998) Crystallization of sodium-birnessite and accompanied phase transformation. Chemistry of Materials 10:1561-1568. DOI: 10.1021/cm970745c.

Malinowski E.R. (1978) Theory of error for target factor-analysis with applications to mass-spectrometry and nuclear magnetic-resonance spectrometry. Analytica Chimica Acta-Computer Techniques and Optimization 2:339-354.

Manceau A., Marcus M.A., Tamura N. (2002) Quantitative speciation of heavy metals in soils and sediments by synchrotron X-ray techniques, in: P. A. Fenter, et al. (Eds.), Applications of Synchrotron Radiation in Low-Temperature Geochemistry and Environmental Sciences. pp. 341-428.

Mandernack K.W., Post J., Tebo B.M. (1995) Manganese mineral formation by bacterial-spores of the marine Bacillus, strain SG-1 - Evidence for the direct oxidation of Mn(II) to Mn(IV). Geochimica Et Cosmochimica Acta 59:4393-4408. DOI: 10.1016/0016-7037(95)00298-e.

McKenzie R.M. (1989) Manganese oxides and hydroxides, Minerals in Soil Environments, Soil Science Society of America, Madison, WI. pp. 439-463.

Murray K.J., Tebo B.M. (2007) Cr(III) is indirectly oxidized by the Mn(II)-oxidizing bacterium Bacillus sp strain SG-1. Environmental Science & Technology 41:528-533. DOI: 10.1021/es0615167.

Music S., Ristic M., Tonkovic M. (1986) Sorption of chromium(VI) on hydrous iron-oxides. Zeitschrift Fur Wasser Und Abwasser Forschung-Journal for Water and Wastewater Research 19:186-196.

Negra C., Ross D.S., Lanzirotti A. (2005) Oxidizing behavior of soil manganese: Interactions among abundance, oxidation state, and pH. Soil Science Society of America Journal 69:87-95.

Newville M. (2001) EXAFS analysis using FEFF and FEFFIT. Journal of Synchrotron Radiation 8:96-100. DOI: 10.1107/s0909049500016290.

Ozturk S., Kaya T., Aslim B., Tan S. (2012) Removal and reduction of chromium by Pseudomonas spp. and their correlation to rhamnolipid production. Journal of Hazardous Materials 231:64-69. DOI: 10.1016/j.jhazmat.2012.06.038.

Pal A., Paul A.K. (2004) Aerobic chromate reduction by chromium-resistant bacteria isolated from serpentine soil. Microbiological Research 159:347-354. DOI: 10.1016/j.micres.2004.08.001.

Perez D.V., De Campos R.C., Meneguelli N.A. (2004) Effects of soil sample storage treatment on the composition and Fe, Al, and Mn speciation of soil solutions obtained by centrifugation. Water Air and Soil Pollution 151:195-214.

Peterson M.L., Brown G.E., Parks G.A. (1996) Direct XAFS evidence for heterogeneous redox reaction at the aqueous chromium/magnetite interface. Colloids and Surfaces a-Physicochemical and Engineering Aspects 107:77-88. DOI: 10.1016/0927-7757(95)03345-9.

Post J.E. (1999) Manganese oxide minerals: Crystal structures and economic and environmental significance. Proceedings of the National Academy of Sciences of the United States of America 96:3447-3454. DOI: 10.1073/pnas.96.7.3447.

Post J.E., Veblen D.R. (1990) Crystal-Structure Determinations of Synthetic Sodium, Magnesium, and Potassium Birnessite Using TEM and the Rietveld Method. American Mineralogist 75:477-489.

Puzon G.J., Roberts A.G., Kramer D.M., Xun L.Y. (2005) Formation of soluble organo-chromium(III) complexes after chromate reduction in the presence of cellular organics. Environmental Science & Technology 39:2811-2817. DOI: 10.1021/es048967g.

Puzon G.J., Tokala R.K., Zhang H., Yonge D., Peyton B.M., Xun L.Y. (2008) Mobility and recalcitrance of organo-chromium(III) complexes. Chemosphere 70:2054-2059. DOI: 10.1016/j.chemosphere.2007.09.010.

Rai D., Sass B.M., Moore D.A. (1987) Chromium(III) hydrolysis constants and solubility of chromium(III) hydroxide. Inorganic Chemistry 26:345-349. DOI: 10.1021/ic00250a002.

Ramirez-Diaz M.I., Diaz-Perez C., Vargas E., Riveros-Rosas H., Campos-Garcia J., Cervantes C. (2008) Mechanisms of bacterial resistance to chromium compounds. Biometals 21:321-332. DOI: 10.1007/s10534-007-9121-8.

Ross D.S., Hales H.C., Shea-McCarthy G.C., Lanzirotti A. (2001) Sensitivity of soil manganese oxides: Drying and storage cause reduction. Soil Science Society of America Journal 65:736-743.

Saleh A.M., Jones A.A. (1984) The crystallinity and surface characteristics of synthetic ferrihydrite and its relationship to kaolinite surfaces. Clay Minerals 19:745-755. DOI: 10.1180/claymin.1984.019.5.05.

Santelli C.M., Webb S.M., Dohnalkova A.C., Hansel C.M. (2011) Diversity of Mn oxides produced by Mn(II)-oxidizing fungi. Geochimica Et Cosmochimica Acta 75:2762-2776. DOI: 10.1016/j.gca.2011.02.022.

Saratovsky I., Gurr S.J., Hayward M.A. (2009) The Structure of manganese oxide formed by the fungus Acremonium sp strain KR21-2. Geochimica Et Cosmochimica Acta 73:3291-3300. DOI: 10.1016/j.gca.2009.03.005.

Sarkar B., Naidu R., Krishnamurti G.S.R., Megharaj M. (2013) Manganese(II)-catalyzed and clay-minerals-mediated reduction of chromium(VI) by citrate. Environmental Science & Technology 47:13629-13636. DOI: 10.1021/es401568k.

Schaefer M.V., Gorski C.A., Scherer M.M. (2011) Spectroscopic evidence for interfacial Fe(II)-Fe(III) electron transfer in a clay mineral. Environmental Science & Technology 45:540-545. DOI: 10.1021/es102560m.

Schulze D.G., Sutton S.R., Bajt S. (1995) Determining manganese oxidation-state in soils using x-ray-absorption near-edge structure (XANES) spectroscopy. Soil Science Society of America Journal 59:1540-1548.

Schwertmann U., Fanning D.S. (1976) Iron-manganese concretions in hydrosequences of soils in loess in bavaria. Soil Science Society of America Journal 40:731-738.

Schwertmann U., Taylor R.M. (1989) Iron oxides, in: S. B. Weed (Ed.), Minerals in Soil Environments, Soil Science Society of America, Madison, WI. pp. 379-438.

Shaheen S.M., Tsadilas C.D., Rinklebe J. (2013) A review of the distribution coefficients of trace elements in soils: Influence of sorption system, element characteristics, and soil colloidal properties. Advances in Colloid and Interface Science 201:43-56. DOI: 10.1016/j.cis.2013.10.005.

Soileau J.M., McCracken R.J. (1967) Free iron and coloration in certain well-drained Coastal Plain soils in relation to their other properties and classification. Soil Science Society of America Proceedings 31:248-&.

Somenahally A.C., Mosher J.J., Yuan T., Podar M., Phelps T.J., Brown S.D., Yang Z.K., Hazen T.C., Arkin A.P., Palumbo A.V., *et al*. (2013) Hexavalent chromium reduction under fermentative conditions with lactate stimulated native microbial communities. Plos One 8:11. DOI: 10.1371/journal.pone.0083909.

Stahl R.S., James B.R. (1991a) Zinc sorption by iron-oxide-coated sand as a function of pH. Soil Science Society of America Journal 55:1287-1290.

Stahl R.S., James B.R. (1991b) Zinc sorption by manganese-oxide-coated sand as a function of pH. Soil Science Society of America Journal 55:1291-1294.

Stewart M.A., Jardine P.M., Barnett M.O., Mehlhorn T.L., Hyder L.K., McKay L.D. (2003) Influence of soil geochemical and physical properties on the sorption and bioaccessibility of chromium(III). Journal of Environmental Quality 32:129-137.

Tan W.F., Liu F., Feng X.H., Huang Q.Y., Li X.Y. (2005) Adsorption and redox reactions of heavy metals on Fe-Mn nodules from Chinese soils. Journal of Colloid and Interface Science 284:600-605. DOI: 10.1016/j.jcis.2004.10.049.

Tan W.F., Lu S.J., Liu F., Feng X.H., He J.Z., Koopall L.K. (2008) Determination of the point-of-zero, charge of manganese oxides with different methods including an improved salt titration method. Soil Science 173:277-286. DOI: 10.1097/SS.01b013e31816d1f12.

Tang Y.Z., Zeiner C.A., Santelli C.M., Hansel C.M. (2013) Fungal oxidative dissolution of the Mn(II)-bearing mineral rhodochrosite and the role of metabolites in manganese oxide formation. Environmental Microbiology 15:1063-1077. DOI: 10.1111/1462-2920.12029.

Toner B., Fakra S., Villalobos M., Warwick T., Sposito G. (2005) Spatially resolved characterization of biogenic manganese oxide production within a bacterial biofilm. Applied and Environmental Microbiology 71:1300-1310. DOI: 10.1128/aem.71.3.1300-1310.2005.

Toner B., Manceau A., Webb S.M., Sposito G. (2006) Zinc sorption to biogenic hexagonal-birnessite particles within a hydrated bacterial biofilm. Geochimica Et Cosmochimica Acta 70:27-43. DOI: 10.1016/j.gca.2005.08.029.

Trebien D.O.P., Bortolon L., Tedesco M.J., Bissani C.A., Camargo F.A.O. (2011) Environmental factors affecting chromium-manganese oxidation-reduction reactions in soil. Pedosphere 21:84-89.

Tsu T.C., Yang J.L. (1996) Formation of reactive oxygen species and DNA strand breakage during interaction of chromium(III) and hydrogen peroxide in vitro: Evidence for a chromium(III)-mediated Fenton-like reaction. Chemico-Biological Interactions 102:133-153.

Vasant C., Balamurugan K., Rajaram R., Ramasami T. (2001) Apoptosis of lymphocytes in the presence of Cr(V) complexes: Role in Cr(VI)-induced toxicity. Biochemical and Biophysical Research Communications 285:1354-1360. DOI: 10.1006/bbrc.2001.5335.

Villalobos M., Lanson B., Manceau A., Toner B., Sposito G. (2006) Structural model for the biogenic Mn oxide produced by Pseudomonas putida. American Mineralogist 91:489-502. DOI: 10.2138/am.2006.1925.

Villalobos M., Toner B., Bargar J., Sposito G. (2003) Characterization of the manganese oxide produced by Pseudomonas putida strain MnB1. Geochimica Et Cosmochimica Acta 67:2649-2662. DOI: 10.1016/s0016-7037(03)00217-5.

Vodyanitskii Y.N., Vasil'ev A.A., Lesovaya S.N., Sataev E.F., Sivtsov A.V. (2004) Formation of manganese oxides in soils. Eurasian Soil Science 37:572-584.

Wang H.D., White G.N., Turner F.T., Dixon J.B. (1993) Ferrihydrite, lepidocrocite, and goethite in coatings from East Texas Vertic soils. Soil Science Society of America Journal 57:1381-1386.

Weaver R.M., Hochella M.F., Ilton E.S. (2002) Dynamic processes occurring at the Cr-aq(III)-manganite (gamma-MnOOH) interface: Simultaneous adsorption, microprecipitation, oxidation/reduction, and dissolution. Geochimica Et Cosmochimica Acta 66:4119-4132. DOI: 10.1016/s0016-7037(02)00980-8.

Webb S.M. (2005) SIXpack: a graphical user interface for XAS analysis using IFEFFIT. Physica Scripta T115:1011-1014.

Webb S.M., Tebo B.M., Bargar J.R. (2005a) Structural influences of sodium and calcium ions on the biogenic manganese oxides produced by the marine Bacillus sp., strain SG-1. Geomicrobiology Journal 22:181-193. DOI: 10.1080/01490450590946013.

Webb S.M., Tebo B.M., Bargat J.R. (2005b) Structural characterization of biogenic Mn oxides produced in seawater by the marine bacillus sp strain SG-1. American Mineralogist 90:1342-1357. DOI: 10.2138/am.2005.1669.

White A.F., Peterson M.L. (1996) Reduction of aqueous transition metal species on the surfaces of Fe(II)-containing oxides. Geochimica Et Cosmochimica Acta 60:3799-3814. DOI: 10.1016/0016-7037(96)00213-x.

Wielinga B., Mizuba M.M., Hansel C.M., Fendorf S. (2001) Iron promoted reduction of chromate by dissimilatory iron-deducing bacteria. Environmental Science & Technology 35:522-527. DOI: 10.1021/es001457b.

Wittbrodt P.R., Palmer C.D. (1996) Effect of temperature, ionic strength, background electrolytes, and Fe(III) on the reduction of hexavalent chromium by soil humic substances. Environmental Science & Technology 30:2470-2477. DOI: 10.1021/es950731c.

Xiao W.D., Zhang Y.B., Li T.Q., Chen B., Wang H., He Z.L., Yang X.E. (2012) Reduction kinetics of hexavalent chromium in soils and its correlation with soil properties. Journal of Environmental Quality 41:1452-1458. DOI: 10.2134/jeq2012.0061.

Yang F., Guo J., Dai R.N., Lan Y.Q. (2014) Oxidation of Cr(III)-citrate/tartrate complexes by delta-MnO2: Production of Cr(VI) and its impact factors. Geoderma 213:10-14. DOI: 10.1016/j.geoderma.2013.07.022.

Zachara J.M., Girvin D.C., Schmidt R.L., Resch C.T. (1987) Chromate adsorption on amorphous iron oxyhydroxide in the presence of major groundwater ions. Environmental Science & Technology 21:589-594. DOI: 10.1021/es00160a010.

Zaidel'man F.R., Nikiforova A.S. (2010) Ferromanganese concretionary neoformations: A review. Eurasian Soil Science 43:248-258. DOI: 10.1134/s1064229310030026.

Zhu M.Q., Ginder-Vogel M., Parikh S.J., Feng X.H., Sparks D.L. (2010) Cation effects on the layer structure of biogenic Mn-oxides. Environmental Science & Technology 44:4465-4471. DOI: 10.1021/es1009955.